Ferroelectric and Electromechanical Properties of Sol-gel PZT Films with Single-composition and Compositionally Graded Structures

Panya Khaenamkaew

A Thesis Submitted in Fulfillment of the Requirements for the Degree of Doctor of Philosophy in Physics
Prince of Songkla University
2007

Thesis Title	Ferroelectric and Electromechanical Properties of Sol-gel PZT Films with Single-composition and Compositionally Graded Structures
Author	Mr. Panya Khaenamkaew
Major Program	Physics

Advisory Committee :

……...Chairman
(Assoc. Prof. Dr. Supasarote Muensit)

……...Committee
(Dr. Pattara Aiyarak)

Examining Committee :

……..…….…..Chairman
(Assoc. Prof. Boonlua Phongdara)

……....Committee
(Assoc. Prof. Dr. Supasarote Muensit)

……....Committee
(Dr. Pattara Aiyarak)

……....Committee
(Asst. Prof. Dr. Pruittikorn Smithmaitrie)

……....Committee
(Prof. Dr. Brahim Elouadi)

The Graduate School, Prince of Songkla University, has approved this thesis as fulfillment of the requirements for the Doctor of Philosophy Degree in Physics

……
(Assoc. Prof. Dr. Krerkchai Thongnoo)
Dean of Graduate School

ชื่อวิทยานิพนธ์ สมบัติเฟร์โรอิเล็กตริกและไฟฟ้ากลของฟิล์มพีซีทีที่เตรียมด้วยวิธีโซล-เจลให้มีโครงสร้างแบบส่วนประกอบเดียวและแบบส่วนประกอบแปรเปลี่ยน

ผู้เขียน นายปัญญา แขน้ำแก้ว

สาขาวิชา ฟิสิกส์

ปีการศึกษา 2550

บทคัดย่อ

งานวิจัยนี้เสนอการเตรียมฟิล์มบางพีแซดที ($Pb(Zr_xTi_{1-x})O_3$) สองแบบคือ แบบส่วนประกอบเดียวและแบบส่วนประกอบแปรเปลี่ยน ค่า x คือปริมาณของเซอร์โคเนียมโดยน้ำหนักของส่วนประกอบ โดยฟิล์มทั้งหมดเตรียมขึ้นด้วยวิธีโซล-เจล และนำมาศึกษาโครงสร้างจุลภาค สมบัติเฟร์โรอิเล็กตริกตลอดจนค่าไดอิเล็กตริกและไพอิโซอิเล็กตริกอย่างเป็นระบบ

ฟิล์มแบบส่วนประกอบเดียวมีสัดส่วนของปริมาณเซอร์โคเนียมต่อไทเทเนียม เป็น 30/70 40/60 52/48 60/40 และ 70/30 เตรียมขึ้นโดยการฉาบทีละชั้นบนฐานรอง $Pt/Ti/SiO_2/Si$ ฟิล์มทั้งหมดถูกเผาที่อุณหภูมิ 600 °C ในเวลา 30 นาที จากผลการเลี้ยวเบนของรังสีเอ็ก พบว่าฟิล์มทั้งหมดมีโครงผลึกแบบเพอรอฟสไกท์และเรียงตัวแบบสุ่ม ฟิล์มที่มีสัดส่วนของเซอร์โคเนียมต่อไทเทเนียม 30/70 และ 40/60 โครงผลึกมีเฟสแบบเตตระโกนอล ในขณะที่สัดส่วน 52/48 60/40 และ 70/30 มีเฟสแบบรอมโบฮีดรอล สำหรับโครงสร้างจุลภาคของฟิล์มซึ่งวัดโดยกล้องจุลทรรศน์อิเล็กตรอนแบบส่องกราด พบว่า ฟิล์มทุกสัดส่วนมีความเป็นเนื้อเดียวกันและมีขนาดเกรนในช่วง 80 ถึง100 nm ในช่วงความถี่ 10^2 ถึง 10^5 Hz ค่าคงที่ไดอิเล็กตริกของฟิล์มเฟสรอมโบฮีดรอลสูงกว่าค่าของเฟสเตตระโกนอล ค่าที่มากที่สุดวัดที่ความถี่ 1 kHz คือ 1194 และมีค่าการสูญเสีย 0.02 เป็นของฟิล์มที่มีสัดส่วน 52/48 ซึ่งที่สัดส่วนนี้ฟิล์มจะมีเฟสแบบผสมระหว่างเฟสเตตระโกนอลและเฟสรอมโบฮีดรอล สนามไฟฟ้าบังคับของฟิล์มเหล่านี้ขึ้นอยู่กับสัดส่วนของเซอร์โคเนียมต่อไทเทเนียมอย่างชัดเจน ที่สัดส่วน 52/48 มีสนามไฟฟ้าบังคับเท่ากับ 72 $kV.cm^{-1}$ และมีโพลาไรเซชันตกค้างเท่ากับ 23.7 $\mu C.cm^{-2}$ ทุกฟิล์มมีการวัดค่าคงที่ไพอิโซอิเล็กตริกด้วยระบบอินเทอร์เฟอร์โรมิเตอร์แบบไมเคิลสัน ที่มีกำลังแยกความแตกต่างของระยะการกระจัด 10^{-13} m ฟิล์มที่สัดส่วน 52/48 มีค่าคงที่ไพอิโซอิเล็กตริก d_{33} มากที่สุดคือเท่ากับ 117.5 $pm.V^{-1}$ และมีค่ามากกว่าสองเท่าของฟิล์มที่สัดส่วนอื่นๆ

มีการศึกษาสมบัติของฟิล์มเหล่านี้ในระดับนาโนโดยใช้เทคนิคไพอิโซเรสปอนส์ฟอร์ช ไมโครสโกปี (พีเอฟเอ็ม) เช่นสมบัติการเปลี่ยนสถานะทางไฟฟ้า วงฮีสเทอรีสิสเฉพาะที่และการตอบสนองแบบไพอิโซอิเล็กตริกของโดเมน พบว่า โดเมนของฟิล์มบางพีแซดทีมีลักษณะเป็นสองแบบ คือแบบเหมือนเกาะ และเหมือนรังสีดวงอาทิตย์ จากลักษณะที่ได้ทำให้สามารถวิเคราะห์ได้ว่าฟิล์มมีความหนา 10 nm การตอบสนองต่อไพอิโซอิเล็กตริกในโดเมนระดับนาโนของฟิล์มเหล่านี้จะขึ้นอยู่กับความหนาของฟิล์ม โดยการตอบสนองจะมีค่าเพิ่มขึ้นตามความหนาของฟิล์ม และมีค่ามากที่สุดคือฟิล์มที่มีสัดส่วน 52/48 ผลของการวัดวงฮิสเทอรีสิสเฉพาะที่ ได้ลักษณะคล้ายรูปสี่เหลี่ยม ยืนยันว่าฟิล์มมีการเรียงตัวของโดเมนในทิศทางเดียวกันกับสนามไฟฟ้าที่ให้ ขนาดของเกรนที่วัดได้จากเทคนิคนี้มีค่าเพิ่มขึ้นตามปริมาณเซอร์โคเนียม ทิศทางโพลาไรเซชันของโดเมนที่มีทิศชี้ออกมาจากระนาบของฟิล์ม มีส่วนสำคัญต่อสัญญาณการตอบสนองไพอิโซอิเล็กตริก และสมบัติเฟร์โรอิเล็กตริกของโดเมน

ฟิล์มพีแซดทีที่มีสัดส่วนของเซอร์โคเนียมต่อไทเทเนียมแปรเปลี่ยนตามความหนาเตรียมได้ด้วยวิธีเดียวกันบนฐานรอง $Pt/Ti/SiO_2/Si$ มีสองแบบ คือฟิล์มที่มีสัดส่วนปริมาณเซอร์โคเนียมเพิ่มขึ้นเรียกว่า อัพเกรด และลดลงตามความหนาเรียกว่า ดาวน์เกรด จากการตรวจลักษณะทางจุลโครงสร้างพบว่า ในแต่ละฟิล์มจะมีรอยต่อระหว่างชั้นฟิล์มบางที่มีสัดส่วนแตกต่างกันตามแนวความหนา ในแต่ละชั้นจะมีโครงผลึกแบบเพอรอฟสไกท์ ซึ่งค่าคงที่ของโครงผลึกจะแตกต่างกันสอดคล้องกับสัดส่วนของเซอร์โคเนียมต่อไทเทเนียมในแต่ละชั้น และลำดับของการฉาบชั้นฟิล์มบาง ฟิล์มพีแซดทีที่มีลำดับการฉาบ 40/52/60 มีค่าไดอิเล็กตริกวัดที่ 1 kHz สูงถึง 1182 และฟิล์มนี้มีค่าโพลาไรเซชันตกค้าง 27 $\mu C.cm^{-2}$ มีสนามไฟฟ้าบังคับใกล้เคียงกันกับฟิล์มที่มีสัดส่วนของเซอร์โคเนียมเพียงสัดส่วนเดียว ฟิล์มพีแซดทีที่มีสัดส่วนของเซอร์โคเนียมต่อไทเทเนียมแปรเปลี่ยนตามความหนานี้มีการตอบสนองต่อสมบัติไพอิโซอิเล็กตริกจากภายใน เนื่องจากความแตกต่างของค่าคงที่โครงผลึก ทำให้เกิดรอยต่อที่ไม่เข้ากันพอดีระหว่างชั้นของฟิล์ม โพลาไรเซชันภายในระนาบ และความเค้นภายใน สมบัติดังกล่าวนี้ของฟิล์มทำให้ฟิล์มที่มีปริมาณเซอร์โคเนียมแปรเปลี่ยนตามความหนาเหมาะสมสำหรับการประยุกต์เป็นหน่วยความจำแบบนอน-โวลาไทล์ ในขณะที่ฟิล์มพีแซดทีที่มีปริมาณเซอร์โคเนียมเพียงค่าเดียว มีความเหมาะสมสำหรับการประยุกต์เป็นสิ่งประดิษฐ์ประเภทแอคซูเอเตอร์

Thesis Title	Ferroelectric and Electromechanical Properties of Sol-gel PZT Films with Single-composition and Compositionally Graded Structures
Author	Mr. Panya Khaenamkaew
Major Program	Physics
Academic Year	2007

ABSTRACT

This work studies the fabrication of $Pb(Zr_xTi_{1-x})O_3$ (PZT) thin films of two types: single-composition and compositionally graded structures. Hence, the x value refers to the zirconium content by weight. All of the films were prepared using a sol-gel method and were systematically investigated for their microstructure, ferroelectric, dielectric and piezoelectric properties.

Single-composition PZT films with fractions of the zirconium content of 30/70, 40/60, 52/48, 60/40 and 0.70/30 were deposited layer-by-layer on $Pt/Ti/SiO_2/Si$ substrates. The PZT films were fired at 600 °C for 30 min. X-ray diffraction was used to examine the crystallization of the films and the pervoskite with random orientation was observed. The films with Zr/Ti ratios of 30/70 and 40/60 crystallized in the perovskite tetragonal phase while it was the rhombohedral for the 52/48, 60/40 and 70/30 PZT films. The grain size was scanning electron microscopically examined and it was in the range of 80 to 100 nm with dense texture. From the dielectric measurement in the frequency range of 10^2 to 10^5 Hz, the rhombohedral phase PZT films have higher dielectric constant than those of the tetragonal ones. A maximum of the $\varepsilon_r^{'}$ value (1 kHz) of 1194 and dielectric loss of 0.02 were observed in the 52/48 PZT film which is the morphotropic phase boundary (MPB) composition. Strong dependence of coercive field on the Zr/Ti ratio was observed. This field was 72 $kV.cm^{-1}$ for 52/48 PZT film and the corresponding

remanent polarization was 23.7 μC.cm^{-2}. The apparent piezoelectric coefficient d_{33} of the films was measured by a Michelson-type interferometer of a spatial resolution of 10^{-13} m. The largest d_{33} value of 117.5 pm.V^{-1} was obtained from the 52/48 PZT film. This value is more than twice those of the films at lower and higher Zr/Ti ratios.

The nanoscale investigation of the uniform films included switching behavior, local hyteresis and piezoelectric responses were carried out using the piezoresponse force microscopy (PFM). Local ferroelectric domains of the film were observed to have two characteristics: island-like and sun-ray types and the average of the minimum thickness of the film was 10 nm. The piezoresponse of the local domain was increased with thicknesses of the film and reached its maximum response in the 52/48 PZT film. A square-like *P-E* hyteresis loop observed in this film indicated that the domains were well aligned with the applied electric field. The grains of the film at Zr/Ti ratios higher than 52/48 were increased in size. It is the out-of-plane polarization of the domains that played the role in probing ferroelectric domains and the PFM signal.

Sol-gel compositionally graded PZT films were deposited on Pt/Ti/SiO_2/Si substrate into two ways: increasing or decreasing the Zr content along the thickness of the films which are respectively called up-graded, and down graded. From the microstructure investigation, the interfaces between the layers with different Zr/Ti ratios were clearly observed. Each layer crystallized into the perovskite phase with lattice parameters corresponding to the Zr/Ti ratios used in the sequence of the deposition. The (40/52/60) PZT film had the dielectric constant (1 kHz) as high as 1182 and a high dielectric loss. This film had the remanent polarization of 27 μC.cm^{-2} and the coercive field was similar to those of the uniform films. The compositionally graded PZT films show interior piezoelectric response possibly due to the effect of lattice mismatches, in-plane polarization and internal stress caused by the pinning of the substrate. In summary the overall properties of the compositionally graded PZT films are attractive for non-volatile memory device applications while the single-composition PZT films are promising for use in actuator applications.

ACKNOWLEDGEMENTS

I wish to express my sincere and deepest gratitude to my academic advisor Assoc. Prof. Dr. Supasarote Muensit for her constant help, personal attention, inspiring guidance, suggestions and encouragement given to me throughout the period of study, without which it would not have been possible for me to complete this work. I also would like to express my sincere appreciation to Dr. Pattara Aiyarak who has given me valuable advice on the academic as well as personal matters.

I wish to give special thanks to Prof. Dr. Andrei L. Kholkin and his co-worker, Dr. Igore D. Bdikin, for a good time in Portugal. During that period, they allowed tremendous time for discussion about my research many chapters of this dissertation were completed by the dedication of his effort. Prof. Dr. Kholkin has given me spiritual rest whenever I feel difficulties in life in a foreign country.

I would like to thank the examining committee for their suggestions: Prof. Dr. Brahim Elouadi from Université de La Rochelle, France, Assoc. Prof. Boonlua Phongdara, and Asst. Prof. Dr. Pruittikorn Smithmaitrie for taking time out of their busy schedules to evaluate my work.

I show my gratitude for the helping hands from my friends in our research group, Nawal Binhayeeniyi, Abedeen Dasaesamoh, for their cheer. I would like to thank Pol. Capt. Yaowaluck Phermponsagul for her patience. I would not have thought of completing my Ph.D. degree so soon without her encouragement. I would also like to thank all my friends Santi, Pairat, Paitoon, Dhammanoon, Boontham, Nivest, Nattaporn, and others for their kind support. I am indebted to my family, particularly to my mother for her kindness and endless care which always make me happy in mind without fear in any extraneous hurdle.

Finally, I would like to acknowledge the support of the Thailand Research Fund through the Royal Golden Jubilee Ph.D. Program (Grand No.PHD0013/2546), the support of Kasetsart University through the UDC grand and the support of Prince of Songkla University.

Panya Khaenamkaew

TABLES OF CONTENTS

TABLES OF CONTENTS (cont.)

TABLES OF CONTENTS (cont.)

LIST OF FIGURES

LIST OF FIGURES (cont.)

LIST OF FIGURES (cont.)

LIST OF FIGURES (cont.)

LIST OF FIGURES (cont.)

LIST OF TABLES

SYMBOLS

A	=	Electrode Area	Q	=	Charge
C	=	Capacitance	R	=	Resistance
c	=	Stiffness	S_{ij}	=	Strain Tensor
D	=	Dielectric Displacement	T	=	Temperature
d	=	Thickness	T_c	=	Curie Temperature
d_{ij}	=	Piezoelectric Stress Coefficient	t	=	Time
d_{ac}	=	Surface Displacement	V	=	Voltage
E	=	Electric Field	U	=	Thermal Energy
E_c	=	Coercive Field	Z	=	Acoustic Impedance
F	=	Force	ε	=	Permittivity of a Medium
f	=	Frequency	ε_0	=	Permittivity of a Free Space
g	=	Piezoelectric Strain Coefficient	ε_r	=	Relative Permittivity
I	=	Light Intensity	σ_{ij}	=	Stress Tensor
k		Electrical coupling Factor	γ	=	Thermal Expansion
m	=	Electric Current	λ	=	wavelength
P	=	Polarization	ω	=	Angular Frequency
P_r	=	Remanent Polarization	χ	=	Electric susceptibility
P_s	=	Saturation Polarization	$tan\delta$	=	Loss Tangent

2ME	=	2-methoxyethanol
CSD	=	Chemical Solution Deposition
FeRAM	=	Ferroelectric Random Access Memory
PFM	=	Piezoresponse Force Microscopy
PLD	=	Pulsed Laser Deposition
PZT	=	$Pb(Zr_xTi_{1-x})O_3$
RAM	=	Random Access Memory
SPM	=	Scanning Probe Microscopy
XRD	=	X-ray Diffraction

CHAPTER 1

INTRODUCTION

1.1 Statement of the Problem

In recent years, there has been an increasing interest in ferroelectric thin films, particularly those that present a perovskite-type crystalline structure, displaying also large values of spontaneous polarization. These materials are of great interest for a wide range of applications such as non-volatile memories, dynamic random access memories (Kholkin *et al*., 2002), solid state displays, infrared detectors, pyroelectric and piezoelectric sensors, microwave devices, electro-optic and integrated-optic devices (Muralt, 2000). The perovskite oxides, owing to their large values of spontaneous polarization, and to their simple crystal structure, are among the most studied ferroelectrics (Whatmore *et al*., 2003). Among the lead-based peroveskites, particular research interest has been devoted to lead zirconate titanate ($Pb(Zr,Ti)O_3$ or PZT) compound which is probably best known for the ferroelectric, piezoelectric and dielectric properties.

Piezoelectric materials have been used extensively in the design of sensors and actuators. Several designs of piezoelectric actuators have been investigated (Uchino and Giniewicz, 2003). PZT and other lead-based relaxor materials are widely used as actuators because of their excellent electromechanical properties. The use of piezoelectric sensor and actuator systems for the active vibration suppression and shape control is fast becoming an essential tool in the design of smart structures and systems. The piezoelectric sensor is able to respond to the vibrations and generate a voltage due to the direct piezoelectric effect.

However, all these design suffer from uneven distribution of the mechanical stresses or stressed metal to ceramic joins or both, which in turn results in lifetime limitations of the devices. In order to reduce high stress concentration at the mid-interface that exist in the standard bimorph actuators while maintaining high bending displacement, ferroelectric films with composition gradients normal to the substrate is introduced.

This new type of ferroelectric films have been reported to exhibit striking new properties not observed in conventional ferroelectric films (Bao *et al.*, 2000). Many authors believe that this structure can optimize the stress distribution, increase the reliability and lifetime of devices made from these materials such as piezoelectric actuator (He *et al.*, 2001).

The most notable property of these graded ferroelectric devices (GFDs) is the large *dc* polarization offset they develop when driven by an alternating electric field. Furthermore, the direction of the offset is related to the direction of the composition gradient with respect to the substrate (Ban, Alpay and Mantese, 2003). These offsets have been reported to have a strong temperature dependence giving rise to possible pyroelectric applications in addition to other potential sensor, actuator, and energy converter applications (Brazier, McElfresh, and Mansour, 1998). However experimental measurements regarding to their ferroelectric domains and piezoelectric coefficient appear to be lacking. Some issues related to the polarization gradient (something similar with the occurrence of the built-in potential in *p-n* semiconductor junctions) are not well understood. A comprehensive understanding on these properties of composition gradients material related to the overall properties of the GFDs should have significant value.

The present work is proposing to fabricate PZT films of high purity over the deposition area and the effects of the perovskite compositions on the microstructure and ferroelectric properties are discussed. Experimental results obtained from ferroelectric and piezoelectric measurements for the PZT films with homogeneous layers and composition gradients structure are presented and discussed. Quatitative investigations using piezoresponse force microscopy (PFM) and a macroscopically study using an interferometric technique are applied for the characterization of PZT thin films.

1.2 Thesis Outline

The thesis consists of six chapters. In the present chapter, the statement of the problem is addressed. In addition, research objectives are also presented.

Chapter 2 describes an overview of the ferroelectric, piezoelectric and other related properties to perovskite materials, focusing on PZT. Various techniques for the fabrication of PZT with homogeneous layers and PZT with composition gradients normal to the substrate are also described.

Chapter 3 specifies the procedure used for the fabrication of PZT thin films, focusing on single-composition PZT thin films. Measurements of the physical, ferroelectric and piezoelectric properties are described and the results obtained are discussed.

Chapter 4 presents the fabrication and characterization of compositionally graded PZT thin films. The overall properties of the films with composition gradients are experimentally reported.

The background devoted to the local probe-based technique: the piezoresponse force microscopy (PFM) for characterizing the nanoscale properties of the films such as switching behavior, local hysteresis and piezoelectric responses of the PZT films were presented in chapter 5.

Chapter 6 summaries the conclusions stated in various chapters of the present work and the prognosis for future investigation is given.

1.3 Objectives of Research

The objectives of this work are the following:

1. To prepare PZT thin films of two types: single-composition and compositionally graded by using a two-step sol-gel processing.
2. To investigate the effect of Zr/Ti ratio on the microstructure and ferroelectric properties of single-composition PZT films.
3. To observe the microstructure and ferroelectric properties of graded PZT thin films.
4. To characterize the piezoelectric response in PZT thin films.

CHAPTER 2

BACKGROUND THEORY

In this chapter, an effort is made to introduce the basic principles governing ferroelectricity and piezoelectricity of perovskite ferroelectric materials. The processing of ferroelectric ceramics in general and important applications of ferroelectric materials are reviewed.

2.1 Introduction to Ferroelectricity and Piezoelectricity

2.1.1 Basic concept of ferroelectricity

Ferroelectricity is a phenomenon which has been discovered in 1921. The name refers to certain magnetic analogies, though it is somewhat misleading as it has no connection with iron (ferrum) at all. Ferroelectricity has also been called Seignett electricity (mainly in Russian literature), as Seignett or Rochelle Salt (RS) was the first material found to show ferroelectric properties such as a spontaneous polarization on cooling below the Curie point, ferroelectric domains and a ferroelectric hysteresis loop (Haertling, 1999; Danglish and Kemmitt, 2000). A number of investigations on ferroelectric materials came in the 1950's, leading to the widespread use of barium titanate ($BaTiO_3$) based ceramics in capacitor applications and piezoelectric transducer devices. Since then, many other ferroelectric ceramics including lead titanate ($PbTiO_3$), lead zirconate titanate (PZT), lead lanthanum zirconate titanate (PLZT), and relaxor ferroelectrics like lead magnesium niobate (PMN) have been developed and utilized for a variety of applications (Haertling, 1999). With the development of ceramic processing and thin film technology, many new applications have emerged. The most expanded use of ferroelectric ceramics is still the areas of dielectric ceramics for capacitor applications, ferroelectric thin films for non volatile memories, piezoelectric materials for medical ultrasound imaging and actuators, and electro-optic materials for data storage and displays (Callister, 1997).

Ferroelectric materials are dielectric materials characterized by a reversible spontaneous polarization. The polarization behavior in an electric field is highly non-linear and exhibits hysteresis loop (*P*-*E* loop), as shown in Fig. 2.1a. The hysteresis loop is characterized by two important parameters, including the coercive field E_c (or coercivity) and the remanent polarization P_r (or remanance). The coercivity is the field required to reduce the polarization *P* to zero, the remanance is the polarization at zero applied field. The value obtained by extrapolating the polarisation in the high field region to zero is called the saturation polarization P_s (Haertling, 1999).

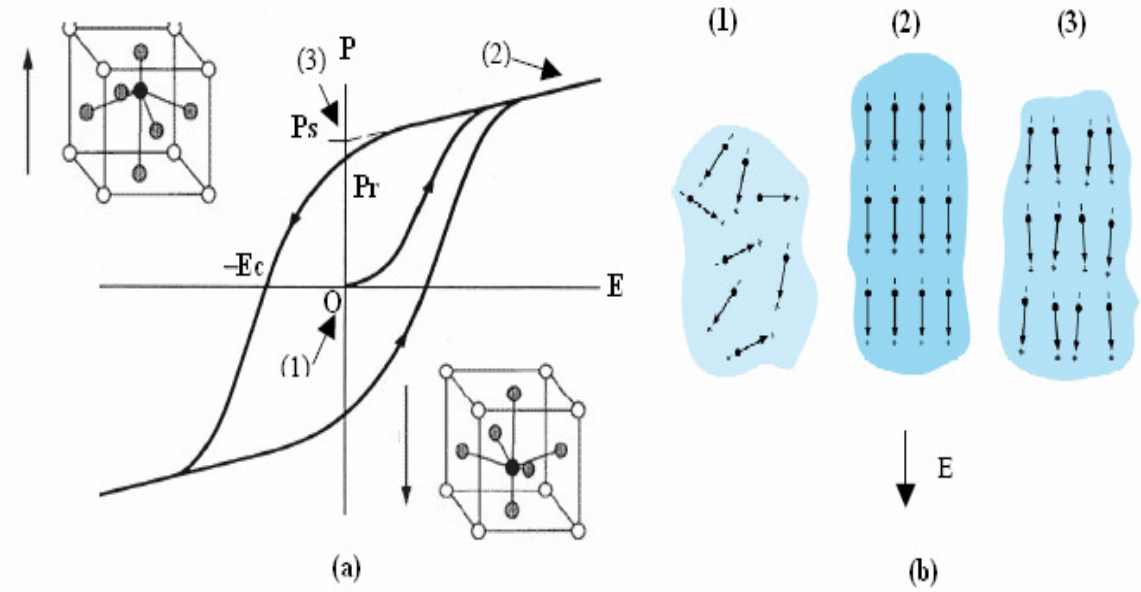

Figure 2.1 (a) A ferroelectric hysteresis loop. The positive and negative saturation polarizations correspond to the two "up" and "down" states of the crystal (Jona, 1993). (b) Orientation of dipoles: (1) without electric field, $P = 0$; (2) domains align in the applied field direction, $P = P_s$; and (3) the electric field is decreased to zero, $P = P_r$.

Ferroelectricity results from the presence of permanent dipole moments that align in the direction of an external electric field. For example, in $Pb(Zr,Ti)O_3$, the dipole moment is caused by the displacement of either the Ti^{4+} or Zr^{4+} cations relative to the centre of the oxygen octahedron around the cation. The two-stable off-center positions correspond to the two different orientations of dipole moment. Adjacent dipoles tend to orient themselves in the same direction, which

induces a spontaneous polarization. Regions of uniform polarization are called domains, separated by domain walls. In ferroelectric materials, the domain walls are extremely narrow, often not more than one or two lattice layers. The response of the domains to the applied electric field, as shown in Fig. 2.1b, determines the shape of the hysteresis loop. In the absence of an electric field, the domains are randomly distributed, resulting in a net zero polarization. In an electric field, the domains tend to align in the field direction by movement of the domain walls and rotation of the dipoles and the polarization reaches the maximum value P_s. When the electric field is removed, domains cannot return to their original states, yielding a non-zero polarization P_r (Jaffe, Cook and Jaffe, 1971).

Different from normal dielectrics, in ferroelectrics the dielectric constant is a non-linear function of applied field, and can be evaluated from the derivative of the polarization to the applied field. Basically, there are two contributions to the dielectric constant: the intrinsic component, which involves the switching of the dipole configurations, and the extrinsic component, which involves the domain wall motion (Chaim *et al.*, 1974; Xu *et al.*, 2001). The necessary condition for a crystal to exhibit ferroelectricity is that the crystal structure is non-centrosymmetric. The ferroelectric state is usually a low temperature, crystalline form with the non-centrosymmetric characteristics. A structural phase transition from non-centrosymmetric to centrosymmetric upon heating induces a transition from the ferroelectric to the paraelectric state. The temperature at which this transition takes place is called the ferroelectric Curie temperature, denoted by T_C. At T_C, the dielectric constant (ε) exhibits a maximum value. Above T_C, the relationship between ε and the temperature follows the Curie-Weiss law:

$$\varepsilon = \frac{C}{T - T_0} \tag{2.1}$$

where C is the Curie constant and T_0 is the Curie-Weiss temperature, which in most cases equal to or slightly different from T_C.

P-E loops can be used as a fingerprint to identify the material. Typical hysteresis loops obtained from various ferroelectric ceramics are presented in Fig.2.2:

(a) a linear tracing from a $BaTiO_3$ capacitor; (b) a non-linear loop from a memory ferroelectric PZT; (c) a narrow non-linear loop from a relaxor $(Pb,La)(Zr,Ti)O_3$ (PLZT) and (d) a double loop typical for an antiferroelectric $Pb(Sn,Zr)O_3$ (PSZT) (Haertling, 1999).

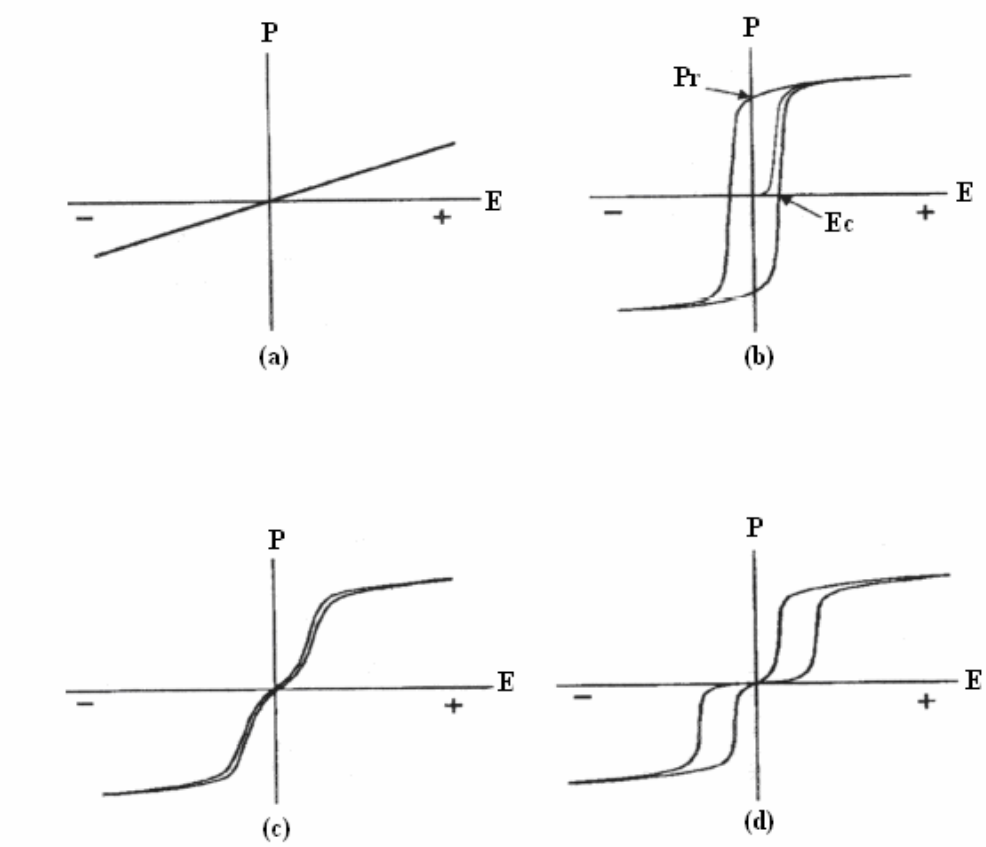

Figure 2.2 Hysteresis loops of various ferroelectric ceramics: (a) linear $BaTiO_3$ capacitor, (b) ferroelectric PZT, (c) relaxor 8/65/35 PLZT, (d) antiferroelectric PSZT (Haertling, 1999; Chaim *et al*., 1974; Xu *et al*., 2001).

2.1.2 ferroelectric thin film

Ferroelectric materials have been commercially important to the electronics industry for more than 50 years. Ferroelectrics have been used in the form of bulk ceramics (thicker than 1 mm). Until 1980s, methods have been developed to fabricate ferroelectrics in the form of thick film (1-20 μm) and thin films (less than 1 μm) (Araujo, Scott and Taylor, 1996). The availability of thin-film ferroelectrics has encouraged the re-examination of previously unrealizable designs, resulting in the

integration of ferroelectrics with semiconductor circuits, and architectures combining the excellent properties of ferroelectrics with micro machined silicon structures. The future appears promising for the development of a new generation of ferroelectric devices, some of which will profoundly affect the evolution of the electronics industry over the next several years.

2.1.3 Piezoelectricity: basic concept, constitutive equations and measurements

Piezoelectricity is one of the property of a group of dielectric materials called ferroelectrics. These materials are characterized by a domain structure that can be modified by an electric field. The piezoelectric effect manifests as a spontaneous potential difference across the opposite faces of a volume of material when under an applied stress. This potential is directly proportional to the mechanical stress applied to it. The inverse is also true, *i.e*. application of an electric field causes strain in a volume of piezoelectric material.

The illustration in Figure 2.3 demonstrates the piezoelectric effect. This explains the origin of the word piezoelectricity as “piezin” is the Greek word for “to press”. The original poled volume of material experiences the electric field and transforms into the inner volume. This has created the extension in the z direction (poled direction), while contraction in both x- and y-axis directions, due to constant sample volume.

On the atomic scale the piezoelectric effect is attributed to a unit cell transformation from a centrosymmetric structure to one with no centre of symmetry. Of the twenty-one non-centrosymmetric crystal classes twenty are piezoelectric, of which 10 are polar (Moulson and Herbert, 1990). A traditional piezoelectric material is barium titanate (ferroelectricity identified in 1945) (Bell and Moulson, 1985), which is commonly used in capacitors due to its high permittivity. The unit cell arrangement of barium titanate consists of a highly charged titanium ion situated in the centre of an oxygen octahedral cage, which is surrounded by a cubic lattice of barium ions. The titanium ion has more than one minimum energy position as thermal energy is sufficient to allow ions to overcome electrostatic forces (Fink, Beaty and Caroll, 1999). In one of these sites the oxygen cage moves in relation to the barium lattice creating a unit cell dipole. This ceramic and its derivatives have the perovskite

ABO_3 structure. A common ABO_3 perovskite structure has a three-dimensional network as shown in Fig. 2.4.

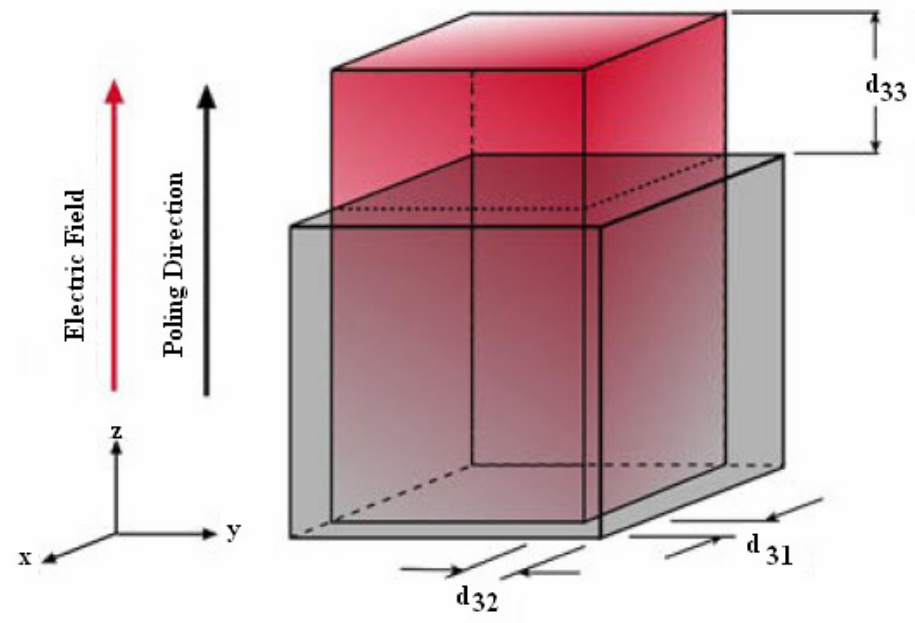

Figure 2.3 Effect of electric field on a poled piezoelectric material, before and after the field is applied (outer and inner cubes, respectively).

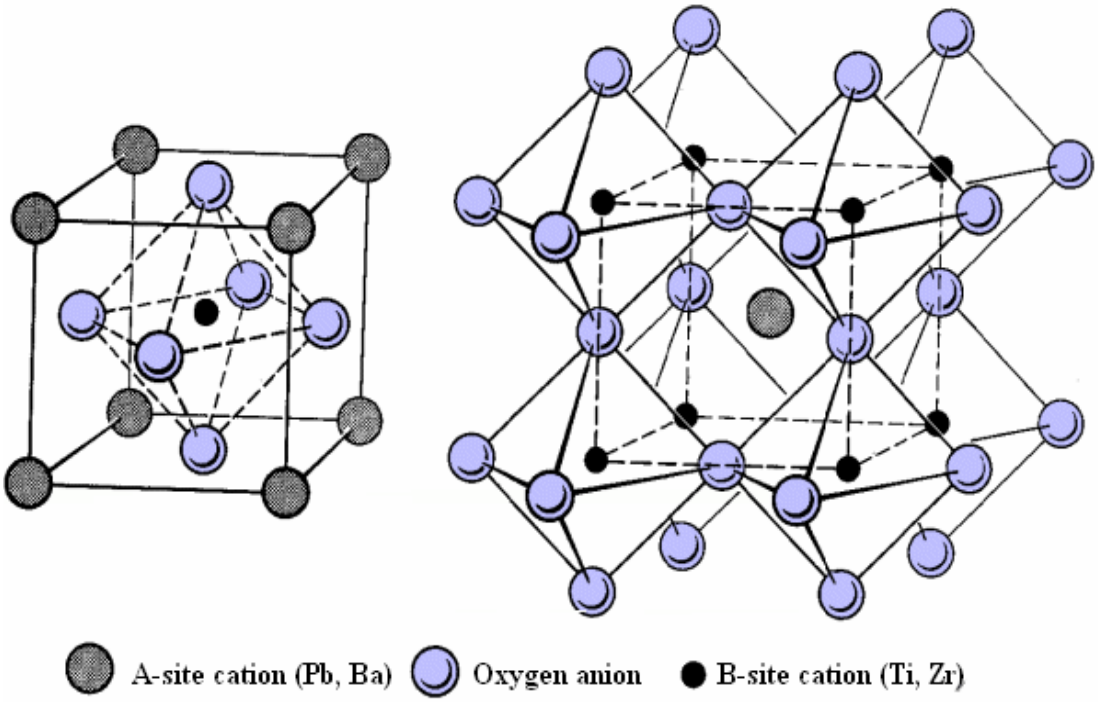

Figure 2.4 A cubic ABO_3 perovskite-type unit cell.

Piezoelectric tensor

The piezoelectric effect varies with direction and it is effected by symmetry change. Since polarization is a vector and stress is a second rank tensor, the physical property relating these two variables must involve three directions:

$$P_j = d_{jkl} T_{kl} \tag{2.2}$$

In general there are 3^3=27 tensor components, but because the stress tensor is symmetric type ($T_{ij} = T_{ji}$), only 18 of the components are independent. Therefore the piezoelectric effect can be described by a 6x3 matrix form of the piezoelectric effect uses only two subscripts: $P_i = d_{ij} T_j$ where $i = 1-3$, and $j = 1-6$. Written out it is

$$\begin{pmatrix} P_1 \\ P_2 \\ P_3 \end{pmatrix} = \begin{pmatrix} d_{11} & d_{12} & d_{13} & d_{14} & d_{15} & d_{16} \\ d_{21} & d_{22} & d_{23} & d_{24} & d_{25} & d_{26} \\ d_{31} & d_{32} & d_{33} & d_{34} & d_{35} & d_{36} \end{pmatrix} \begin{pmatrix} T_1 \\ T_2 \\ T_3 \\ T_4 \\ T_5 \\ T_6 \end{pmatrix} \tag{2.3}$$

For a strain- charge piezoelectric, strain tensors are written as;

$$\begin{pmatrix} S_1 \\ S_2 \\ S_3 \\ S_4 \\ S_5 \\ S_6 \end{pmatrix} = \begin{pmatrix} d_{11} & d_{21} & d_{31} \\ d_{12} & d_{22} & d_{32} \\ d_{13} & d_{23} & d_{33} \\ d_{14} & d_{24} & d_{34} \\ d_{15} & d_{25} & d_{35} \\ d_{16} & d_{26} & d_{36} \end{pmatrix} \begin{pmatrix} E_1 & E_2 & E_3 \end{pmatrix} \tag{2.4}$$

The strain-charge for a material of the 6mm crystal class such as poled piezoelectric ceramics PZT can be written as:

$$\begin{pmatrix} S_1 \\ S_2 \\ S_3 \\ S_4 \\ S_5 \\ S_6 \end{pmatrix} = \begin{pmatrix} 0 & 0 & d_{31} \\ 0 & 0 & d_{32} \\ 0 & 0 & d_{33} \\ 0 & d_{15} & 0 \\ d_{15} & 0 & 0 \\ 0 & 0 & 0 \end{pmatrix} \begin{pmatrix} E_1 & E_2 & E_3 \end{pmatrix} \tag{2.5}$$

Constitutive equations, describing direct and inverse piezoelectricity and electrostriction, can be derived from the Gibbs free energy and the elastic Gibbs function (Nye, 1985). For simplicity, it is assumed that factors such as applied stresses, temperature, magnetic field, *etc.*, are constant and that the strain is due entirely to the electric field. Under these conditions, the strain can be expressed as:

$$S_{ij} = d_{kij} E_k + M_{klij} E_k E_l \tag{2.6}$$

The first term on the right of Eq.(2.6) represents the inverse piezoelectric effect, with d_{kij} is the third rank piezoelectric tensor. The second term gives the quadratic dependence of strain on the field. This term is the electrostriction, and M_{klij} is a fourth-rank tensor.

For piezoelectric thin films deposited on a thick substrate, the thin film is always clamped to the substrate, therefore the ratio strain/field (or the electric displacement/stress) does not represent the piezoelectric coefficient d_{33} of the free sample but an effective coefficient $d_{33\text{eff}}$ (Yao and Tay, 2003). It can be shown that, for converse piezoelectric effect, such as for the interferometer and vibrometer methods (Lefki and Dormans, 1994):

$$d_{33eff} = \left(\frac{\partial S_3}{\partial E_3} \right) = d_{33} - 2d_{31} \frac{s_{13}^E}{s_{11}^E + s_{12}^E} \tag{2.7}$$

where S is the strain,

E is the electric field,

T is the stress,

s_{ij} are mechanical compliances of the piezoelectric film and

d_{31} is the transverse piezoelectric coefficient.

If we use the s_{ij} values for a typical soft lead zirconate titanate (PZT) ceramics such as PZ23 from http://www.ferroperm-piezo.com/, Ferroperm MatData, we can obtain:

$$d_{33eff} = d_{33} + 1.59 d_{31} \approx 0.62 d_{33} \tag{2.8}$$

The mechanical properties of PZT thin films are not expected to be the same as the bulk ceramics, therefore the precise numerical relationships between the $d_{33\text{eff}}$ and d_{33} are not expected to be the same as above and may be sample dependent. Nevertheless, it is expected that the effective piezoelectric coefficient is always smaller than the free standing piezoelectric coefficient.

Piezoelectric Coefficients

Piezoelectric materials are characterized by a domain structure that is generated by the minimization of internal energy by local charge displacement, *i.e.* polarization. Domains are regions of "homogenous" polarization (Dennis, 1972). Twinning is the formation of these domains to balance the domain wall energy, elastic and electric field energy as shown in Fig. 2.5.

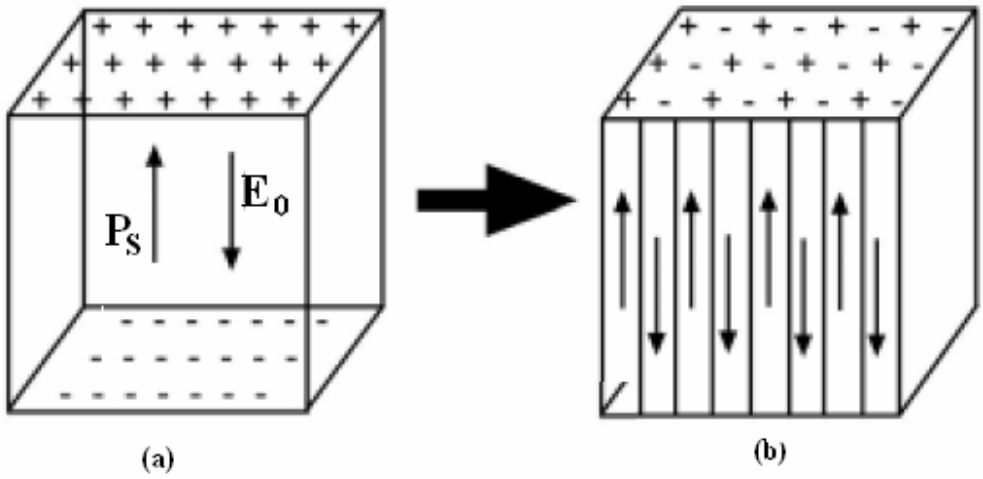

Figure 2.5 (a) Charge associated with spontaneous polarization, P_S, and electric field generated, E_0, (b) formation of 180° domains to minimize electrostatic energy (Moulson and Herbert, 1990).

An equilibrium domain configuration is established only if sufficient time is allowed for wall mobility. The pattern generated will depend on the electrical and mechanical stress conditions (Arlt, 1990). The electrostatic conditions defining the domain pattern change when an external field is applied and may result in displacement of the domain walls. The surface energy of the wall will be increased when it is set in motion because of the inertia of the ions which change position slightly as their dipole moment changes direction on passage of the wall. The vibration motion of the domain wall as an extrinsic contribution to polarization response of ferroelectric materials was a subject of many theoretical and experimental studies. There are two types of domain, named 90° and 180° domains as shown in Fig. 2.6.

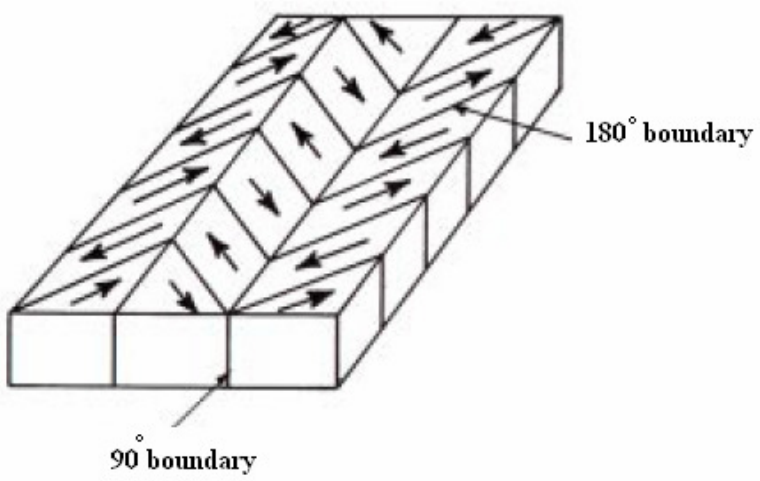

Figure 2.6 Schematic diagram of 90° and 180° domain (Moulson and Herbert, 1990).

However, clamping by adjacent grains hinders the formation of any domain configuration. As the tetragonal structure is anisotropic a change of domain direction by 90° will require a change in shape. This is different to magnetic domains that are not related to crystal structure but to the electron configuration. A domain wall width of 80 Å has been reported (Dennis, 1972), but may depend on the grain size. Material deformation occurs by cooperative twinning in adjacent grains and a sufficiently high internal stress can maintain the materials shape (Fig. 2.7).

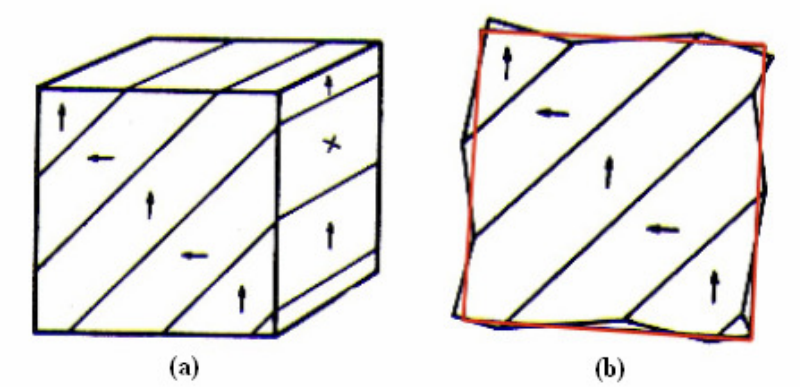

Figure 2.7 (a) Small stressed grain domain configuration and (b) deformation in the free grain (Jaffe, Cook and Jaffe, 1971).

Note that surface grains will twin differently compared to bulk grains due to reduced clamping stresses. An un-poled piezoelectric will have randomly orientated domains that produces no overall polarization. Poling requires the alignment of 180° domains and rotation of 90°domains (Sayer *et al*., 1981). The intention of poling is to cause as many domains as possible to be aligned in the poling direction (Sayer *et al*., 1981). Domains can be switched (90°domain rotated while 180° domains reversed) by electrical fields due to the ferroelectric properties of the material (Ogawa, 2000). Application of mechanical stresses can only produce 90° domain rotation due to crystal dimension anisotropy (Zhu and Yang, 1997).

The polarization is only allowed along certain directions depending on the crystallographic class as depicted in Fig. 2.8. As such not all domains will be precisely aligned to the poling direction but will be as close as the crystal orientation permits if given sufficient energy and time.

The greater the number of polarizable directions the closer the polar axes can align to poling field to increase the piezoelectric properties. In polycrystalline piezoelectrics the maximum attainable polarization can be given as a fraction of the single crystal value. For a tetragonal perovskite there are six polar directions giving a fraction of 0.83. In practice the value is limited by internal strains that inhibit 90° domain switching. The switching of 180° domain can be almost totally accomplished (Moulson and Herbert, 1990).

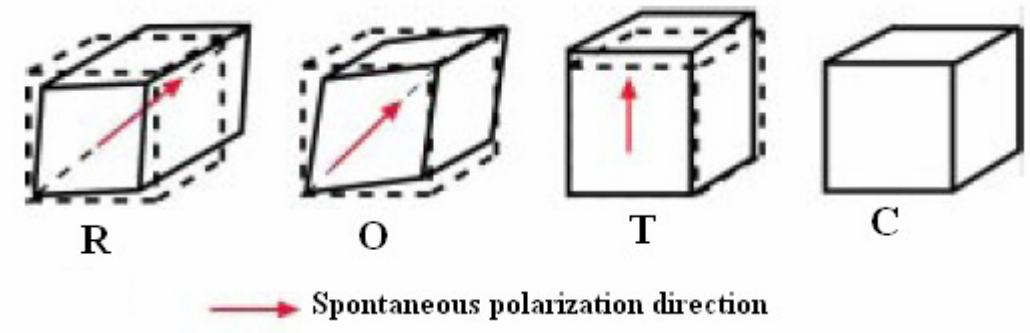

Figure 2.8 Direction of spontaneous polarization in (R) rhombohedral, (O) orthorhombic, (T) tetragonal and (C) cubic crystals of barium titanate (Moulson and Herbert, 1990; Rosen, Hiremath and Newnham, 1992).

Piezoelectric Measurements

Conventionally, the techniques for piezoelectric measurement of thin films fall into two categories: direct measurement and indirect measurement. With the former one relies on a direct probe of either the displacement induced by applied electric field or charge amount produced by imposing a load, from which d_{33} or e_{31} can be extracted out. The indirect measurement looks into the intrinsic linkage between the mechanical properties (stress and strain) and the electrical ones (voltage or charge), utilizing piezoelectric effects such as bulk or surface acoustic wave. An updated but incomplete list of those techniques in terms of the underlying mechanisms is given in Fig. 2.9.

In this study, a single-beam optical interferometry was selected for a piezoelectric measurement of a PZT thin film. Because this technique have many advantages. In general, optical interferometry technique is extremely high resolution and high data reliability (Zhang, Pan and Cross, 1988; Kholkin *et al*., 1998). Although this technique is suffered with clamped sample, many authors were used the correction term for confident clamped data. The correction factor of the interferometer technique was reported elsewhere (Zhang, Pan and Cross, 1988; Kholkin *et al*., 1998; Guy, Muensit, and Goldys, 1999; Muensit and Khaenamkaew, 2002; Khaenamkeaw, Muensit, and Aiyarak, 2003).

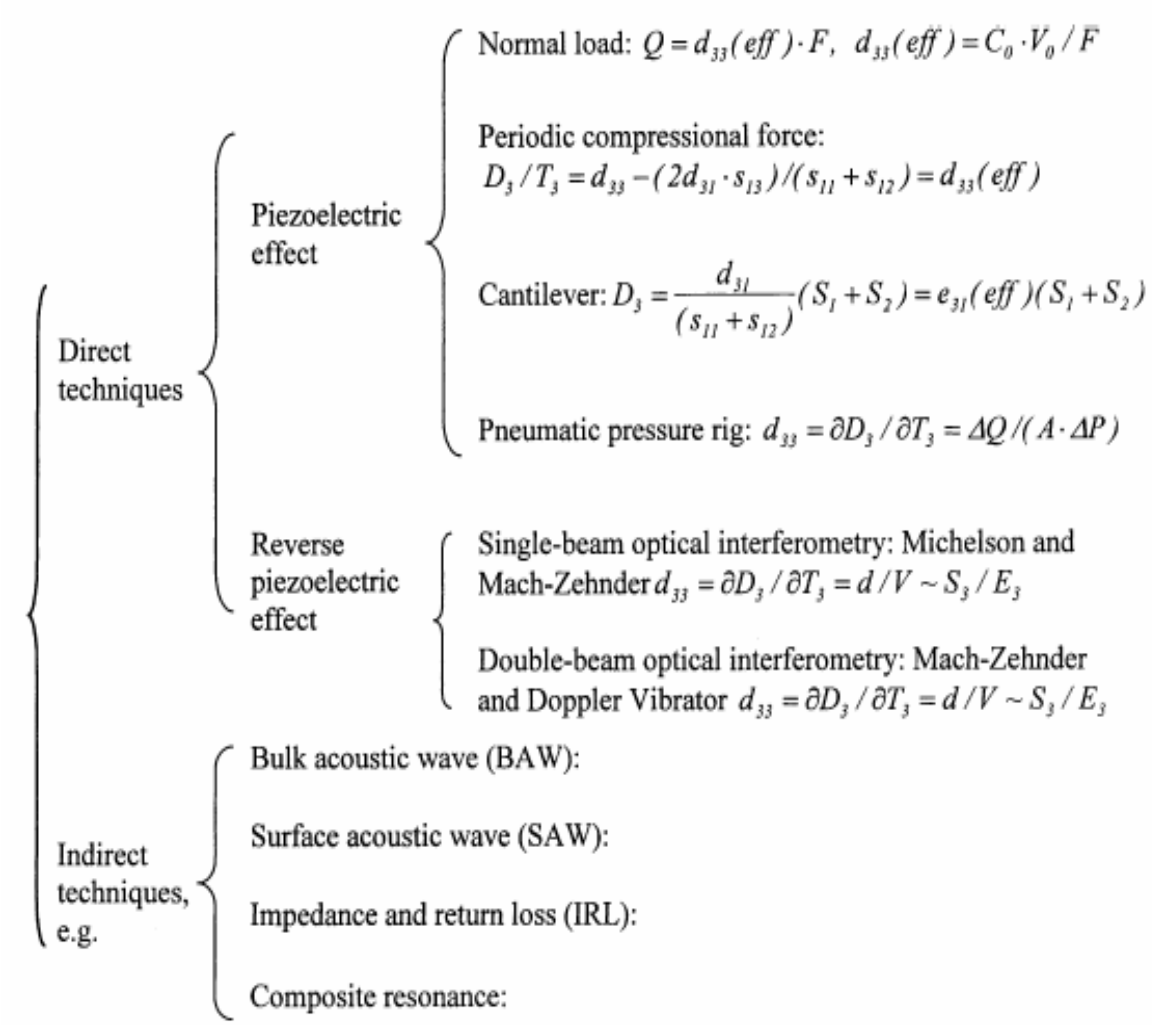

Figure 2.9 A classification of currently employed techniques for piezoelectric coefficient measurement and their principles (Liu *et al.*, 2002).

The principle of the optical system is as follow. The polarized laser beam is focused by a condenser lens before being separated by a beam splitter into two equal beams. The probing beam is directed to the sample surface coated with top electrode and reflected back to the same beam splitter. It recombines with the beam reflected from the reference mirror in the reference arm and produces an interference pattern at the detection plane. The interferometer's optimized operation should be at the peak sensitivity point, *i.e.* the $\frac{\lambda}{4}$ position, which is achieved with the help of the feedback circuit connected to retain the system exactly at the point. When the sample

is driven by an *ac* signal of amplitude V_0, the corresponding interferometric intensity change is detected by a photodiode and monitored by a lock-in amplifier. The intensity change is linearly proportional to the sample surface displacement, d_{ac} ($d_{ac} << \lambda$). Because the interferometry has an extra-high resolution in displacement ($<10^{-12}$ m), the piezoelectric coefficient of ultra-thin films can be evaluated with good reliability. The details and methods of the interferometric technique are clearly described in chapter 3.

Applications of piezoelectric materials

Piezoelectric materials have widespread applications as transducers, such as sensors and actuators. Transducers are used to convert energy from one form to another, such as in sensors that give the robotic hand (Fig. 2.10) sufficient sensitivity to handle the bulk or large structures such as sonars, and hydrophones (Rosen, Hiremath and Newnham, 1992). Actuators, fuel injection system, use the controllable deformation by the piezoelectric effect to achieve high precision and accuracy for positioning, for laser optics. Applications for ceramic actuators are increasing due to their high reliability and chemical inertness, for example spark ignitors and valves in fuel injection systems.

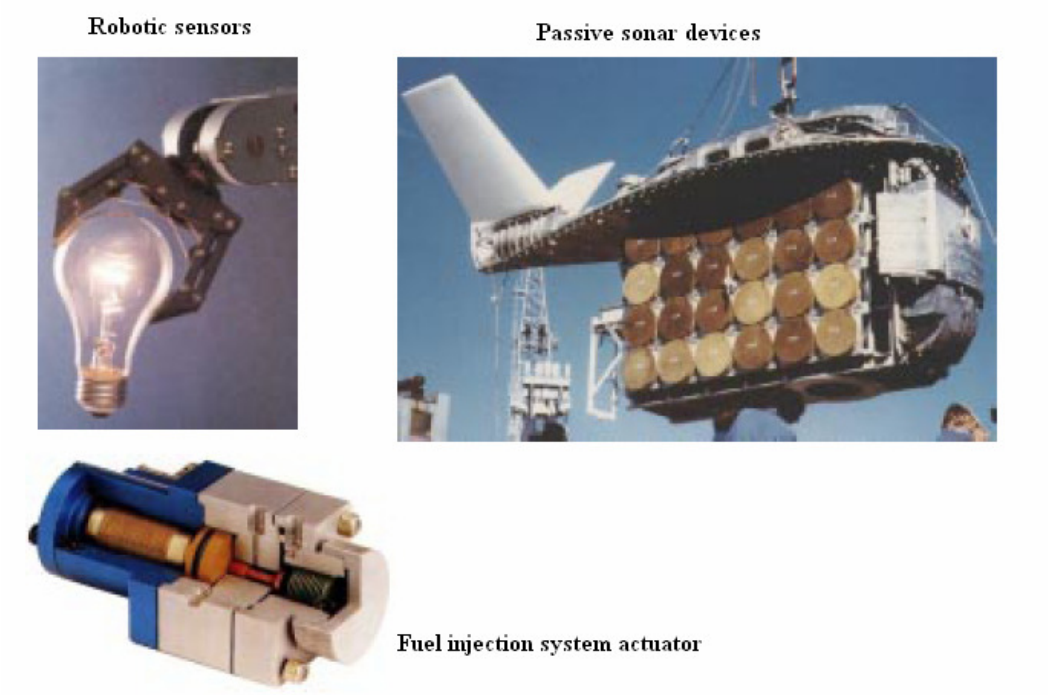

Figure 2.10 Examples of applications of piezoelectric materials.

2.1.4 Other related properties and applications of ferroelectric materials

Electro-optic properties. By varying the ferroelectric polarization with an electric field, one produces a change in the optical properties of the ferroelectrics. The most important ones are the quadratic electro-optic effect and the biased quadratic electro-optic effect (Haertling, 1999).

Pyroelectricity. This property relates to the ability to produce electric charges on the crystal faces as a result of a temperature change (Kingery, Bowen, and Uhlmann, 1976; West, 1985).

Ferroelasticity. A crystal that has two or more stable orientational states and can be switched from one to the other by an external mechanical stress is called ferroelastic. Various potential applications of ferroelectric materials in commercial devices, exploiting their special properties, are presented in Fig. 2.11. These include high-dielectric constant storage capacitors, piezoelectric microactuators, infrared sensors, electro-optic light valves and thin film memories.

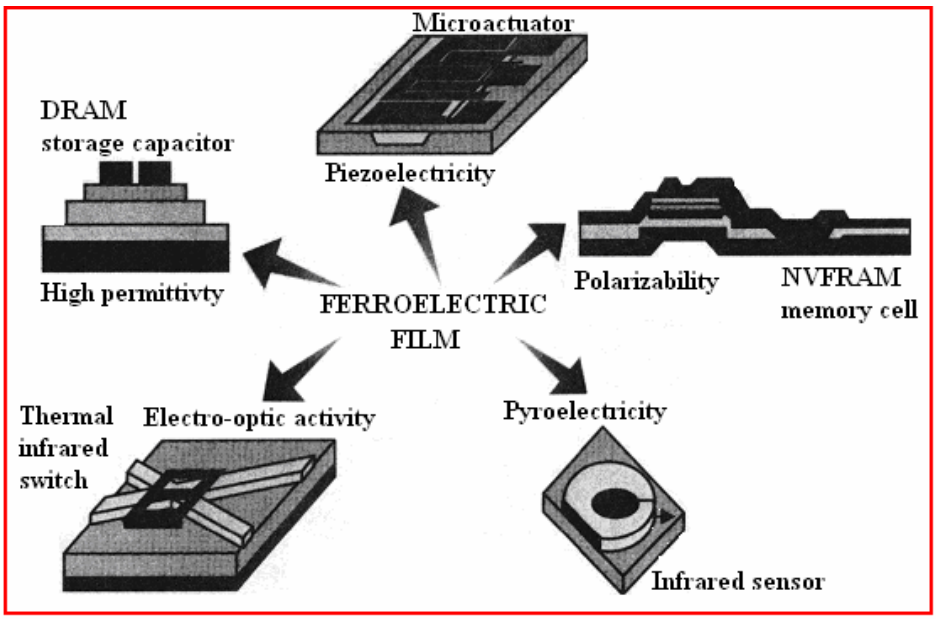

Figure 2.11 Examples of applications of ferroelectric films.

2.2 Lead Zirconate Titanate ($Pb(Zr_xTi_{1-x})O_3$): single composition and compositionally graded films

2.2.1 Single-composition PZT films

PZT can be regarded to date as the best ferroelectric material for various applications in technology, especially for ferroelectric memories. It has the highest polarization (36 $\mu C.cm^{-2}$) and the lowest coercive field ($\geq$ 20 $kV.cm^{-1}$) (Newnham, 1997). In PZT crystals, lead and oxygen atoms appear at the corners and face centers, respectively. Octahedrally coordinated titanium or zirconium ions are located at the centre of the unit cell. Solid solutions containing less than 45 mole percent $PbTiO_3$ are rhombohedral, while those containing more than this amount are tetragonal (Kittel, 1986). Curie temperatures can vary from 220 °C to 490 °C, depending on the composition of PZT (Newnham, 1997). The phase diagram in Fig. 2.12 shows the structural changes at the Curie temperature and the morphotropic phase boundary (MPB), separating the rhombohedral and tetragonal structure at about 45 mole percent $PbTiO_3$. Very large values for the dielectric constant and the piezoelectric electromechanical coupling factor are observed near this phase boundary

(see Fig. 2.13) (Jaffe and Roth, 1954). For large polarization, the composition near the MPB is preferred. It is believed that the tetragonal phase with six equivalent domain states (in the <100> directions) and the rhombohedral phase with eight domain states (in the <111> directions) co-exist for these compositions, resulting in 14 possible different directions of alignment over a wide temperature range (Cross, 1996).

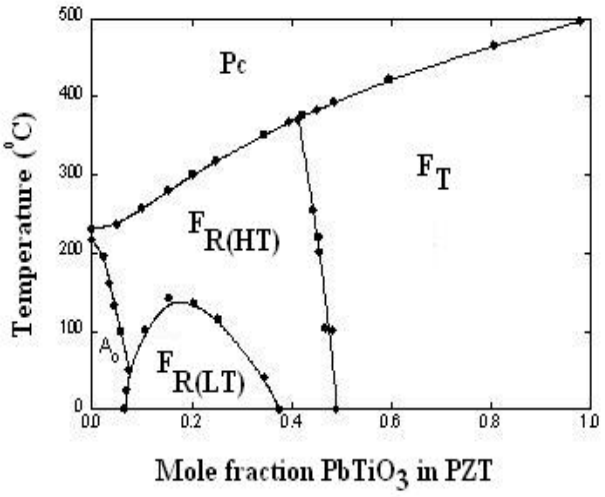

Figure 2.12 Phase diagram of $Pb(Zr,Ti)O_3$ system (Newnham, 1997).

Recently, the discovery of a new monoclinic phase in PZT system in the vicinity of the MPB has been reported (Noheda *et al*., 1999; Noheda *et al*., 2001). The monoclinic structure can be considered as a "bridge" between the tetragonal and rhombohedral phases in PZT. The piezoelectric strain occurs, not along the polar axes but along the directions that induce the monoclinic distortions.

Initial studies of PZT were mainly focused on the anomalous behaviors of the dielectric constant and piezoelectric coupling of the bulk materials around MPB. Since the onset of ferroelectric memory application, extensive work on PZT thin films have been conducted in a wide composition range. The results indicate that nano-structured PZT thin films exhibit different properties from PZT bulk materials. They display higher coercive fields and somewhat lower remanent polarizations than bulk materials (Scott and Araujo, 1989). The hysteresis characteristics of the thin films depend on composition crystal structure, morphology, particle size and distribution, *etc*., and, therefore, are strongly dependent on the film fabrication.

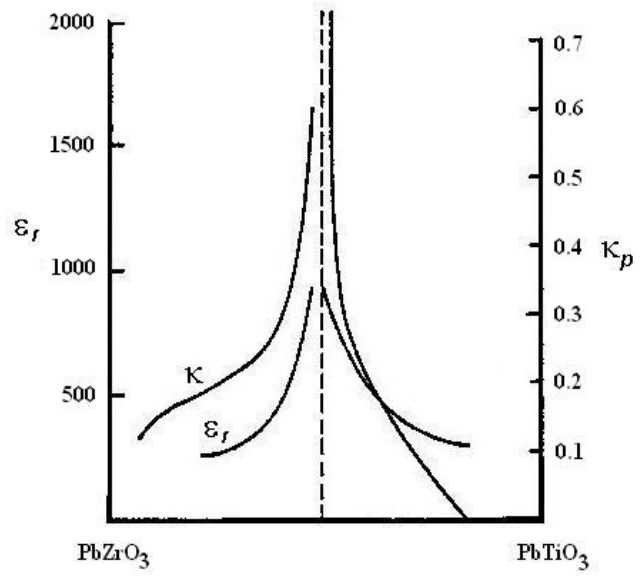

Figure 2.13 Composition dependence of the dielectric constant and the electromechanical coupling factor in PZT (Jaffe and Roth, 1954).

2.2.2 Compositionally graded PZT films

Polarization-graded ferroelectrics are distinguished from homogenous ferroelectrics in that the electric dipole moment density varies with position in graded ferroelectrics (Mantese and Schubring, 2001). This new class of ferroelectrics expands the applications and understanding of ferroelectric heterostructures and their related electric properties. As a result of the spatial variation of the polarization, polarization-graded ferroelectrics show unusual phenomena and properties that are not routinely observed for homogenous bulk ferroelectrics and their thin film counterparts.

Unlike homogenous ferroelectrics, which are characterized by a symmetric hysteresis loop with respect to the polarization and applied field axes, graded ferroelectric devices display strikingly new behavior, the most notable being a translation of the hysteresis loop along the polarization axis (Schubring *et al.*, 1992). The shift in the hysteresis loops are attributed to a "built-in" potential, in analogy with the asymmetric current-voltage characteristics resulting from the "built-in" potential across chemically doped regions in semiconductor diode junctions (Mantese *et al.*, 1995; Mantese and Schubring, 2001). Due to the charge offset, a giant pseudo-

pyroelectric response was reported in graded ferroelectrics (Jin *et al.*, 1998; Mohammed *et al.*, 1998). Other interesting properties for graded ferroelectrics include a diffuse phase transition accompanied with a broadening in the dielectric response with temperature (Schubring *et al.*, 1992; Slowak *et al.*, 1999; Zhu *et al.*, 2002). Recently, Mantese and his co-workers have extended the concept of graded ferroelectrics and concluded that graded ferroelectric structures are capable of interchanging thermal/electric/mechanical energy, leading to novel devices based on graded ferroelectrics, such as transpacitor and other energy storage devices (Schubring *et al*., 1999; Mantese and Schubring, 2001; Mantese, Schubring, and Micheli, 2001; Mantese, Schubring, and Micheli, 2002).

Compositional grading is the most common way to introduce a polarization gradient in ferroelectric materials. In a study of the potassium tantalate niobate thin film with gradient in composition, Schubring *et al*. reported an unidirectional charge flow which results in a measurable hysteresis charge offset (Schubring *et al.*, 1992). A smearing in the dielectric permittivity curves with respect to temperature has been found with a giant effective pyroelectric coefficient.

Consider a mono-domain ferroelectric of thickness L sandwiched between two metallic electrodes with the easy axis of polarization along the z-axis such that $P1 = P2 = 0$, $P3 = P = f(z)$, as shown in Fig.2.14.

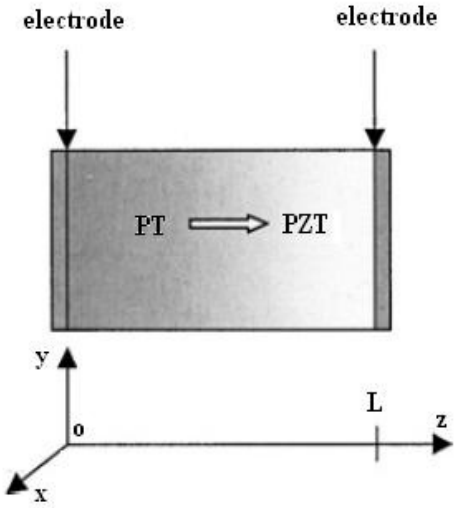

Figure 2.14 Schematic diagram showing a compositionally graded lead zirconate titanate bar and the coordinate system used in the model (PT: lead titanate, $PbTiO_3$, PZT: lead zirconate titanate, $Pb(Zr_xTi_{1-x})O_3$) (Alpay, Ban, and Mantese, 2003).

A linear relationship between the zirconium concentration and the position along the *z*-direction is assumed, and the ferroelectric is homogeneous along the *x*- and *y*-directions, reducing the problem to only one dimension. Accordingly, the free energy per unit area can be expressed by (Landau and Lifshitz, 1980):

$$F(z) = \int_0^L [F_P(z) + F_{el}^i(z) + F_E(z)]dz \tag{2.9}$$

where $F_P(z)$, $F_{el}^i(z)$ and $F_E(z)$ are the energy contributions from polarization, electric field and stress respectively. The first term $F_P(z)$ can be expressed in the spirit of Landau as an expansion in terms of even powers of the polarization:

$$F_{pl}(z) = \frac{1}{2}\alpha P^2 + \frac{1}{4}\beta P^4 + \frac{1}{6}\gamma P^6 + \frac{1}{2}A\left(\frac{dP}{dz}\right)^2 \tag{2.10}$$

accompanied by a gradient energy term. In relation (Eq. 2.10), α, β, γ, and A are the free energy expansion coefficients. The temperature dependence of the dielectric stiffness, α, is given by the Curie-Weiss law, (IEEE standard on Ferroelectric, 1986)

$$\alpha = \frac{(T - T_0)}{\varepsilon_0^{'} C} \tag{2.11}$$

where T_0 and C are the Curie-Weiss temperature and constant, respectively, and $\varepsilon_0^{'}$ is the permittivity of free space. The compositional inhomogeneity in the material system is reflected through the composition dependence of the Landau coefficients. Coefficient A can be approximated as $\delta^2|\alpha|$, where δ is the characteristic length along which the polarization varies. The second term of Eq. (2.9), $F_{el}^i(z)$, is the internal elastic energy due to the variation of the self-strain, *i.e.*, $x^0(z) = Q_{12}\left[P^2(z) - \langle P\rangle^2\right]$, which is a result of the change of the lattice parameter within the compositionally graded unconstrained ferroelectric bar. It can be defined as (Alpay, Ban, and Mantese, 2003):

$$F_{el}^i(z) = \overline{C}\left\{Q_{12}\left[P^2(z) - \langle P\rangle^2\right] + \left(z - \frac{L}{2}\right)\kappa\right\}^2 \tag{2.12}$$

where Q_{12} is the electrostrictive coefficient, $\overline{C} = C_{11} + C_{12} - \frac{C_{12}^2}{C_{11}}$ is an effective elastic constant, C_{ij} are the elastic moduli at constant polarization, $\langle P\rangle$ is the average

polarization and κ is the radius of curvature resulting from the bending moment due to misfit between "layers" given by:

$$\kappa = \frac{24}{L^3}\int_0^L \left(z - \frac{L}{2}\right) x^0(z)dz \tag{2.13}$$

The last term $F_E(z)$ in Eq. (2.9) represents the energy contribution from the electric field and is given by:

$$F_E(z) = -\frac{1}{2}E^D P(z) - EP(z) \tag{2.14}$$

In Eq. (2.14), E is the external electric field along the z-direction and E^D is the depolarization field which we assume to be small due to the finite conductivity of the material as well as local compensation by defects such as oxygen vacancies in perovskite ferroelectrics. The minimization of the free energy with respect to the polarization yields the Euler-Lagrange equation:

$$A\frac{d^2P}{dz^2} = \left\{\alpha + 4\overline{C}Q_{12}\left[\left(z - \frac{L}{2}\right)\kappa - Q_{12}\langle P\rangle^2\right]\right\}P + \left(\beta + 4\overline{C}Q_{12}^2\right)P^3 + \gamma P^5 - E \tag{2.15}$$

Equation (2.15) can be solved numerically to determine the polarization profile across the ferroelectric bar in the z-direction employing the boundary conditions $\frac{dP}{dz} = 0$ at $z = 0$ and $z = L$ which correspond to complete charge compensation at the ferroelectric/electrode interfaces. The coefficients α , β , and γ , and the elastic constants for $Pb(Zr_xTi_{1-x})TiO_3$ are obtained by averaging the corresponding parameters of $PbTiO_3$ and $PbZrO_3$ (Noheda *et al.*, 1995).

2.2.3 Asymmetrical charge offset and dielectric properties

The polarization profile then can be used to calculate the charge offset per unit area ΔQ based on the one-dimensional Poisson's Eq.2.16:

$$\Delta Q = \frac{k}{L}\int_0^L z\left(\frac{dP(z)}{dz}\right)dz \tag{2.16}$$

where k is the ratio of the capacitance of the graded ferroelectric C_F and the capacitance of a load capacitor C_Q (Sawyer and Tower, 1930). In Fig. 2.15, the

charge offset $\frac{\Delta Q}{\Delta Q_{\max}}$ was plotted as a function of the barium concentration X_{Ba} on one end of the ferroelectric (the other end has a fixed concentration corresponding to pure $BaTiO_3$). ΔQ is defined as the magnitude of the shift of the origin of the $Q-E$ hysteresis loop, as schematically illustrated in the inset of Figure 2.15 $\Delta Q_{\max}$ is the maximum charge offset.

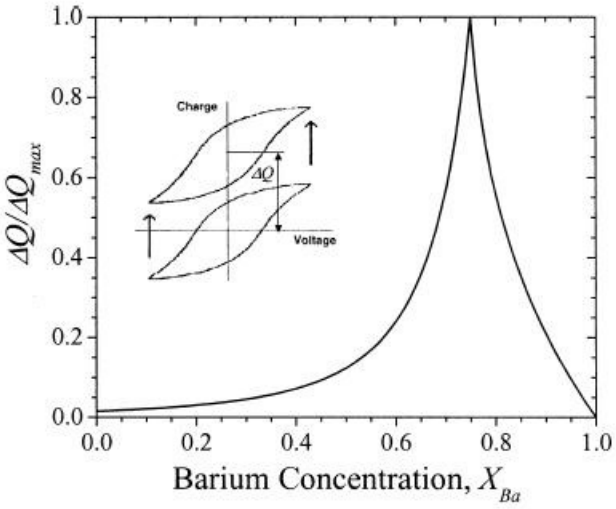

Figure 2.15 The calculated charge offset as a function of the minimum barium concentration X_{Ba} on one end of the ferroelectric (the other end has a fixed concentration corresponding to pure $BaTiO_3$)
(Ban, Alpay, and Mantese, 2003).

Figure 2.15 shows that the polarization gradient results in a charge offset and the magnitude of the charge offset strongly depends on the composition gradient. For compositionally homogenous materials (X_{Ba} =1), there is no charge offset. ΔQ is not a monotonic function of the composition gradient. A maximum charge offset may be obtained at a critical grading corresponding to the onset of paraelectric region with no spontaneous polarization in the ferroelectric bar.

Compositionally graded ferroelectrics exhibit dispersed dielectric susceptibility as a function of temperature (Schubring *et al.*, 1992; Slowak *et al.*, 1999; Zhu *et al.*, 2002). The broadness of dielectric susceptibility is inherently linked with the distribution of the phase transition temperature resulting from the composition gradient across the ferroelectric. Calculating the polarization change ΔP for $E = 0$ and $E \neq 0$ respectively, we can obtain a position dependent dielectric susceptibility profile as:

$$\chi(z) = \frac{1}{\varepsilon_0}\frac{\Delta P(z)}{E} \tag{2.17}$$

and the mean susceptibility of the ferroelectric bar is given by:

$$\chi_m = \frac{L}{\int_0^L \frac{1}{\{\chi(z)+1\}} dz} - 1 \tag{2.18}$$

Figure 2.16 shows χ_m as a function of temperature for various compositionally graded $Ba_xSr_{1-x}TiO_3$. In contrast to a sharp peak of the dielectric susceptibility corresponding to the ferroelectric-paraelectric phase transformation at the Curie temperature for bulk homogenous ferroelectric, a typical dispersed dielectric susceptibility response with the temperature is predicted for compositional graded $Ba_xSr_{1-x}TiO_3$ ferroelectrics. The maximum in the susceptibility is broadened as a result of the compositional grading. It is not surprising that the extent of the broadening of the susceptibility displays a close relationship with the imposed composition gradient. As seen in this figure (Fig. 2.16), the dielectric susceptibility is significantly flattened with respect to the temperature for $Ba_{0.5}Sr_{0.5}TiO_3$–$BaTiO_3$ graded ferroelectric. However, the broadening is less pronounced for a $Ba_{0.75}Sr_{0.25}TiO_3$–$BaTiO_3$ graded ferroelectric. A steeper composition gradient can give rise to broader maximum of the dielectric susceptibility. The exact same feature has been documented experimentally in compositionally graded $Ba_xSr_{1-x}TiO_3$ ferroelectric thin films where more pronounced broad plateau region of the permittivity with the variation of the temperature was observed for $Ba_{0.5}Sr_{0.5}TiO_3$–$BaTiO_3$ graded thin film compared with $Ba_{0.75}Sr_{0.25}TiO_3$–$BaTiO_3$ graded film (Slowak *et al.*, 1999).

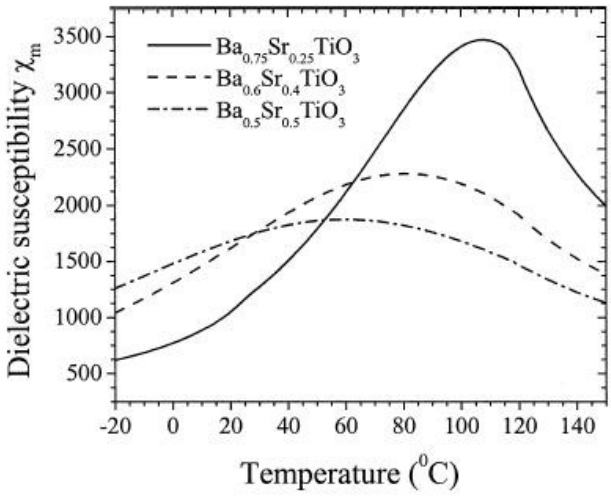

Figure 2.16 Dielectric susceptibility χ_m as a function of temperature for Various compositionally graded $Ba_xSr_{1-x}TiO_3$ ferroelectric systems (Ban, Alpay, and Mantese, 2003).

Another important aspect of the theoretically calculated dielectric susceptibility is that the broad plateau of susceptibility is shifted towards lower temperatures with an increase in the compositional gradient, as indicated in Figure 2.16. This is understandable because the "average" Curie temperature of the graded ferroelectric decreases with increasing compositional gradient. This result suggests that a high dielectric susceptibility with less temperature dependence at a desirable temperature can be achieved by appropriately tailoring the composition gradient.

2.2.4 Fabrication of $Pb(Zr_xTi_{1-x})O_3$ and $Pb(Zr_xTi_{1-x})O_3$ graded film

Several methods are in current use for depositing thin films, each of which has its merits and disadvantages. The methods can be classified into three groups:

-Physical vapour deposition (PVD), e.g. RF sputtering and pulse laser deposition

-Chemical vapour deposition (CVD), e.g. metal-organic chemical vapour deposition

-Chemical solution deposition (CSD), e.g. sol-gel

Although PVD and CVD techniques are currently favoured by the semiconductor industry-partly because of their existing investment and experience in using these techniques, CSD is a useful research and development tool requiring very little capital expenditure. The quality of the films is comparable across all three methods (Danglish and Kemmitt, 2000).

A wide range of CSD processes has been developed for ferroelectric thin film fabrication. Sol–gel methods, in which the metal cations are taken up into solution as alkoxides (for Zr and Ti) or acetates (for Pb and many dopant ions such as Mn) are usually based on chelating solvents such as 2-methoxyethanol (2ME) (Budd, Dey, and Payne, 1985; Gurkovotch and Blum, 1985), acetic acid with alcohols and stabilisers such as acetyl acetone and ethylene glycol (EG) (Yi, Wu, and Sayer, 1988; Schwartz *et al*., 1992) and diols (Phillips and Milne, 1991). There has been a move to eliminate the use of 2ME, because of its carcinogenic and teratogenic properties, leading to a greater emphasis on the use of simple alcohol solvents such as ethanol or methanol (Zhang, Whatmore and Vickers, 1999). Metal-organic decomposition processes that use metal carboxylates (*e.g.* Pb-2-etyhylhexanoate, Ti-di-methoxy-di-neodecanoate) in solvents such as butanol or xylene have also been explored with success (Klee *et al*., 1993), but the sol–gel processes are far more popular. The popularity of the sol–gel processes is probably because the amount of carbon in the films is much lower than the MOD processes. On the other hand, while sol–gel solutions are certainly stable enough to be used for weeks; sol ageing during storage is an issue that needs to be addressed, certainly from the aspect of industrial acceptability (Zhang and Whatmore, 2001).

2.3 Sol-gel process for $Pb(Zr_xTi_{1-x})O_3$ and $Pb(Zr_xTi_{1-x})O_3$ Graded Film

The general principle involved in the solution deposition of perovskite films is to prepare a “homogeneous” solution of the necessary cation species that may later be applied to a substrate. The fabrication of thin films by this approach involves four basic steps:

(i) synthesis of the precursor solution;

(ii) deposition by spin-casting or dip-coating, where drying processes usually begin depending on the solvent;

(iii) low-temperature heat treatment for drying, pyrolysis of organic species (typically 300-400 °C), and formation of an amorphous film;

(iv) higher temperature heat treatment for densification and crystallization of the coating into the desired oxide phase (600-1100 °C).

For most solution deposition approaches, the final three steps are similar despite differences in the characteristics of the precursor solution, and for electronic devices, spin-casting has been used almost exclusively. Depending upon the solution route employed, different deposition and thermal processing conditions may be employed to control film densification and crystallization for the preparation of materials with optimized properties.

Solution preparation of perovskite materials generally involves the use of metalloorganic compounds that are dissolved in a common solvent. The starting reagents are typically metal alkoxide compounds, $M(OR)_x$, where M is a metal and R is an alkyl group, metal carboxylates, $M(OOCR)_x$, and metal β-diketonates, $MO_x(CH_3\text{-}COCHCOCH_3)_x$. The selection of the starting reagents is dictated by solubility and reactivity considerations and the type of solution precursor species desired. The synthetic strategy used will define solution precursor properties such as equivalent solids content, extent of oligomerization and cation interaction, degree of homogeneity and reactivity, type and number of modifying ligands, and precursor size, structure, and shape. The solution route used will also determine the intermixing of the metal species, whether formation of a network versus formation of individual inorganic phases occurs, the carbon content of the films, the temperature at which pyrolysis of organic species occurs, the weight loss associated with oxide formation, the densification and crystallization behavior of the film, and stress development within the film. As will be discussed below, solution chemistry variations (*i.e.*, differences in precursor structure and solvent) can have a significant impact on the processing behavior of the as-deposited film. While some of these effects are now well understood, others are less clear, partly because of the difficulty in characterizing the solution precursor and the resulting amorphous film. In addition to precursor

characteristics, film processing behavior, such as substrate wetting, can also play a role in determining the solution chemistry that must be developed. Film properties that can necessitate changes in solution chemistry include poor thickness uniformity (striations), crack formation, crystallization behavior and phase purity, and compositional no uniformities. (Yi and Sayer, 1991; Schwartz *et al*., 1997)

For the production of perovskite thin films, the most frequently used CSD approaches may be grouped into three categories:

(1) Sol-gel processes that use 2-methoxyethanol as a reactant and solvent (Budd, Dey, and Payne, 1985; Budd, Dey and Payne, 1986; Coffman and Dey, 1994).

(2) Chelate processes that use modifying ligands such as acetic acid (Takahashi *et al.*, 1990; Yi and Sayer, 1991; Schwartz, Assink and Headley, 1992).

(3) Metalloorganic decomposition (MOD) routes that use water-insensitive metal carboxylate compounds (Vest and Xu, 1988; Haertling, 1991; Ito, 1997).

Other approaches that have also been used, but less extensively, include the nitrate method (Ng and Cima, 1994), the citrate route (Baythoun and Sale, 1982), and the Pechini process (Falter *et al.*, 1989).

During solution synthesis, the chemical interactions that take place between the starting reagents will depend on both the reactivity of the compound and the solution preparation conditions, such as reflux temperature. In true sol-gel processing routes, the reactivity of the reagents is high, and if alcohol exchange occurs or if modifying ligands are used, the structure of the species in solution can bear little resemblance to the starting compounds. In this case, the species that are generated are frequently oligomeric in nature and can contain more than one type of cation (Chae *et al.*, 1994; Ma and Payne, 1994). In contrast, for the long-chain carboxylate compounds that have been historically used in MOD routes (Vest and Xu, 1988), such as zirconium 2-ethylhexanoate, reactivity is low and the chemical interactions between the different precursor compounds is minimal.

2.3.1 Sol-gel with 2-methoxyethanal route

Although other alcohols have also been utilized, the solvent, 2-methoxyethanol (CH_3-OCH_2CH_2OH), is the most extensively used in the chemical synthesis of perovskite materials. Processes based on 2-methoxyethanol (Budd, Dey, and Payne, 1985) are most appropriately considered sol-gel processes and the key

reactions leading to the formation of the precursor species are hydrolysis and condensation of the alkoxide reagents, in which metal-oxygen-metal (M-O-M) bonds are formed:

Hydrolysis:

$M(OR)_x + H_2O$ ------- $M(OR)_{x-1}(OH) + ROH$

Condensation (alcohol elimination):

$2M(OR)_{x-1}(OH)$ ------- $M_2O(OR)_{2x-3}(OH) + ROH$

Condensation (water elimination):

$2M(OR)_{x-1}(OH)$ ------- $M_2O(OR)_{2x-2} + H_2O$

Prehydrolysis of less reactive alkoxides may also be used to improve solution compositional uniformity.

Another key reaction in the use of this solvent is the alcohol-exchange reaction that results in a decrease in the hydrolysis sensitivity of starting reagents such as zirconium *n*-propoxide and titanium isopropoxide used in the production of PZT films:

Alcohol exchange:

$M(OR)_x + xR'OH$ ------- $M(OR')_x + ROH$

where OR is a reactive alkoxy group and OR′ is the less reactive methoxyethoxy group. 2-Methoxyethanol has also been found to be beneficial in the dissolution of carboxylate precursors such as lead acetate. In this case, by refluxing the lead acetate precursor in 2-methoxyethanol, one of the acetate groups is replaced, resulting in the formation of the soluble lead precursor, $Pb(OOCCH_3)(OCH_2CH_2OCH_3)\bullet 0.5H_2O$. Lead carboxylate compounds are usually employed due to the instability of lead alkoxides and their limited commercial availability. A typical process involves refluxing lead acetate and the alkoxide compounds in methoxyethanol in separate reaction vessels. This is followed by combining the solutions, further refluxing, distillation, and dilution to the desired volume. Prior to film formation, the stock solution prepared by the above process is then hydrolyzed to promote oligomerization.

The reactions that occur during PZT solution preparation have been extensively studied using spectroscopic techniques (Coffman and Dey, 1994; Ramamurthi and Payne, 1990). Similar reactions between precursor compounds and 2-methoxyethanol have been also noted in the processing of $Pb(Zn_{1/3}Nb_{2/3})O_3$ (Francis, Payne and Wilson, 1990). These studies have elucidated certain aspects of the structure of the solution precursors. Some studies have indicated that the precursors formed in the lead zirconate titanate and lead titanate deposition solutions are apparently small, mixed metal oligomers, (Ramamurthi and Payne, 1990; Coffman and Dey, 1994) while others have indicated that the A-site precursor may not be intimately involved in the formation of the gel network (Sengupta *et al*., 1995; Lakeman, Xu and Payne, 1995). In particular, the results of Sengupta and co-workers of EXAFS (Extended X-ray Absorption Fine Structure) investigations of PZT gels indicate that separate networks of Ti-O-Ti, Zr-O-Ti, and Pb-O-Pb exist within the gel structure. This would seem to indicate that "intimate" mixing of the starting reagents has not taken place. In terms of controlling the extent of intermixing and stoichiometry of the precursor species, there have been a number of efforts to synthesize stoichiometric precursors with structures similar to the final crystal structure of the desired perovskite phase.

The motivation behind these efforts is that stoichiometric precursors with structures similar to the crystalline phase should undergo crystallization at lower heat treatment temperatures. Most attempts have resulted in mixed metal species with a cation stoichiometry different than that of the perovskite material. Examples in the synthesis of $PbZrO_3$ and $PbTiO_3$ include $[PbZr_2(\mu4\text{-}O)_2(OOCCH_3)_4\text{-}(OCH2CH_3)_6]_2$ and $[PbTi_2(\mu4\text{-}O)(OOCCH_3)(OCH_2\text{-}CH_3)_7]_2$ (Chae *et al.*, 1994; Ma and Payne, 1994). These results indicate the importance that thermodynamic sinks can play in the synthesis of these materials (Boyle and Schwartz, 1994). However, while the stoichiometry of the precursor species may not match that of the crystalline perovskite, this has not inhibited the production of high quality perovskite films by this processing route.

It has also been demonstrated that through manipulation of the above reactions, *i.e.*, by controlling the reflux, catalysis, and hydrolysis conditions, the nature of the resulting solution precursors and gels may be controlled, allowing for control of material properties. The initial interpretation of these effects was based on the more extensive investigations that had taken place for the silica system. It was noted that many of the catalyst (acid or base) and hydrolysis effects in perovskite materials paralleled to those for silica sol-gel processing using tetraethyl orthosilicate (TEOS). For example, in the production of lead titanate gels, acidic catalysis conditions resulted in gels that seemed more capable of polymeric rearrangement, while gels prepared under basic catalysis conditions exhibited more phase separation and were more highly textured. Other physical properties of gel-derived lead titanate powders, namely, surface area and pore characteristics, also indicate a strong similarity in the processing behavior (hydrolysis and catalysis effects) of these materials to silica (Schwartz, Payne and Holland, 1989). Solutions prepared with higher levels of hydrolysis resulted in powders with greater surface areas and pore volumes.

Solution processes based on the use of methoxyethanol are perhaps the most widely used of any of the CSD routes, primarily due to the ability of this solvent to solubilize a variety of starting reagents. When properly carried out, sol-gel processes offer excellent control and reproducibility of process chemistry, and nonhydrolyzed solutions exhibit minimal aging effects.

Once the precursor solution has been prepared, films are typically formed by spin casting, spraying, or dip coating, as illustrated in Fig. 2.17. After deposition, the desired ceramic phase is subsequently obtained by heat treatment.

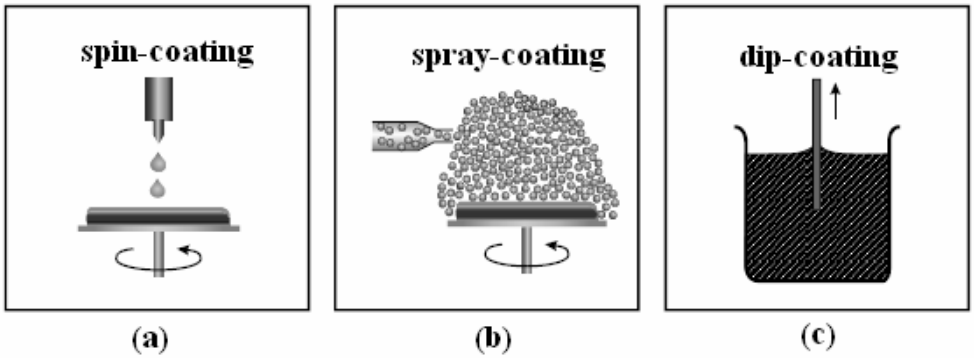

Figure 2.17 Illustration of the commonly used coating techniques

At the laboratory scale, spin deposition is usually achieved with a photoresist spinner and the substrate is typically either a planar single crystal oxide, or an electroded Si wafer (Fig.2.17a). The substrate is held in place on the spinner by applying a vacuum to the backside of the wafer through a chuck that is at the end of the spinner motor shaft. The wafer is typically flooded with solution during a 'static dispense' using a syringe with a 0.2 μm filter. The wafer is then accelerated rapidly to 1000 to 8000 rpm. The angular velocity and the spinning time, together with the solution viscosity, can be used to control the thickness of the wet film. This characteristic and the solute concentration will, in turn, determine the thickness of the final ceramic film. Birnie has reported solution characteristics and deposition conditions that can result in striation development in the films (Birnie, 2001; Haas *et al*., 2001).

The spray-coating technique potentially offers the advantage of conformal film deposition on non-planar structures (e.g., steps, stacks or trenches) on semiconductor chips (Fig. 2.17b). This technique is based on the transformation of the coating solution into an aerosol by means of an ultrasonic nebulizer or appropriate pressuredriven, nozzle-based atomizer (McMillan *et al*., 1992; Huffmann, 1995). Compared to spin and dip coating, the solution viscosity must be reduced significantly in order to facilitate the nebulizing process and the formation of sufficiently small droplets. The misted solution is transferred into the deposition chamber by a carrier gas where the droplets settle onto the wafer surface by gravitation, or more efficiently, by an electrostatic field. In this later case, the aerosol is electrically charged by a corona discharge before entering the chamber (McMillan *et al*., 1992; Han, Gu, and Ma, 1997). The step coverage and conformal nature of the films deposited on non-planar surfaces by spray-coating has also been studied: for 400-nm steps, films that were ~200 nm thick demonstrated thickness variations of < 20% (McMillan *et al*., 1992). The key of improving conformal coverage is the reduction of the solution droplet size. By using a Venturi nozzle rather than an ultrasonic nebulizer, it is possible to reduce the droplet size to ~100 nm. However, since the deposition

efficiency obtained by gravitation decreases with droplet size, electrostatic enforcement is desirable in this case.

Dip-coating (Figs. 2.17c and 2.18). involves the formation of a film through a liquid entrainment process that may be either batch or continuous in nature. Brinker and Scherer present an excellent review of the various factors that govern the dip-coating process (Brinker and Scherer, 1990). For the batch method (Scriven, 1988), the general steps include immersion of the substrate into the dip-coating solution, start-up, where withdrawal of the substrate from the solution begins, film deposition, solvent evaporation, and continued drainage as the substrate is completely removed from the liquid bath (Brinker and Scherer, 1990). Depending on the rate of substrate withdrawal, solvent volatility and film thickness, the extent of overlap of these different processes can vary dramatically. The thickness of the film that is formed in dip coating is governed by factors that include viscous drag, gravitational forces, and the surface tension in the concavely curved meniscus among others (Brinker and Scherer, 1990). For dip-coating from sol–gel solutions, the characteristics of the precursor (sticking probability), aggregation and gelation behavior also play a key role in defining both the thickness and nature of the film that is formed (Brinker and Scherer, 1990). To characterize the changes that occur in the nature of the film during the formation process, a variety of probe molecules have been incorporated into the sol (Hunderford *et al.*, 2002). These have allowed for in situ characterization of film/process properties, such as solvent composition in the entrainment and drying line regions, as well as measurements of the drying-induced pressure that is developed (Bornside, Macosko, and Scriven, 1987).

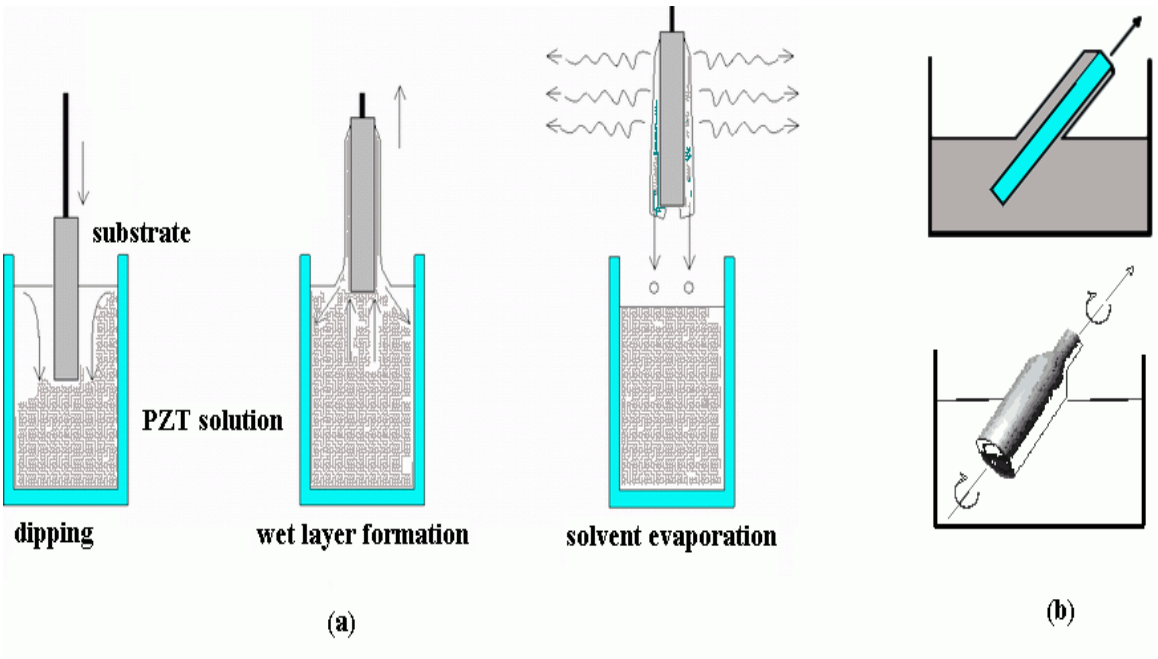

Fig. 2.18 (a) dipping of the substrate into the coating solution, (b) general shape of substrate in dip-coating process.

Thin films with excellent properties have been prepared by sol-gel for a number of materials including PZT (high dielectric constant and ferroelectric hysteresis), $LiNbO_3$ (electro-optic coefficient), (Hirano and Kato, 1988; Eichorst and Payne, 1988) $BaTiO_3$ (high dielectric constant), (Hayashi *et al*., 1993) and YBCO (high critical current capabilities) (Lourdes *et al*., 1995). However, for the non-chemist, the procedures involved in solution synthesis can be rather complex. Thus, while the control over precursor characteristics is good, the process simplicity is low. In addition, 2-methoxyethanol is a known teratogen, which presents a significant safety concern and inhibits its use in most manufacturing facilities (Schwartz, 1997).

CHAPTER 3

FERROELECTRIC AND PIEZOELECTRIC PROPERTIES OF SINGLE-COMPOSITION PZT FILMS

3.1 Introduction

As mentioned in earlier chapters, PZT are of great interest for various applications including non-volatile memories, piezoelectric micro-actuators, pyroelectric detectors and microelectromechanical systems (MEMS) (Auciello *et al*., 1998). Ferroelectric and piezoelectric properties of PZT films depend on many condition parameters, including the composition, crystallographic structure, grain size and preferential orientation. It is well known that the PZT ceramic with the composition near the MPB region crystallizes in a two-phase system which are the tetragonal and rhombohedral perovskite phases and possess the maximum values of the relative permittivity and the piezoelectric coupling factor.

In this chapter, the fabrication of PZT films with uniform Zr content is described. Effect of Zr/Ti ratio on the microstructure and ferroelectric properties of the films are systematically investigated. Owing to the challenging of the measurement of an electrically-induced displacement in a film (Liu *et al*., 2002), an illustration of using an optical interferometry for measuring small displacements relating to the piezoelectricity of the films was presented in this chapter.

3.2 Review of Previous Work

Sol-gel techniques have rapidly drawn attention for the fabrication of ferroelectric thin films. The most common method for sol-gel synthesis involves hydrolysis and condensation of metal alkoxides followed by drying and densification of resulting gels in order to produce a ceramic material. PZT thin films have been prepared by sol-gel methods using a variety of metal organic precursors and solvent systems. The most widely used system is the methoxyethanol route. This method was

first reported by Budd, Dey and Panye (1985) and they used this techniques to prepare $PbTiO_3$, $PbZrO_3$, PZT and PLZT thin films. Several research groups have used acetylacetone (Tohge, Takahashi, and Minami, 1991) and acetic acid (Yi, Wu and Sayer, 1988) to stabilize Zr and Ti alkoxide.

One of the factors controlling thin film properties is the chemical characteristics of the solid solution (or "sol" in brift) of the ceramics. Thin films prepared from different solutions normally show different physical and electrical properties. The sols using n-propanol as a solvent gave large PZT grain of the order of 2 μm, while the film prepared by using 2-methoxyethanol as solvent resulted in a fine PZT grain of 0.2 μm (Hseueh and Mecartney, 1990). Another solvents are the methoxybuthanol which gave a large rosette structure in a matrix of a nanocrystalline phase, the methoxyethanol giving a rough surface with a fine grain of 0.1-0.2 μm, and the acetic acid which lead to the films with grain size below 0.1 μm. The films prepared using the acetic-acid based route were (100) preferred oriented (Khamanker *et al.*, 1994). The acetic-acid based film also likely showed a square hysteresis loops with higher E_c and P_r .

The effect of Zr source on properties of PZT thin films was reported by Tu and Milne (1995). Zr-acetylacetonate and Zr-n-propoxide were used as Zr-sources in the sol preparation. The films prepared from Zr-acetylacetonate were highly (111) oriented with small grain sizes and had good electrical properties. Boyle *et al*., (1997) reported the ageing effect of the sols. Those films prepared from aged sols (>10 days) showed surface nucleated grains, leading to opacity of the films.

The employment of rapid heating was suggested to reduce PbO losses by volatilization and reduce thermally activated film/substrate interactions (Hu *et al*., 1992). The high surface area of a thin film is expected to cause more lead loss than a bulk ceramics. About 3-6% of lead loss for films annealed at 700°C was reported in the literature (Kwok, Desu and Kammerdiner, 1993). Exceed Pb content in the starting sols can also change the microstructure. Toewee, Boulton, and Uhlmann (1992) observed that the grain size of PZT thin films increased with the amount exceed Pb. To obtain the desired ferroelectric and piezoelectric properties, the composition and crystal orientation of PZT film are the key factor. The investigation of the Zr/Ti ratio dependence of the electrical properties of the PZT film is, therefore

essential. However, the Zr/Ti ratio dependence of the electrical properties in (111) textured films has been rarely reported in the literature. Most often, the properties of randomly oriented films were studied (Pandey *et al*., 2004; Gong *et al*., 2004).

3.3 Materials and Methods

3.3.1 Preparation of the PZT sol-gel solutions

In this work, the procedure of the preparation of precursor solution was based on that proposed by Budd, Dey and Payne (1985). 0.6 M $Pb(Zr,Ti)O_3$ solutions were prepared by using zirconium propoxide ($C_{12}H_{28}O_4Zr$, Aldrich, 99% purity, 70 wt% in n-propanol), titanium iso-propoxide ($C_{12}H_{28}O_4Ti$, Aldrich, 97% purity) and lead acetate trihydrate as starting materials, and 2-methoxyethanol ($CH_3OCH_2CH_2OH$, Ajax Finechem) as solvent. Physio-chemical properties of these materials are listed in Table 3.1. The quantities of these precursors are shown in Table 3.2.

Table 3.1 Physio-chemical properties of precursor materials.

Precursor Material	Molecular Weight ($g.mol^{-1}$)	Density ($g.ml^{-1}$)	Boiling point (ºC)
Lead acetate trihydrate	379.33		
Zirconium propoxide*	327.58	1.05	208
Titanium isopropoxide	284.25	0.966	240
2-Methoxyethanol	76.10	0.965	124

* Zirconium propoxide 70 wt % in propanol

Table 3.2 Quantity of the precursors required to prepare 50 ml of a 0.6 M PZT solutions with various Zr/Ti ratios. (Units in ml are in brackets)

Zr/Ti / Precursor	Zr content (g)				
	70/30	60/40	52/48	40/60	30/70
Lead acetate trihydrate	13.655	13.655	13.655	13.655	13.655
Zirconium propoxide	9.827 (9.4)	8.422 (8.0)	7.3 (7.0)	5.614 (5.3)	4.211 (4.0)
Titanium isopropoxide	2.558 (2.6)	3.411 (3.5)	4.093 (4.2)	5.116 (5.3)	5.969 (6.2)
2-Methoxyethanol	14	14	14	14	14

At first, lead acetate trihydrate ($C_4H_6O_4Pb{\cdot}3H_2O$, Riedel-de Haen, 99% purity) is dissolved in 2-methoxyethanol and mixed during 30 min. To compensate the lead loss during crystallization process, and to decrease the annealing temperature of the PZT perovskite phase, 10 wt% of lead acetate was added to the solution (Perez, Vilarinho, and Kholkin, 2004). Distilled the solution until became white powder by increasing the temperature up to 130 ºC. 2-methoxyethanol was then added and refluxed for 3 hours. This process was followed by the addition of zirconium propoxide to the lead solution and it was refluxed during 2 hours. Finally, titanium isopropoxide was added to the solution and mixed for more than 12 hours. The addition of the zirconium propoxide in the second step of the reaction and the refluxing during 2 hours were carried out in order to stabilize the solution and to avoid the formation of the titanium hydroxide. The distillation process was introduced in order to prevent the low molecular weight compounds (such as water or acetic acid) presented in the lead acetate trihydrate and to improve the chemical stability and homogeneity of the lead solution. To maintain the molar concentration after each distillation, 2-methoxyethanol solvent was added to the lead solution. In order to prepare a crack-free film, 4 vol% of formamide (CH_3NO, SIGMA, 99.5%) was added and stirred until the PZT solution became homogeneous. The procedure of the preparation of PZT solution is shown in Fig. 3.1.

3.3.2 Viscosity measurement

Viscosity is a measurement of the resistance of a fluid to deformation under shear stress. It is commonly perceived as "thickness", or resistance to pouring. Viscosity describes a fluid's internal resistance to flow and may be thought of as a measure of fluid friction. The thicker fluid is, the greater its resistance to shear stress and the more rapid the decay of its flow.

For PZT solution, viscosity measurement is one of the main techniques used to study the aging of the sol-gel solution. Any change in the viscosity of the solution with the time after the preparation could be interpreted as a change in the stability of the solution (precipitation, agglomeration, *etc.*). The viscosity measurements were performed using a Carry-Met CSL Digital Rheometer, equipped

with acquisition software, which determines the relation between the viscous shear stress and the shear rate of deformation. The viscosity data, of all the study solutions, were recorded after one day, one month and every month after preparation.

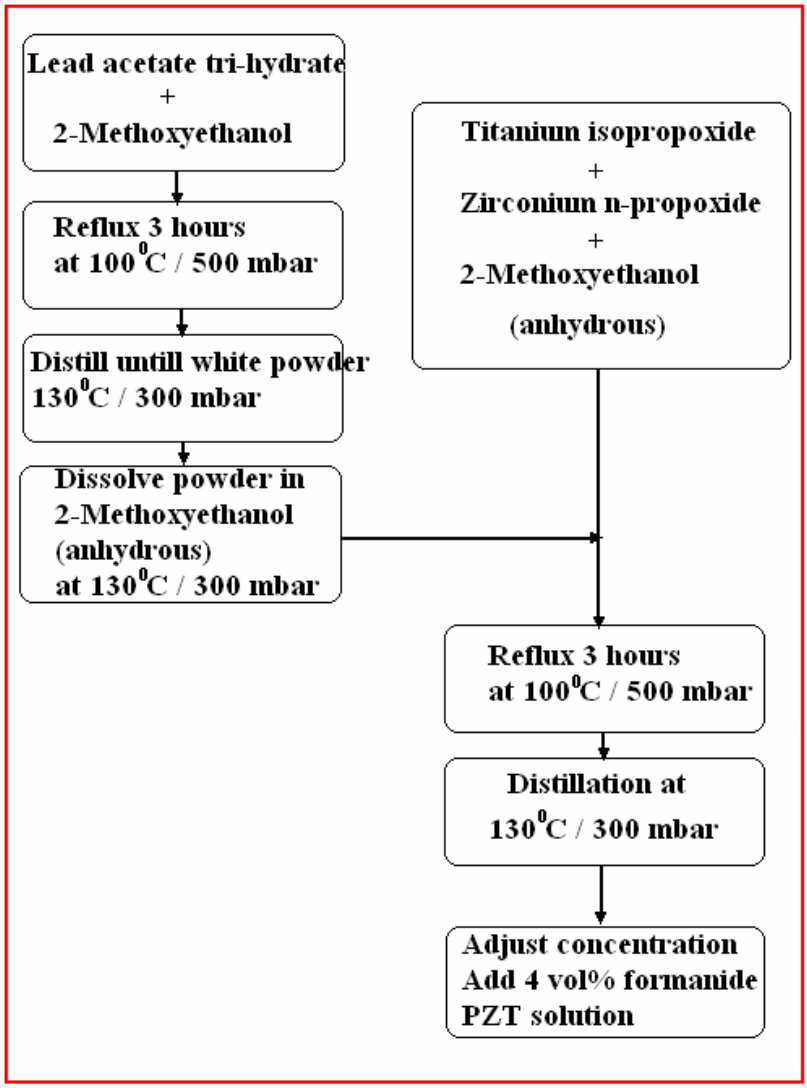

Figure 3.1 Flow chart of the PZT solution process.

3.3.3 Thin film fabrication

50 ml of a 0.6 M PZT solutions were deposited on platinised silicon substrates (INOSTEK, Korea) using a spin-coating technique. The full configuration of the substrate was (111)Pt/TiO_2/SiO_2/Si; the Pt layer was 1500 Å in thickness, the Ti adhesion layer, 200 Å, and the thermally grown SiO_2, 3000 Å in thickness. The Pt was polycrystalline with a (111) orientation. Before the coating process, the substrates

were cut into pieces of ~1 cm^2 area, and cleaned ultrasonically with a series of cleaning solvents: trichloroethylene, acetone and 2-propanol. Finally, any residual organics were removed using an oxygen gun and a hot plate at 230 ºC.

Fig. 3.2 shows the steps of the preparation of thin films (Gurkovotch and Blum, 1985). The PZT solution was dropped onto the substrate and spun at 3000 rpm for 30 s. After each deposition, the film was dried at 200 ºC for 1 min and subsequently pyrolysis at 400 ºC for 5 min. The deposition was repeated 5 times each before firing at 600 ºC for 30 min in air.

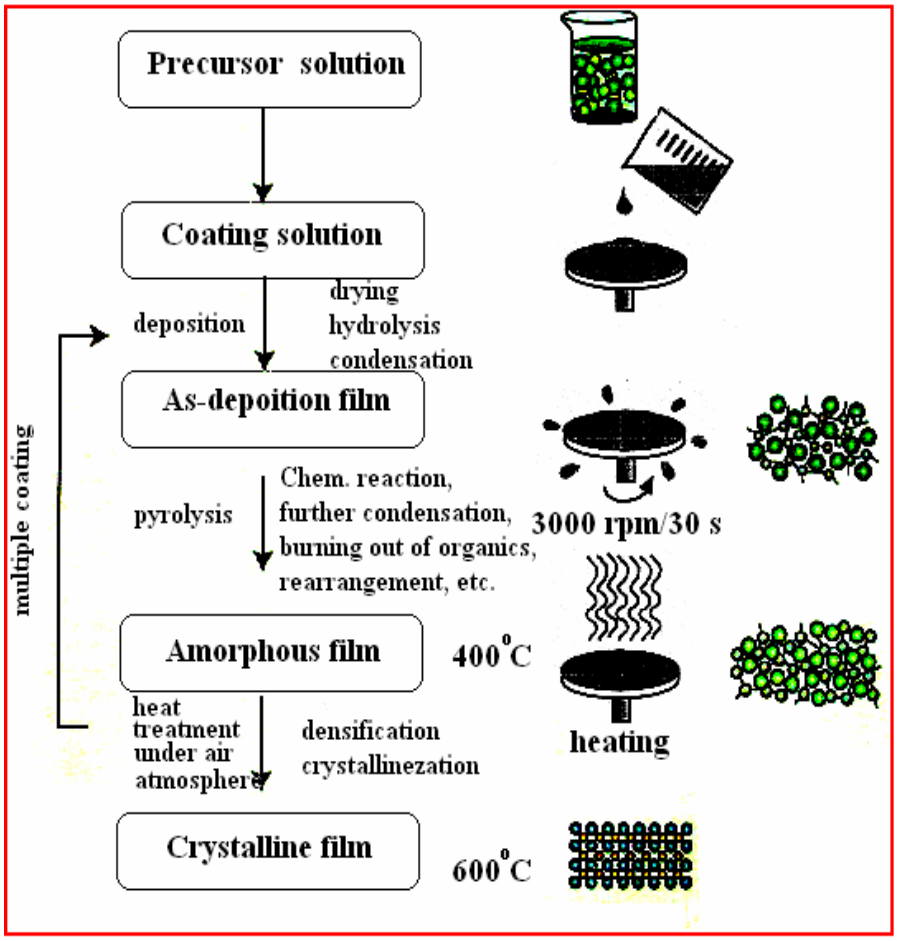

Figure 3.2 Flow chart of the PZT thin film fabrication.

3.3.4 X-ray and microscopic characterization

The crystal structure and texture of the $Pb(Zr_xTi_{1-x})O_3$ films were examined by X-ray diffraction (XRD) technique (Philips X-Pert diffractometer, monochromatic Cu Kα). The patterns were recorded at a scan rate of 3º per min

from 20° to 60° for phase and texture analyses. Scanning electron microscopy (SEM) was performed using an S-4100 Hitachi instrument for microtexture investigation.

3.3.5 Electrical characterization

For the electrical measurements, ~60 nm-thick of gold metal was sputtered through a shadow mask (SPI module sputtering, Inc.) to form an electrode of an area of ~0.3 mm^2 on the surface of the film. Films at the corner were etched away using a 40% hydrofluoric acid, HF solution (Aldrich). This was done to reveal the metallized substrate to act as a bottom electrode. The dielectric constant ($\varepsilon_r^{'}$) and $\varepsilon_r^{'}$ as a function of *dc* bias (*C-V*) measurements were carried out in a frequency range of 10^2 to 10^6 Hz using a Kiethley 3330 LCZ meter. A ferroelectric test module (AIXACT TF Analyzer) was used to observe the ferroelectric properties of the films. The measurement of *P-E* hysteresis loop was carried out by contacting between the top Au electrode and the conductive substrate.

The piezoelectricity in the film was investigated by a modified Michelson interferometer. The arrangement of the interferometer was shown in Fig. 3.3. The operation of the system was described in chapter 2. A He-Ne polarized laser (Uniphase 1135p) was used as a light source. In the measurement, the electroded surface of the film which was ~1.5 mm^2 sputtered gold was used as a mirror surface to reflect the laser beam back into the optical system. An *ac* voltage is applied to the electrodes of the film using a signal generator (HP 8116A). The displacement of the top electrode is assumed to be equal to the entire piezoelectric displacement. The resulting piezoelectric strain in the sample produces a small change in the intensity of the interference pattern which is adjusted to fall on the aperture of a *p-i-n* photodiode detector (BPX 65). The detector converts the small changes of intensity into an electrical signal.

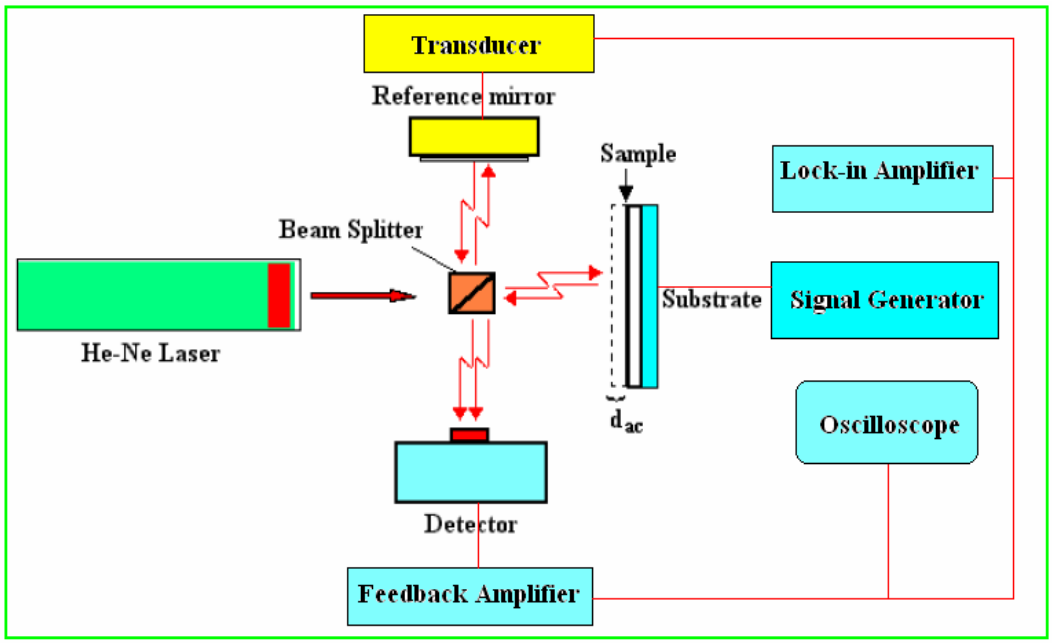

Figure 3.3 Schematic diagram of the experimental set up for the d_{ij} determination using a Michelson interferometer

The output from the detector is measured using a lock-in amplifier (Stanford Research Systems 830). The reference input for the lock-in is driven directly from the signal generator. The output from the lock-in amplifier was measured as V_{out}. Knowing V_{out} and a driving voltage, the magnitude of piezoelectric coefficient can be calculated. In a perovskite film the *c*-axis is usually perpendicular to the plane of the film. If an electric field is applied parallel to the *c*-axis, the d_{33} coefficient can be obtained directly from the ratio of the resultant displacement normal to the film plane to the applied voltage. The relationship determining the piezoelectric coefficient, d_{33} of the films using the interferometer technique is given by (Zhang, Pan and Cross, 1988):

$$d_{33} = \frac{d_{ac}}{V} = \frac{\lambda V_{out}}{2\pi V_{pp} V} \tag{3.1}$$

where V is the *rms* voltage driving the film, V_{pp} is the peak-to-peak voltage corresponding to the change in interference light intensity, λ is the wavelength of the polarized He-Ne laser emission, V_{out} is the output from the lock-in amplifier

measured at the same frequency as the applied *ac* voltage and d_{ac} is a small electric-field induced displacement related to the strain of the film.

Initial performance of the system was checked from the measurements performed on a sample whose piezoelectric coefficient is well-known. The system was electronically stabilized against the mechanical vibration at frequencies below 1 kHz via the use of the feedback amplifier. From 1 kHz to 5 kHz the mechanical displacement varied linearly with driving voltage. At frequencies above 5 kHz, the readings was unstable and extremely high due to the mechanical resonance.

3.4 Results and Discussion

3.4.1 Analysis of the viscosity of the PZT precursors

The viscosity of the PZT precursor was measured using a *Carry-Met* CSL Digital Rheometer, equipped with acquisition software. The viscosity data of all specimen were recorded after one day, one month and every month after preparation. The results are shown in Fig. 3.4.

From the results, the stock solutions were stable against precipitation for at least four months when stored in air. The viscosity of 0.6 M solution prepared using 2-methoxyethanal route was around 5 mPa·s.

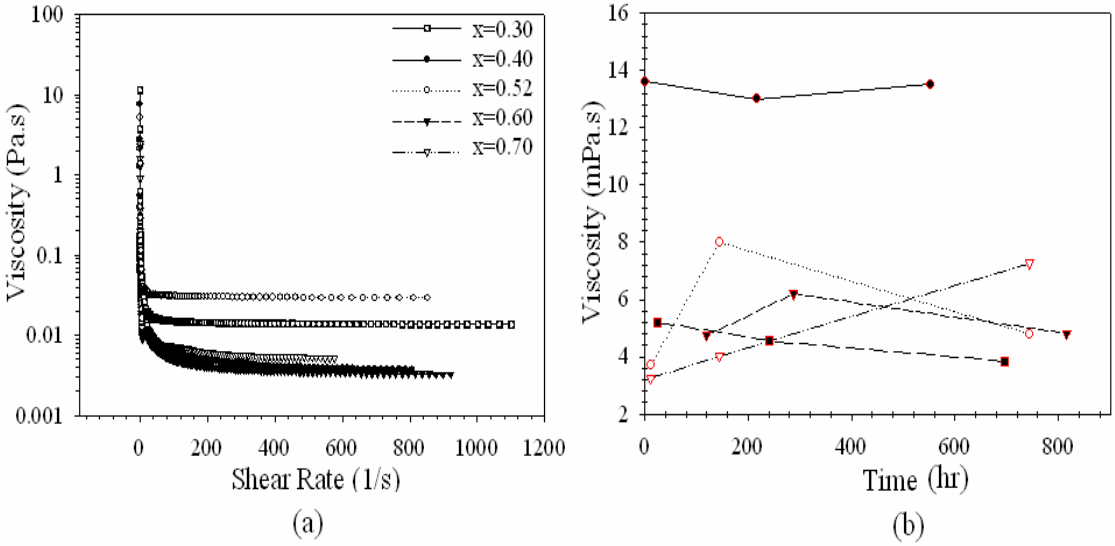

Figure 3.4 (a) Shear rate *vs* viscosity, and (b) viscosity *vs* time of the PZT sols.

3.4.2 X-ray characterization as a function of the composition of PZT

The XRD patterns of PZT thin films deposited on (111)Pt/Ti/SiO_2/Si substrates with the Zr/Ti ratios ranging from 30/70 to 70/30 were shown in Figs. 3.5-3.9.

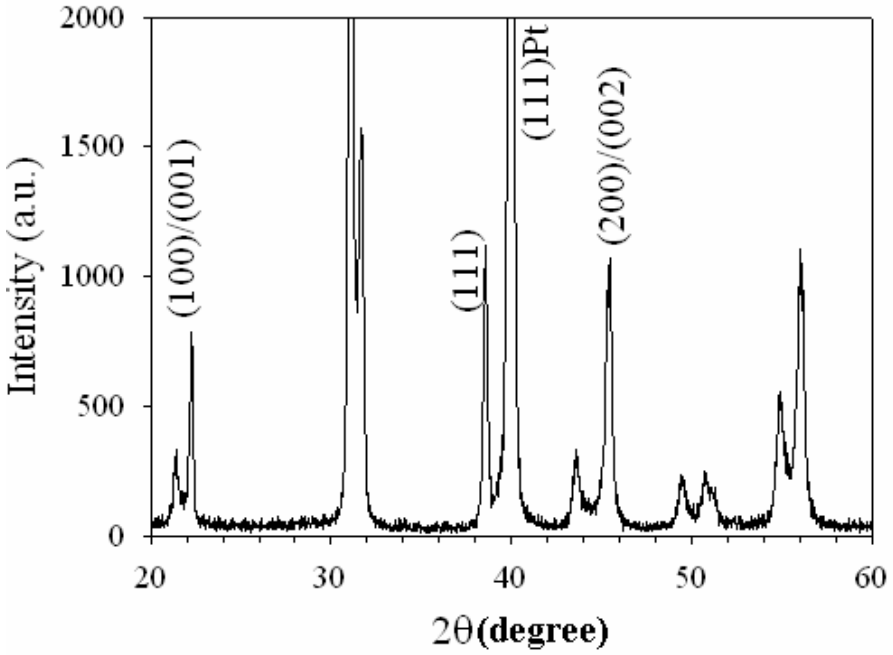

Figure 3.5 XRD pattern of PZT film with x=0.30.

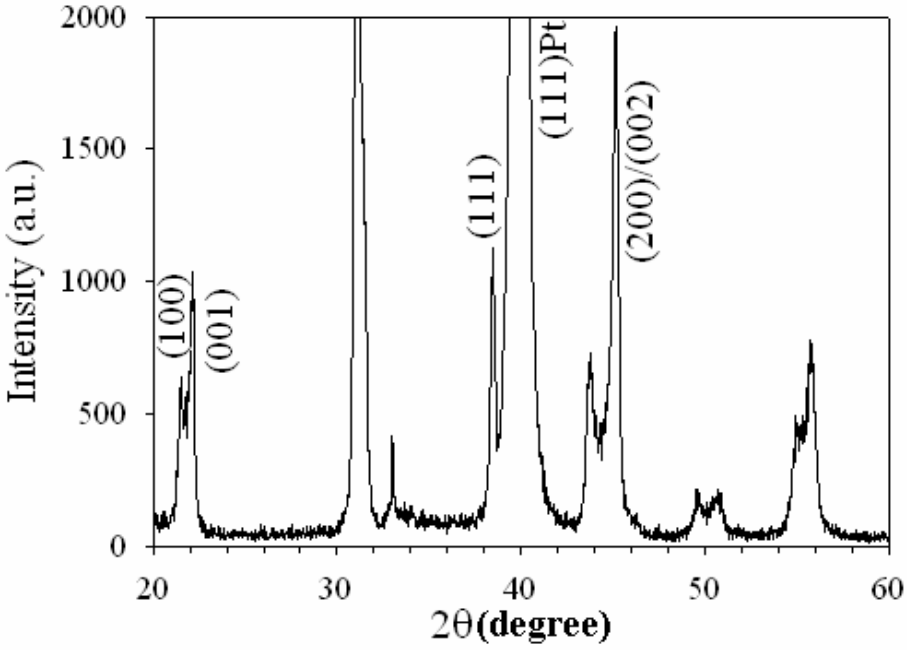

Figure 3.6 XRD pattern of PZT film with x=0.40.

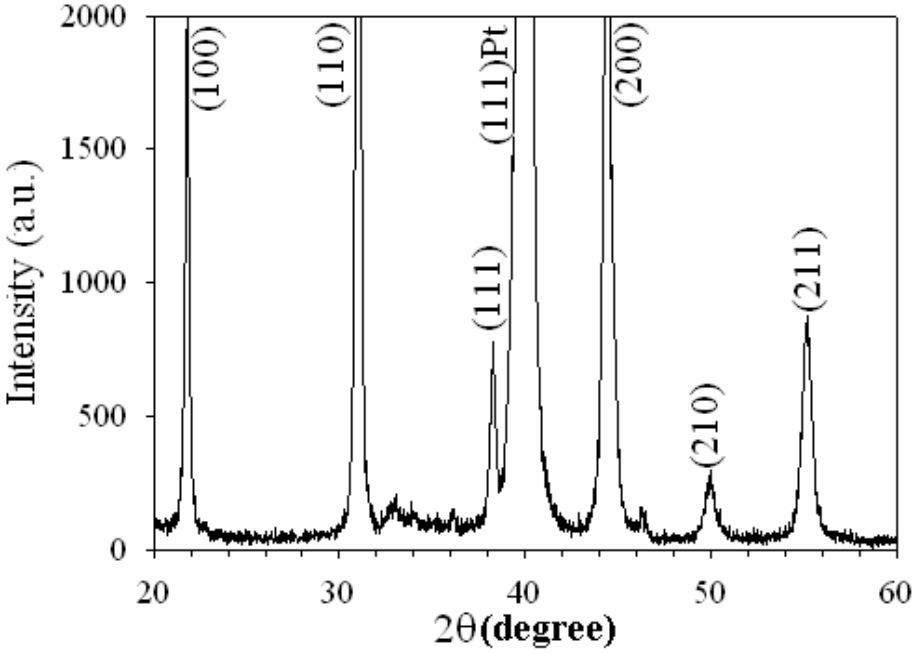

Figure 3.7 XRD pattern of PZT film with x=0.52.

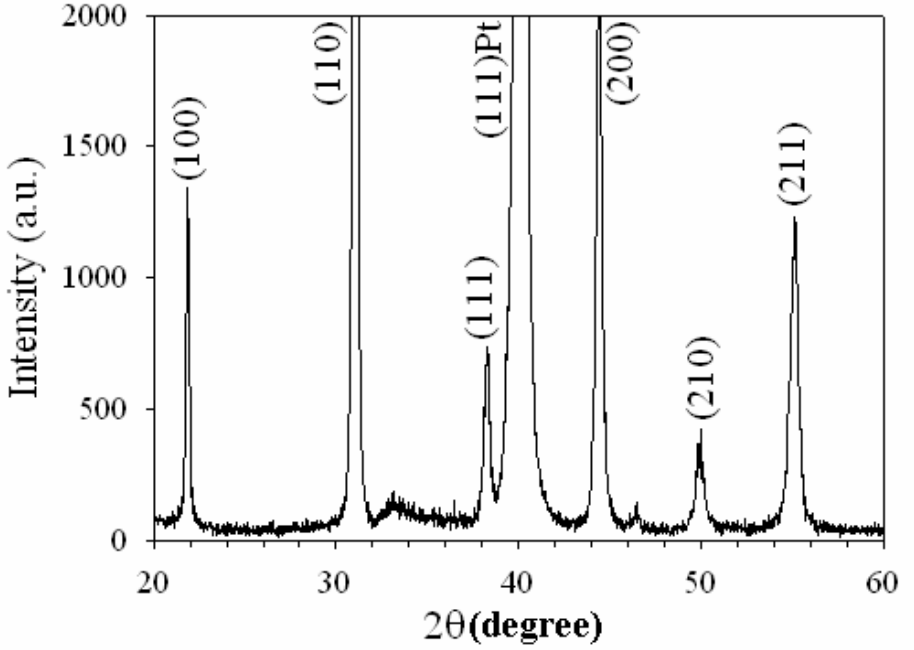

Figure 3.8 XRD pattern of PZT film with x=0.60.

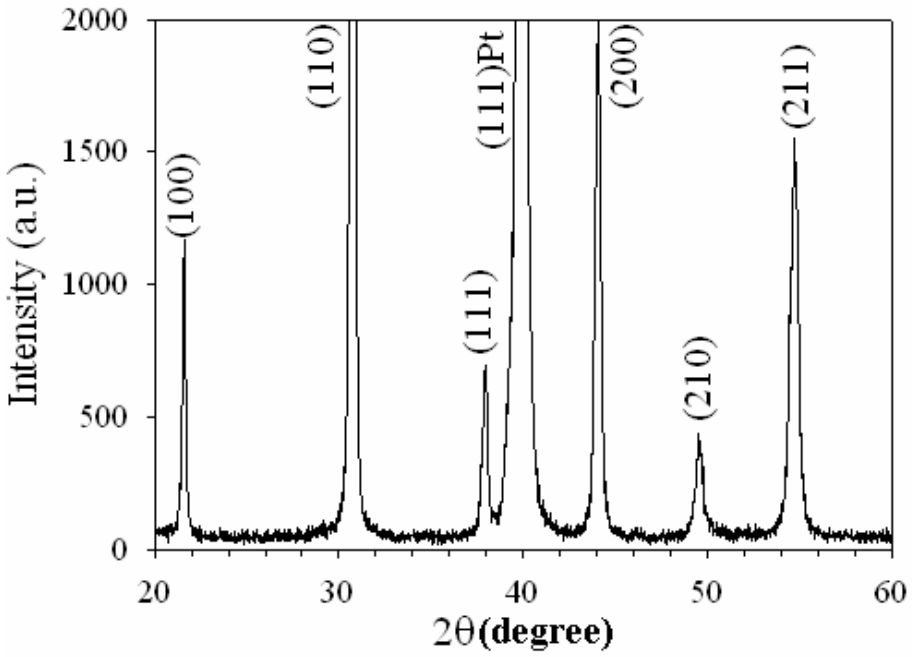

Figure 3.9 XRD pattern of PZT film with x=0.70.

The splitting of the peaks at 2θ of 21.7˚ 31.2˚ and 44.8˚ (in Fig.3.5 and Fig.3.6) can be clearly observed in the film fabricated from the solution with a changing Zr/Ti ratio from 30/70 to 40/60. This means that these films crystallize in the tetragonal phase. The splitting peaks are the nature of tetragonal and rhombohedral crystallographic structure of the films. For the tetragonal structure (100) and (001) is the splitting of the rhombohedral peak at 2θ near 22˚, (110) and (101) of R(*hkl*) at 31.5˚, (200) and (002) of R(*hkl*) at 44.5˚, (220) and (202) of R(*hkl*) at 50˚, (210) and (201) of R(*hkl*) at 50˚, (112) and (211) of R(*hkl*) at 56˚. The films fabricated from the solution with Zr/Ti ratios of 70/30, 60/40 and 52/48 displayed single (unsplit) peaks due to the predominance of the rhombohedral phase. Calculated lattice parameters corresponding to the XRD data were summarized in Table 3.3. Average lattice constants as a function of Zr/Ti ratio were illustrated in Fig. 3.10.

Table 3.3 Summary of the Bragg planes, 2θ, d_{hkl}, and lattice parameters of the uniform PZT films with the Zr/Ti ratios ranging from 30/70 to 70/30.

Zr/Ti	(hkl)	2θ	d_{hkl} (Å)	Lattice parameters (Å)
30/70	(001)	21.42	4.1490	c_t=4.1490
	(100)	22.28	3.9908	a_t=3.9908
	(110)	31.64	2.8283	a_t=3.9998
	(111)	38.52	2.3375	a_t=4.0011
40/60	(001)	21.52	4.1300	c_t=4.1300
	(100)	22.14	4.0157	a_t=4.0157
	(110)	31.34	2.8547	a_t=4.0371
	(111)	38.44	2.3422	a_t=4.0216
52/48	(100)	21.80	4.0776	a_r=4.0776
	(110)	31.02	2.8834	a_r=4.0777
	(111)	38.26	2.3528	a_r=4.0751
60/40	(100)	21.86	4.0665	a_r=4.0665
	(110)	31.08	2.8780	a_r=4.0701
	(111)	38.30	2.3505	a_r=4.0711
70/30	(100)	21.60	4.0702	a_r=4.1149
	(110)	30.74	2.9091	a_r=4.1140
	(111)	37.92	2.3731	a_r=4.1103

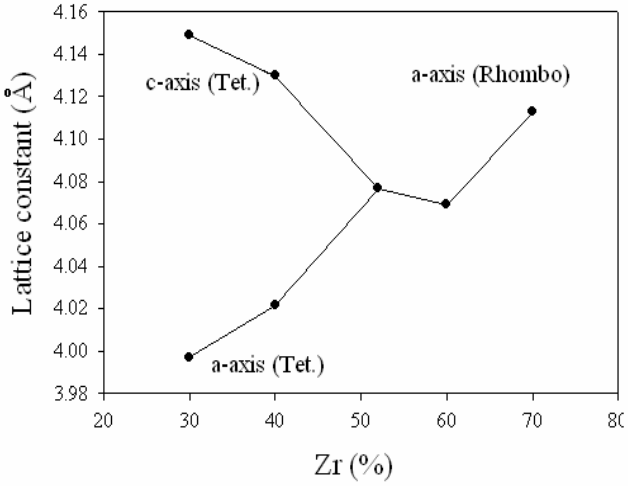

Figure 3.10 Average lattice constants *vs* Zr/Ti ratios of the PZT films.

3.4.3 Microstructure characterization as a function of the composition of PZT

The SEM micrographs of the PZT films with different Zr/Ti ratios are shown in Figs. 3.11-3.14.

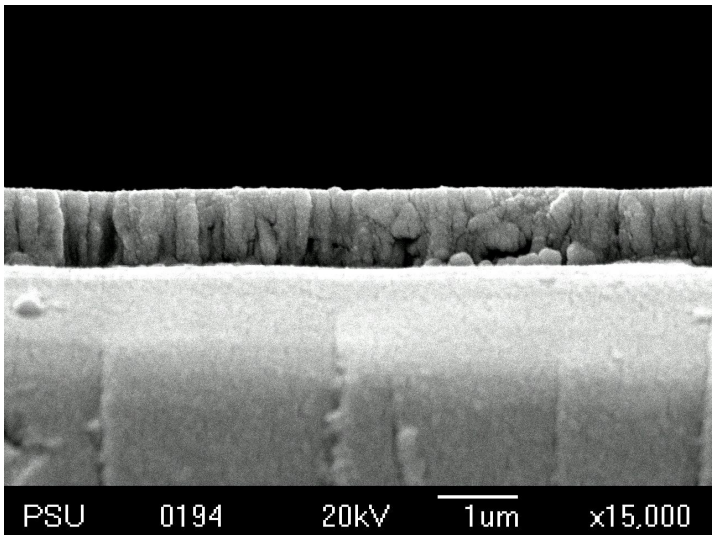

Figure 3.11 SEM cross sectional image of the 1-μm thick PZT film (x=0.52).

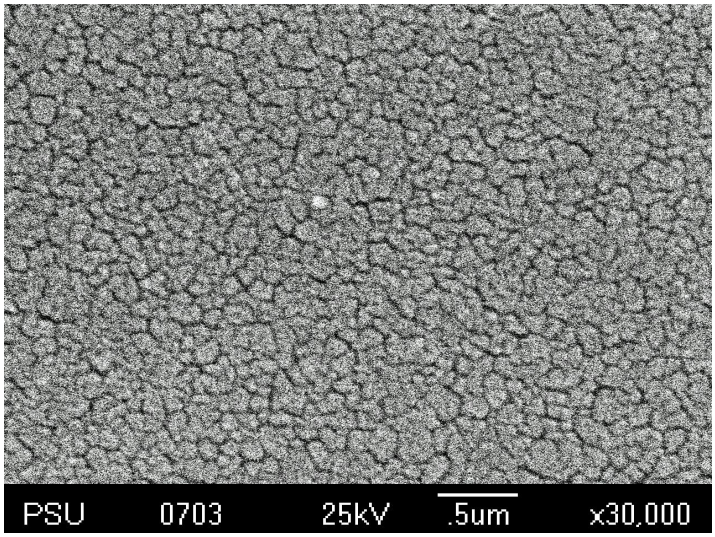

Figure 3.12 SEM planar image of 1-μm thick PZT film (x=0.3).

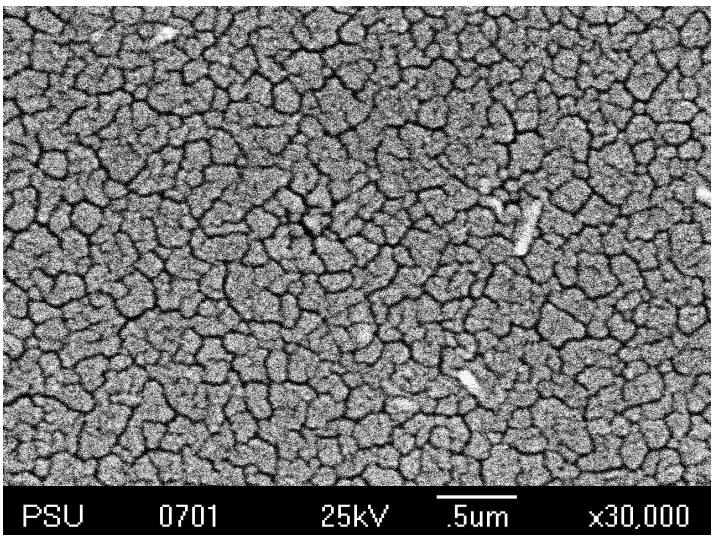

Figure 3.13 SEM planar image of 1-µm thick PZT film (x=0.52).

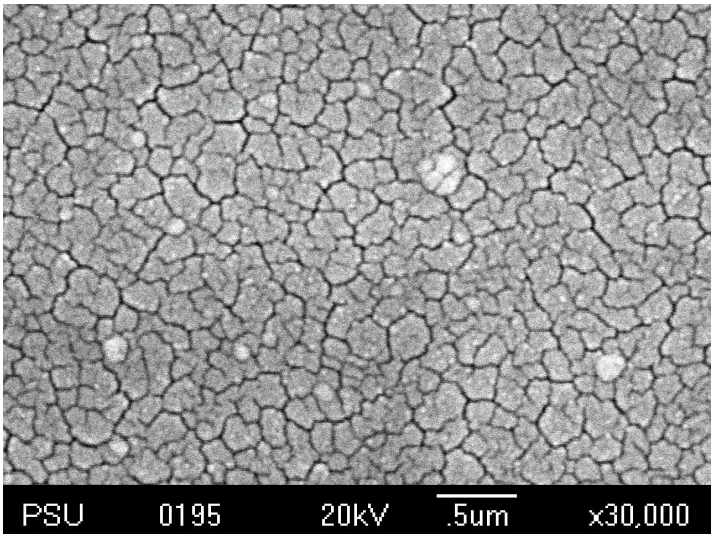

Figure 3.14 SEM planar image of 1-µm thick PZT film (x=0.7).

Cross-sectional SEM micrograph indicated a well-aligned columnar structure (Fig.3.11). The SEM micrographs (Figs. 3.12-3.14) show the surface texture of continuous and fine grain of the PZT films. The composition-dependent grain size of the films was observed. The Zr-rich film has a relatively larger grain than that of Ti-rich films. It is related to the growth energy which is different in different crystallizing phases. This trend is similar to those reported in the literature (Zhang and Whatmore, 2001; Kim *et al.*, 2003).

3.4.4 Electrical characterization as a function of the composition of PZT

The electroded film was measured the dielectric constant within the frequency range of 10^2 to 10^6 Hz, and the results are presented in Fig. 3.15. Values of the dielectric constant ($\varepsilon_r^{'}$) and dielectric loss ($\tan\delta$) measured at 1 kHz for all films are summarized in Table 3.4. The *P-E* hysteresis loops recorded for all films are shown in Fig.3.16.

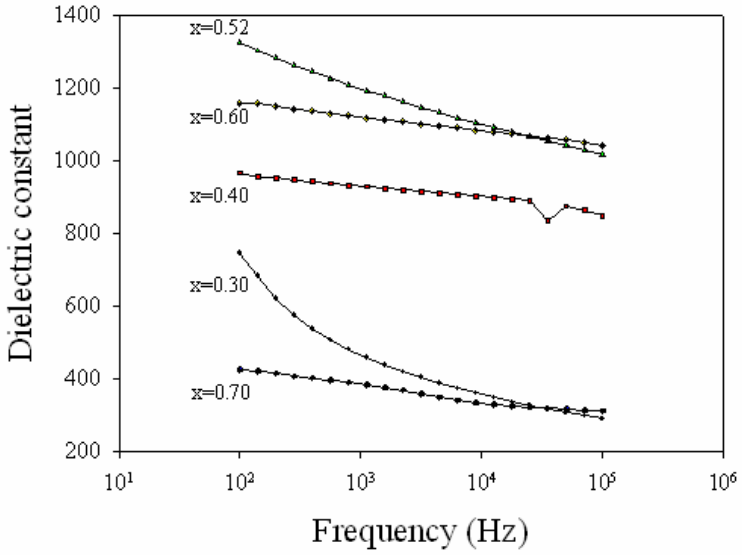

Figure 3.15 Dielectric constant *vs* frequency of the PZT films with different x values.

Table 3.4 The dielectric constant and dielectric loss tangent at 1 kHz of all uniform PZT films studied in this work.

Zr/Ti	30/70	40/60	52/48	60/40	70/30
$\varepsilon_r^{'}$	458	929	1194	1119	384
tan δ	0.012	0.026	0.025	0.047	0.393

$\varepsilon_r^{'}$ values are much larger in the rhombohedral films and its maximum value was from the film at a Zr/Ti ratio of 52/48. This composition is located at the MPB, where there is a peak in the spontaneous polarization and the reorientation of domains under applied field is maximized (Bell and Moulson, 1985).

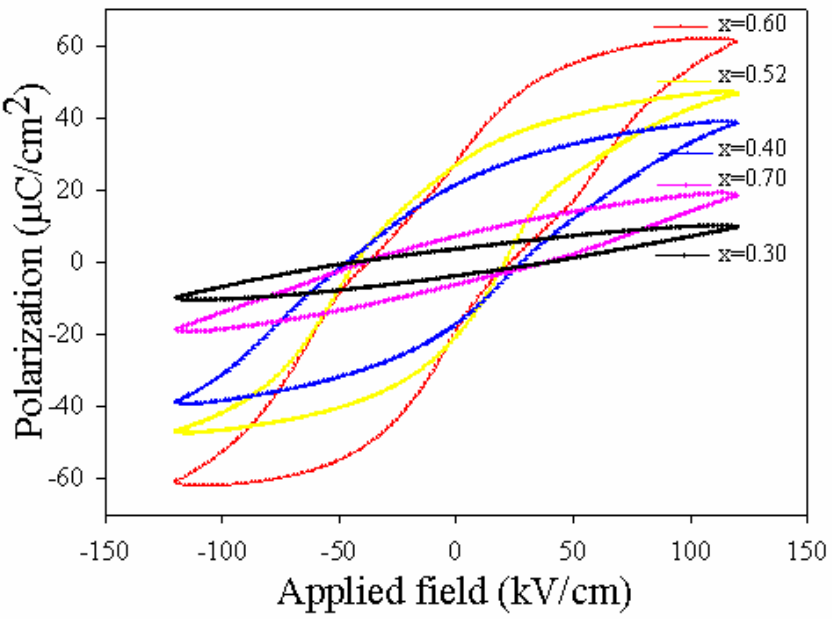

Figure 3.16 *P-E* hysteresis loops for $Pb(Zr_xTi_{1-x})O_3$ films.

Table 3.5 *P-E* hysteresis data for PZT films.

$Pb(Zr_xTi_{1-x})O_3$	P_r ($\mu C.cm^{-2}$)	P_s ($\mu C.cm^{-2}$)	E_c ($kV.cm^{-1}$)
x=0.3	14.7	38.4	32
x=0.4	19.2	31.8	87
x=0.52	23.7	45.0	72
x=0.6	20.1	53.7	20
x=0.7	7.6	31.2	91

Figure 3.16 illustrates the *P-E* hysteresis loop of the PZT films with different compositions. The film with MPB composition exhibits the highest saturation and remanent polarization among all the films studied. This trend is similar to the bulk data and this behavior has been also found elsewhere (Klee *et al.*, 1993; Gong *et al.*, 2004). The *C-V* curves (Fig. 3.17) reveal the dielectric nonlinearity and

hysteresis in ferroelectric thin films. The expected butterfly-type shapes are the natural result of switching behavior where the maximum occurs near the coercive voltage. This is due to the large number of coexisting domain walls at these voltages.

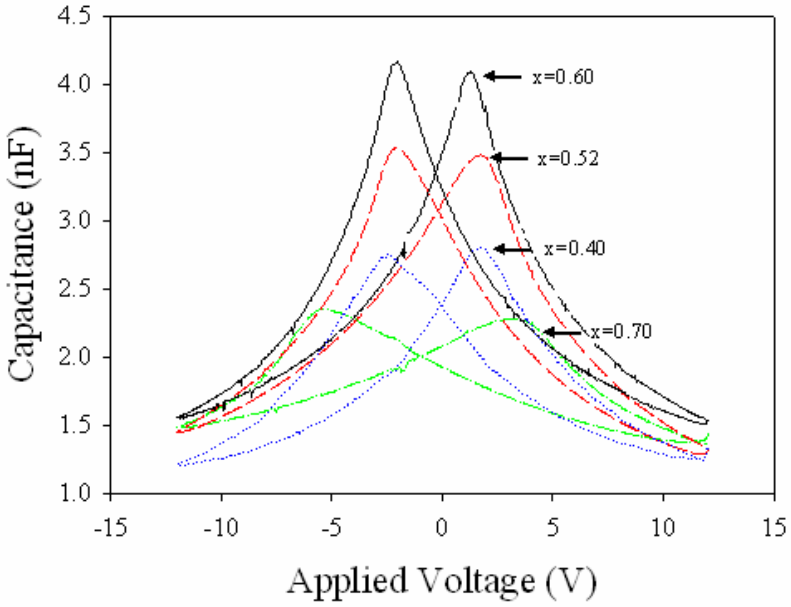

Figure 3.17 *C-V* curves for PZT films with different x values along the solid solution $Pb(Zr_xTi_{1-x})O_3$.

Figs. 3.18-3.20 show the piezoelectric response of poled PZT thin films measured at 5 kHz. The piezoelectric coefficient d_{33} for each film was determined from a slope of each graph by the use of Eq. 3.1. Owing to a film was rigidly glued to a substrate, the measured coefficient is the so-called clamped or apparent value. These values were listed in Table 3.6.

Table 3.6 The piezoelectric coefficient d_{33} of poled films of the system $Pb(Zr_xTi_{1-x})O_3$.

PZT film composition	Clamped d_{33} ($pm.V^{-1}$)
x = 52 (unpoled)	11.6 ± 0.5
x = 40	44.3 ± 0.5
x = 52	117.5 ± 0.5
x = 60	41.0 ± 0.5

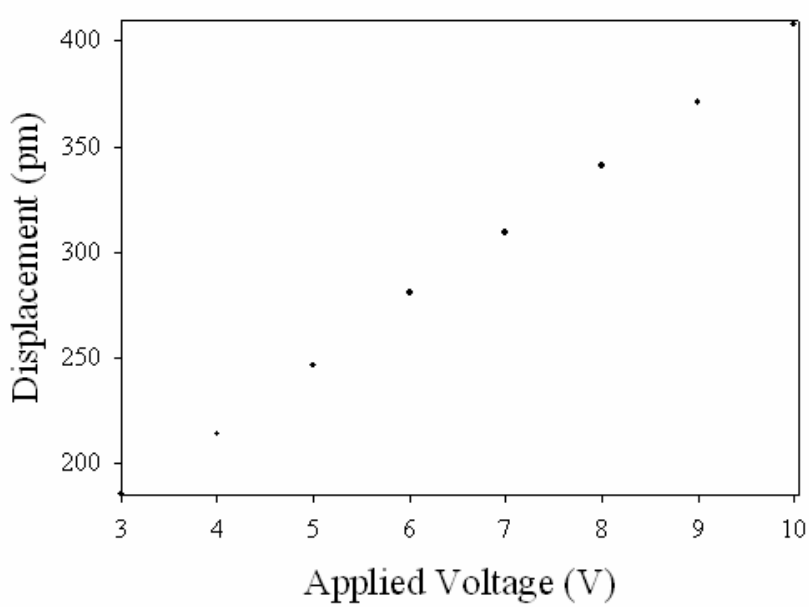

Figure 3.18 Variation of surface displacement with applied voltage for 200 nm-$Pb(Zr_xTi_{1-x})O_3$ film (x=0.40).

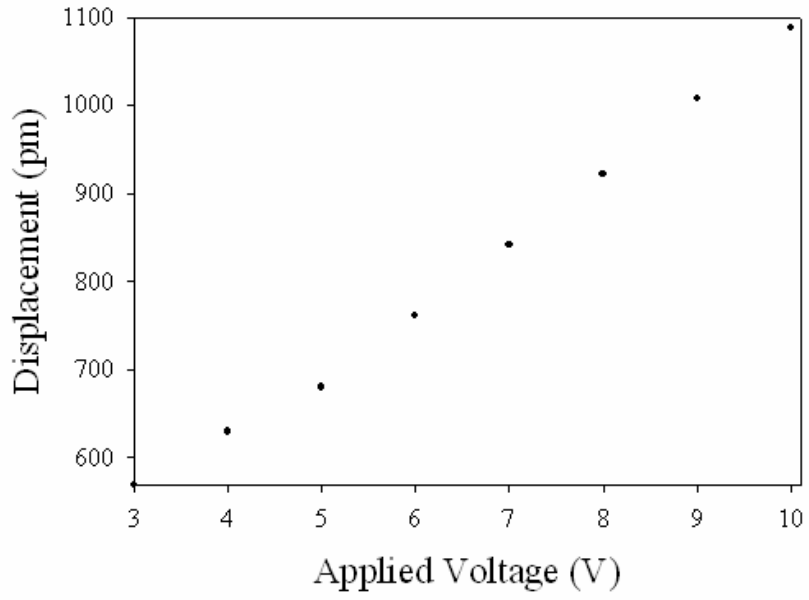

Figure 3.19 Variation of surface displacement with applied voltage for 200 nm-$Pb(Zr_xTi_{1-x})O_3$ film (x=0.52).

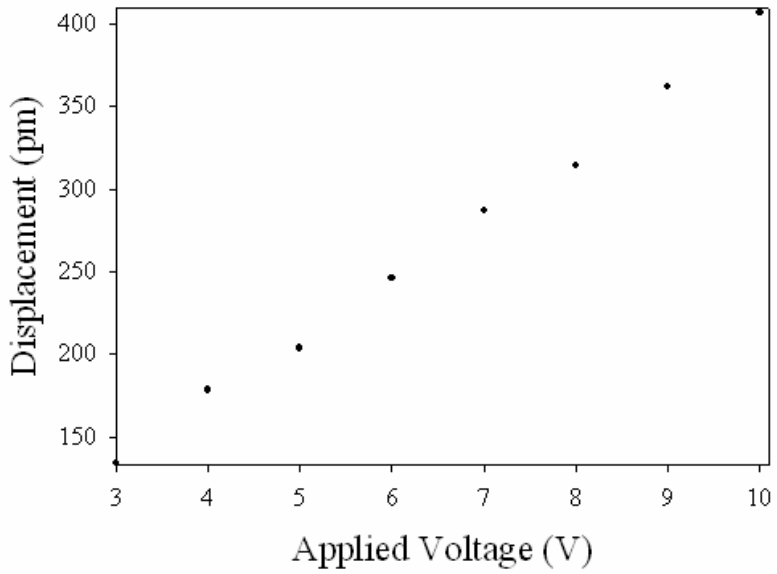

Figure 3.20 Variation of surface displacement with applied voltage for 200 nm-$Pb(Zr_xTi_{1-x})O_3$ film (x=0.60).

The largest d_{33} coefficient value of 117.5 $pm.V^{-1}$ was obtained from the poled PZT film with MPB composition. The peaking in the d_{33} coefficient of the 52/48 PZT film is identical to that of the bulk PZT ceramic but the magnitude was considerably smaller. All of the films required a minimum electric field to produce a linear displacement-applied voltage response. These fields are 25 $MV.m^{-1}$ for 52/48 PZT, and 15-20 $MV.m^{-1}$ for the other films. The measured displacement at a zero applied field was possibly due to the clamping effect which leads to the built-in strain in a structure.

As the MPB PZT thin film exhibits a large d_{33} coefficient, this film is attractive for MEMS applications such as actuator, sensor, and transducer structures for most MEMS application based on piezoelectric laminated beams and membranes (Uchino, 2000). A piezoelectric film sandwiched between a bottom and a top electrode (Fig.3.21) senses the strains caused by deflections, or actuates a bending by means of piezoelectric stresses. In both the direct (sensor) and the converse (actuator) case, the same effective piezoelectric coefficient d_{31eff} is needed to describe the piezoelectric interaction (Muralt, 2000). In this work, d_{31eff} = 59 $pm.V^{-1}$ for the PZT x=0.52 ($d_{31}=d_{33}/2$).

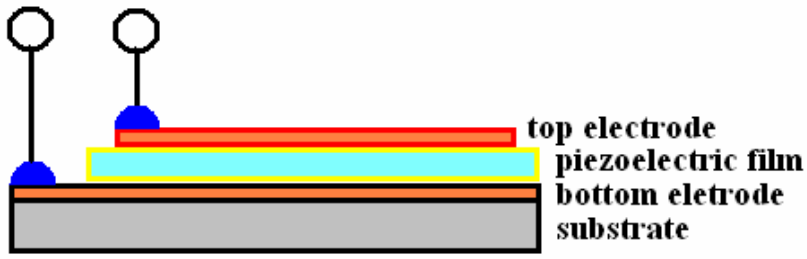

Figure 3.21 Schematic cross section through a piezoelectric laminated cantilever.

3.5 Conclusions

Single-composition $Pb(Zr_xTi_{1-x})O_3$ films (x=0.30, 0.40, 0.52, 0.60 and 0.70) of about 1 μm in thickness were prepared on $Pt/Ti/SiO_2/Si$ substrates at the annealing temperature of 600 ºC by a 2-methoxyethanal sol-gel route. Strong dependence of the microtexture and electrical properties as a function of the composition were observed in these films.

Ferroelectric properties of PZT films were investigated as functions of Zr/Ti ratio. The optimal P_r value of 23.7 $\mu C.cm^{-2}$ was observed for PZT 52/48. The low E_c field of 72 $kV.cm^{-1}$ and high dielectric constant of 1194 suggests that the films are promising for MEMS applications.

The interferometer technique was applied for the measurement of the apparent piezoelectric coefficient d_{33} of the $Pb(Zr_xTi_{1-x})O_3$ films. The coefficient of the films were strongly depended on the Zr/Ti ratio. The d_{33} values were found to be 44.3, 117.5, and 41.0 $pm.V^{-1}$ for the composition x=0.4, x=0.52, and x=0.6, respectively. This result suggests that the piezoelectric properties of the thin film are markedly different than those of a bulk material of identical composition. This difference is apparently due to the clamping effect at the substrate which causes unrelaxed stresses within the films.

CHAPTER 4

FERROELECTRIC AND PIEZOELECTRIC PROPERTIES OF COMPOSITIONALLY GRADED PZT FILMS

4.1 Introduction

Ferroelectric thin films have been developed rapidly in recent years due to their potential for important device applications, including capacitors, infrared detectors, SAW-delay lines, sensors and actuators, optical switches, non-volatile memories, *etc*. (Kholkin *et al*., 2002; Whatmore *et al*., 2003). Recent developments in MEMS have opened new potential applications of ferroelectric thin layers in micro-positioning, actuation and infrared sensors (Muralt *et al.*, 1995; Yi, Wu, and Sayer, 1988). Lead zirconate titanate solid solution $Pb(Zr_x,Ti_{1-x})O_3$ (PZT) is a well known piezoelectric system that can be used as an active element in MEMS for both microsensor and microactuator applications (He *et al*., 2001). Another property is their giant pyroelectric coefficients (Tang, Chan, and Ding, 2003; Tang *et al*., 2004).

The concept of "graded ferroelectric structures" (GFS) was developed at the beginning of 90's. The basic principle of this structure is to have a polarization gradient, that can be induced either by introducing a concentration gradient, a temperature gradient or a stress gradient (Felberg *et al.*, 2001; Poullain *et al*., 2002; Bouregba *et al*., 2003). Among several interesting properties of GFS based on different materials, the most intriguing is the shift up or down along the polarization axis under an applied ac field, leading to a so-called polarization offset (Brazier, McElfresh, and Mansour, 1998, Pintilie, Boerasu and Gomes, 2003; Ban, Alpay and Mantese, 2003a; Bouregba *et al.*, 2003). This unconventional hysteresis behaviour is strongly depend on the direction of the polarization gradient (Brazier, McElfresh, and Mansour, 1998). The subject of GFS is thus very interesting and offers large possibilities for study. In the present work, the PZT solid solution of which the chemistry is well developed has been chosen and the sol-gel method has been used for changing the Zr/Ti ratio from one layer to another to obtain the compositionally

graded PZT films. The properties of component materials are then studied relating to the overall properties of the structure.

4.2 Review of Previous Work

Functionally graded microstructures (FGMs) are inhomogeneous materials of which the material properties vary continuously in one (or more) direction(s). This is achieved by gradually changing the composition of the constituent materials along one direction, usually the thickness direction from one surface to another. FGM was first developed by the Japanese in the late 1980s, Yamanouchi *et al.* (1990). FGMs have found extensive applications in various industries due to their superior thermo-mechanical properties (Obata and Noda, 1996; Praveen and Reddy, 1998).

FGMs with a gradient of piezoelectric properties can be used for ultrasonic transducers and bending actuators (Zhu and Meng, 1996). Actuators usually have a non-uniform distribution of stresses in the metal-ceramic interfaces. In addition, the bonding between the metal and ceramic components may crack or peel off at low temperature and may creep at high temperature, which could lead to reliability and lifetime limitations.

He *et al.*, (2001) present a finite element formulation based on the classical laminated plate theory of the shape and vibration control of the functionally graded material plates with integrated piezoelectric sensors and actuators. Wu *et al.*, (2002) presented a high order theory of piezoelectric generic shells with graded material properties in the thickness direction. This theory examined the electromechanical behavior of different types of charge equations, depending upon whether the driving signal of piezoelectrics is free charge or electric voltage. Takagi *et al.* (2003) investigated the properties of the PZT/Pt composites under purpose of developing a PZT/Pt FGM actuator with enhanced mechanical reliability.

Taya *et al.* (2003) designed FGMs to reduce the stress concentration at the middle interface that exists in the standard bimorph actuators while maintaining high bending displacement. The bending displacements of these actuators are then being measured as a function of applied voltage. The measured data of the bending

displacements versus applied voltage are compared with the predictions by the classical laminate theory (CLT). Chen, Ma and Li (2004) fabricated the FGM monomorph actuator by the electrophoretic deposition (EPD) technique. The fabrication process is described in detail as well as its graded microstructure. The principle of the monomorph is discussed in this work and the expression for the theoretical bending displacement is derived. Good agreement is observed between the theoretical predictions and the experimental results.

Electrical properties of a graded ferroelectric were investigated by many authors. Unlike homogenous ferroelectrics, graded ferroelectric devices display strikingly new behavior, the most notable being a translation of the hysteresis loop along the polarization axis (Schubring *et al.*, 1992).

Bao, Mizutani and Zhang (2000) prepared the compositionally graded (Pb,La)TiO_3 thin films on Pt/Ti/SiO_2/Si substrates. The excellent dielectric properties and large polarization offsets were observed. They suggest that the compositionally graded PLT thin films are promising for various device applications.

In previous work reported by Brazier McElfresh and Mansour (1998) and Bouregba *et al.* (2003), thin film lead zirconate titanate (PZT) capacitors with composition gradients normal to the substrate were fabricated using pulsed laser deposition. These PZT thin film capacitors exhibited large polarization offsets when driven by an alternating electric field. The direction of the offsets depended on the direction of the gradient with respect to the substrate. The largest offset, greater than 400 $\mu C.cm^{-2}$ when driven with a 50 $V.mm^{-1}$ field, was nearly an order of magnitude greater than any results reported for other graded ferroelectric films. They have shown that anomalous hysteresis loops can be obtained in case of graded ferroelectric devices (GFDs) structures. The shift of the hysteresis loop along the polarization axis seems to be produced by the differences between polarization values in the component layers. Vilquin *et al.* (2003a) show that the graded nature of the film alone does not seem to be sufficient to observe a polarization offset. They suggest that asymmetrical leakage currents may be at the origin of this offset. Vilquin *et al.* (2003b) found that the polarization off-set is depending on the crystal orientation and texture of the analyzed samples. They concluded that the graded nature of GFDs alone is not sufficient for observation of polarization offset. Brazier, McElfresh, and Mansour

(1999) reported the origin anomalous polarization offsets in compositionally graded $Pb(Zr,Ti)O_3$ thin films. They suggested that the hysteresis loop offsets are not necessarily due to a large static polarization of the sample. From these results, the hysteresis loop came from the development of a *dc* offset *voltage*, rather than a large static polarization, across the sample capacitor; similarly to the results from Bouregba, Rhun, and Poullain (2005).

Bouregba, Rhun, and Poullain (2005) have demonstrated that significant shifts of hysteresis loops may be observed on non-graded ferroelectric films using a Sawyer-Tower circuit if the input resistance of the oscilloscope channel (R_{osc}) and sense capacitor (C_{st}) are large enough. This is possibly caused by the difference in the work functions of the top and bottom electrodes. The observation of hysteresis offsets are, therefore not the characteristic and exclusive feature of graded structures. The shifts of hysteresis loops can also be originated from asymmetrical leakage currents.

The present chapter contains the fabrication of step-GFS (up and down graded) of the sol-gel PZT films. The ferroelectric and piezoelectric properties of the films are characterized and correlated to the composition of the constituent materials containing in the GFS.

4.3 Materials and Methods

Compositionally graded $Pb(Zr_xTi_{1-x})O_3$ thin films with Zr/Ti ratio varying from 40/60 to 60/40 on $Pt(111)/Ti/SiO_2/Si(100)$ substrates were prepared by a simple sol–gel process (Budd, Dey and Payne, 1985; Perez, Vilarinho and Kholkin, 2004). The nominal compositions of the solutions are $Pb(Zr_xTi_{1-x})O_3$ (x= 0.40, 0.52, and 0.60), the precursor with 10% excess Pb composition was prepared on purpose to compensate for the lead loss in the deposition processing. The PZT solution was prepared in the same procedure as shown in Fig. 3.1.

The PZT solution was spin coated onto $(111)Pt/Ti/SiO_2/Si$ substrates and the sequence of the deposition used were different. From an example shown in Fig. 4.1, the sequences were x=0.40, x=0.52 and x=0.60 and this was an up-graded PZT film which was noted as PZT 40/52/60. For the down-graded PZT film, the

sequence was reversed and the film was noted as PZT 60/52/40. All of the samples were listed in Table 4.1. The spinning speed of 3000 rpm for 30 s was used for the deposition and each deposited layer was dried in air at 150 ºC for 5 min. Each concentration was repeated three times so that the overall structure consisted of nine layers. The graded PZT thin films with nine layers were pre-annealed in air at 400 ºC for 30 min. The following procedure was the annealing at 650 ºC for 30 min using a rapid thermal annealing (RTA) in oxygen atmosphere (Araujo and Eiras, 2000).

Table 4.1 List of samples denoted according to the sequences of the deposition of Zr concentration in the solid solution $Pb(Zr_xTi_{1-x})O_3$

Sample	Sequences of Zr%
M1	x=0.40 and x=0.60
M2	x=0.60 and x=0.40
M3	x=0.40, x=0.52 and x=0.60
M4	x=0.60, x=0.52 and x=0.40

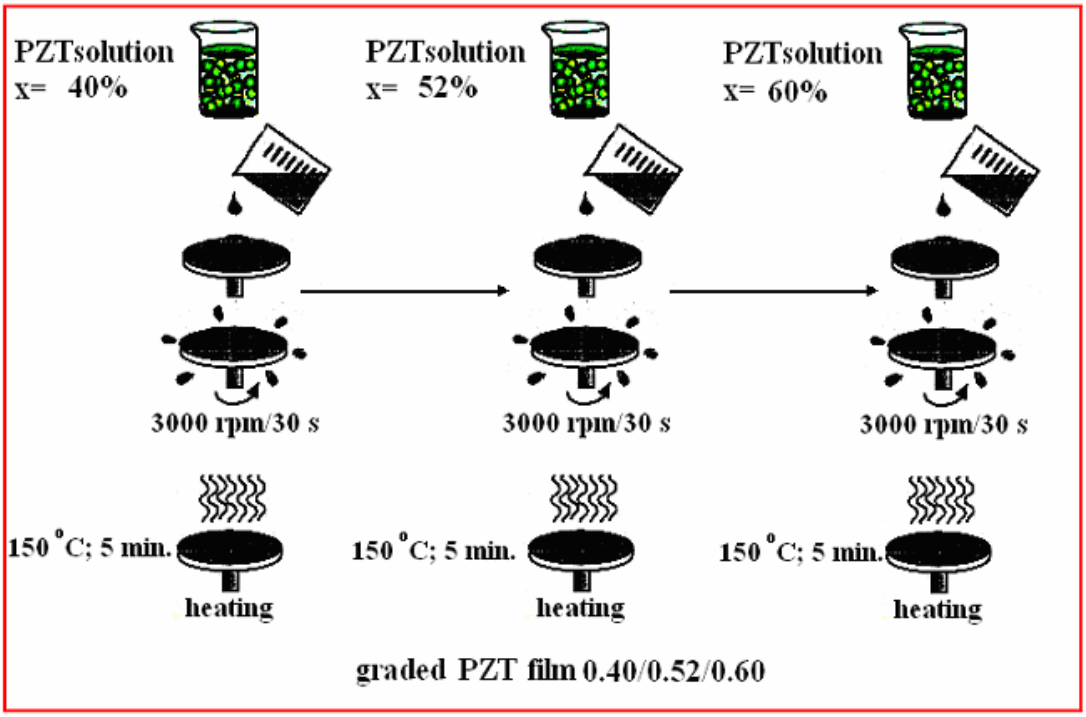

Figure 4.1 Flow chart of the spin coating of the graded PZT film.

The graded PZT thin films on a Pt/Ti/SiO_2/Si substrate were investigated by an X-ray diffractometer (Philips X'pert X-ray diffraction (XRD) system) with Ni filtered Cu Kα radiation. Microstructural analysis was performed by scanning electron microscopy (JEOL 5800) formed by a scanning electron microscope operating at 200 kV (JEOL2000 FX EM) with a Link AN-10000 EDXS system.

In order to investigate the electrical properties of the thin films; 100-nm thick Au layer of 0.8 mm diameter was sputtered on the surface of the films. The ferroelectric hysteresis loop was observed using a TF Analyzer 2000; the dielectric constant and dielectric loss (tan δ) were measured by an HP4284A LCR meter with a small *ac* signal of 100 mV.

The piezoelectric coefficient of the films was measured by using the single-beam Michelson interferometer described earlier in chapter 3.

4.4 Results and Discussion

4.4.1 X-ray characterization of the compositionally graded PZT film

Figures 4.2-4.5 show the XRD patterns of compositionally graded $Pb(Zr_xTi_{1-x})O_3$ films with different sequences of Zr deposition. The XRD data showed a perovskite structure without preferred orientation. For M1 (Fig.4.2) and M3 (Fig.4.4), they were highly (100) and (200) oriented. For M2 (Fig.4.3) and M4 (Fig.4.5), the mixture of perovskite and pyrochlore phases (Py) was observed. This was because the annealing was not enough for a complete crystallization of the perovskite phase. The lattice parameters extracted from and XRD patterns of Figs.4.2-4.5 and Figs.4.6-4.8 are calculated and summaried in Table 4.2. It is noted that the diffraction peaks of the graded films are broad comparing with those of uniform films. This is due to the fact that there are some difference of the lattice constants between the adjacent layers of different Zr content.

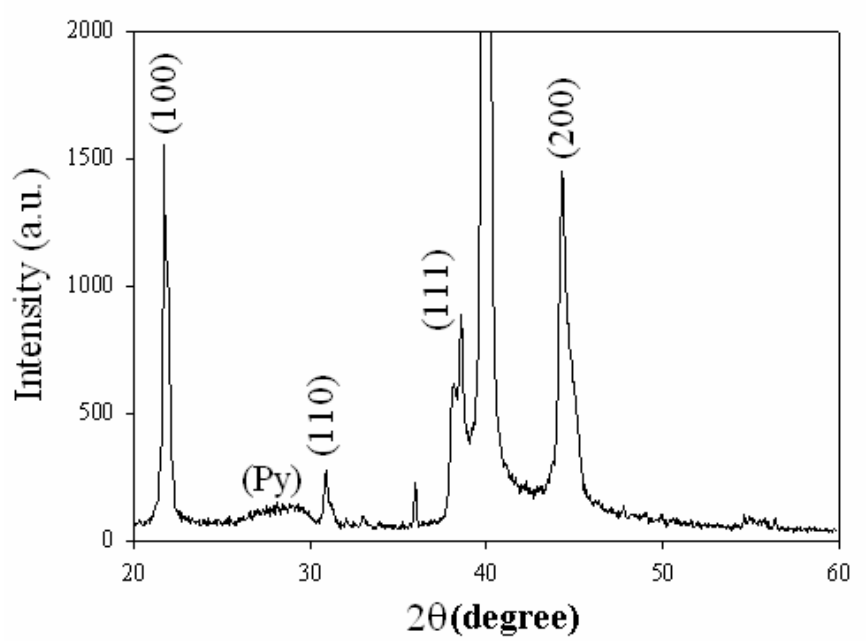

Figure 4.2 XRD pattern of 40/60 graded $Pb(Zr_xTi_{1-x})O_3$ film.

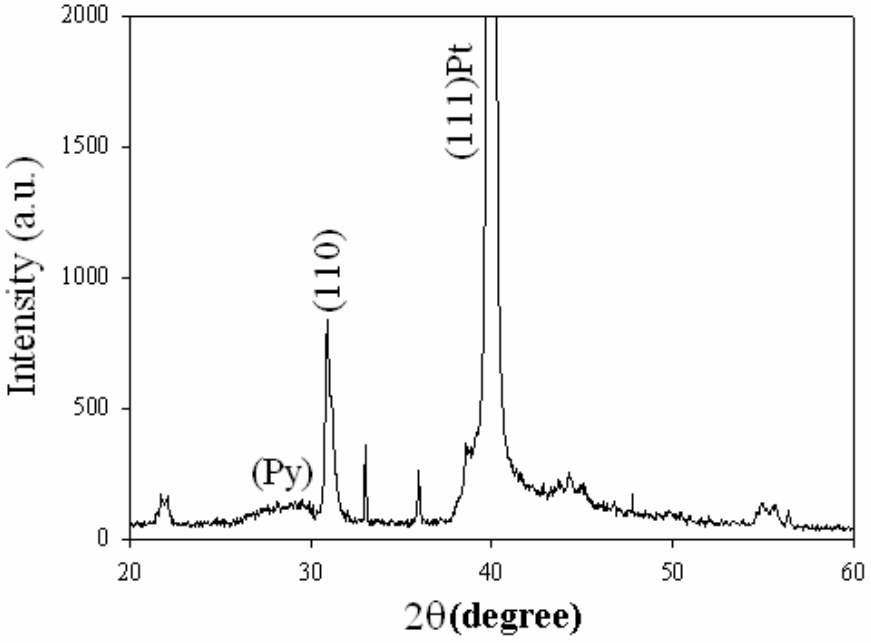

Figure 4.3 XRD pattern of 60/40 graded $Pb(Zr_xTi_{1-x})O_3$ film.

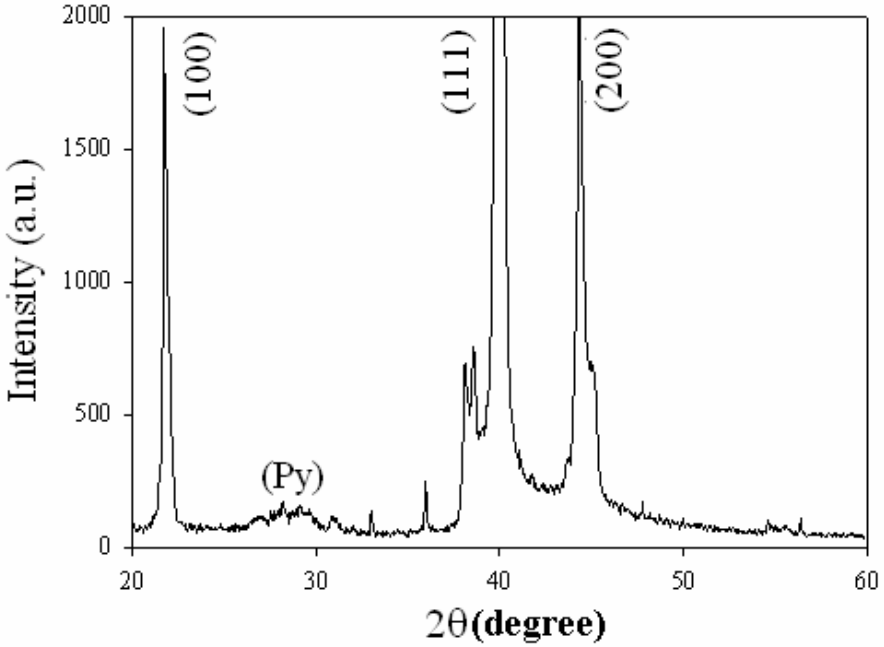

Figure 4.4 XRD pattern of 40/52/60 graded $Pb(Zr_xTi_{1-x})O_3$ film.

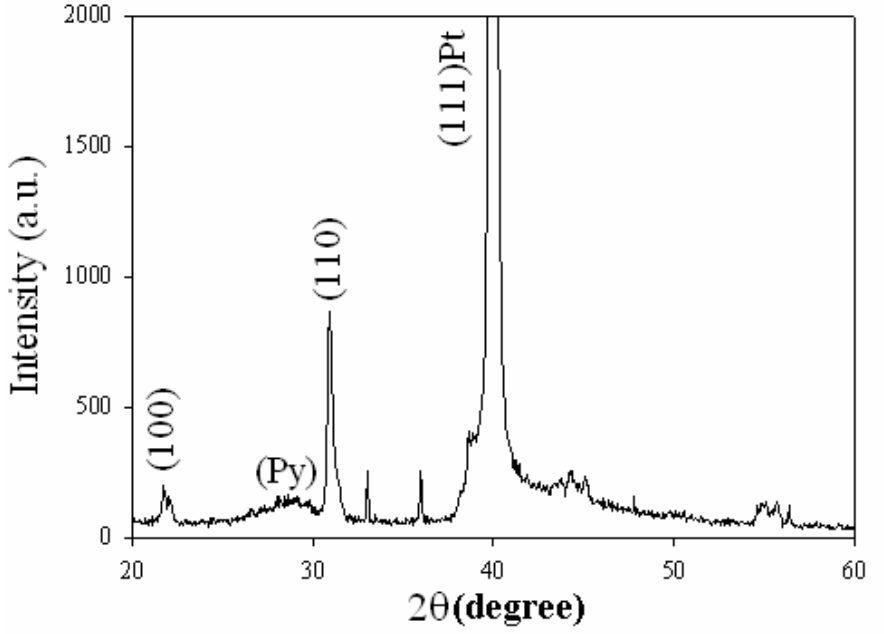

Figure 4.5 XRD pattern of 60/52/40 graded $Pb(Zr_xTi_{1-x})O_3$ film.

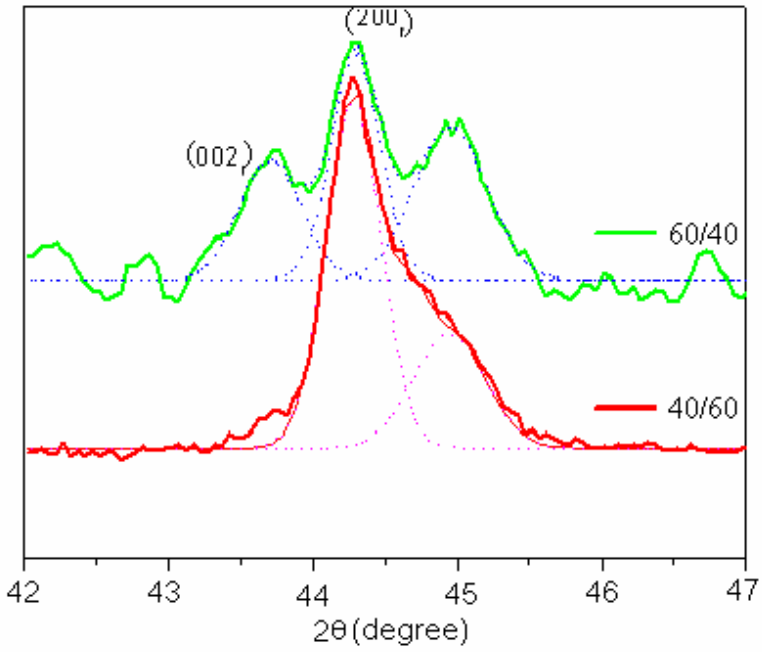

Figure 4.6 XRD spectra of 40/60 and 60/40 graded $Pb(Zr_xTi_{1-x})O_3$ films.

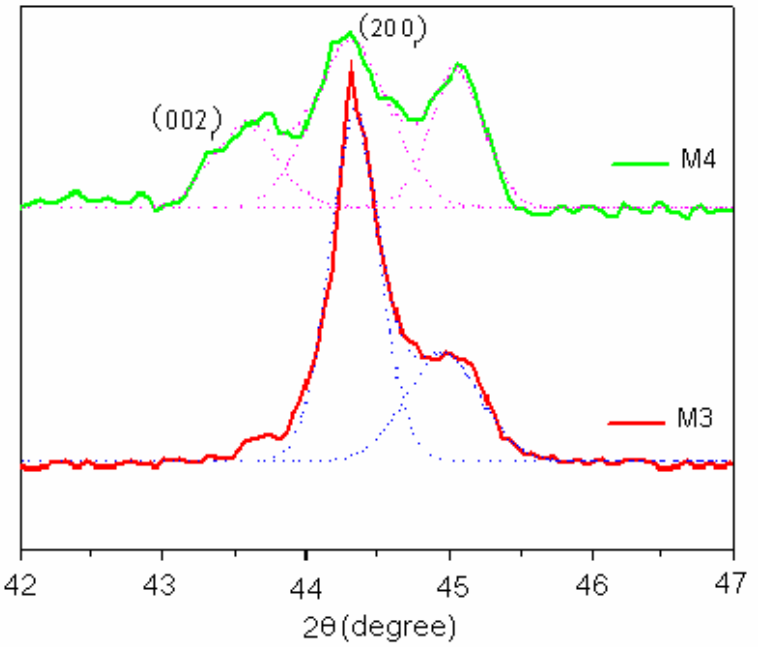

Figure 4.7 XRD spectra of 40/52/60 and 60/52/40 graded $Pb(Zr_xTi_{1-x})O_3$ films.

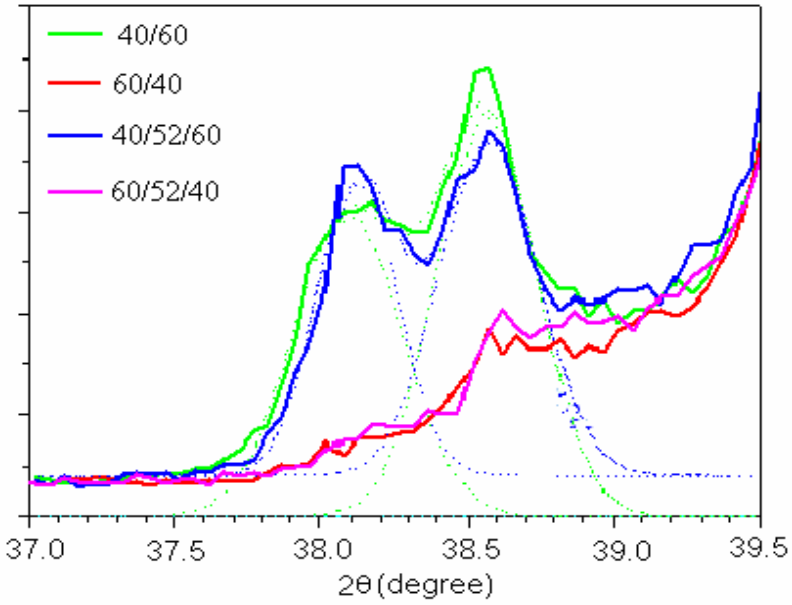

Figure 4.8 Extracted (111) diffraction line in XRD spectra of 40/60, 60/40, 40/52/60 and 60/52/40 graded $Pb(Zr_xTi_{1-x})O_3$ films.

Table 4.2 Summarized parameters extracted from peaks of the graded PZT films.

Sample	Diffraction line	2θ	d_{hkl} Extracted	Parameters (Å)
M1	(100)	21.72	4.0924	$a_t = 4.035$,
	(111)	38.57	2.3346	$a_r = 4.092$,
	(200)	44.27	2.0464	$c_t = 4.075$
M2	(100)	21.72	4.0924	$a_r = 4.091$,
	(110)	30.92	2.8925	a_t=3.9965,
	(111)	38.57	2.3346	$c_t = 4.143$
M3	(100)	21.77	4.0831	$a_t = 4.033$,
	(111)	38.57	2.3346	$a_r = 4.087$,
	(200)	44.87	2.0204	$c_t = 4.070$
M4	(100)	22.07	4.0283	$a_r = 4.088$,
	(111)	30.92	2.8925	$a_t = 4.025$,
				$c_t = 4.155$

4.4.2 Microstructure characterization of the compositionally graded PZT film

Figure 4.9 and 4.10 illustrate the surface texture of continuous and fine-grained microstructure without crack of the PZT films. This means that the grain size of the film is independent of the direction of the gradient compositions of the graded structure up- and down-graded of the PZT films.

Figure 4.11 is a representative cross-sectional SEM images for graded films. The well-defined layers of different x values were observed in PZT M1 (x=0.40/0.60) film. There is no apparent depletion from each other. The total thickness of the three layers is 1 μm and 2 μm for the two layers. The film has grain sizes in a range of 80–100 nm (Fig.4.12). There was a sign of depletion between x=0.40 and 0.52 layers in PZT M4 (x=0.60/0.52/0.40) (Fig.4.13). This is due to the energy growth during the heat treatment process in the x=0.52 layer which is very similar to that of x=0.40 layer (Song, 1998).

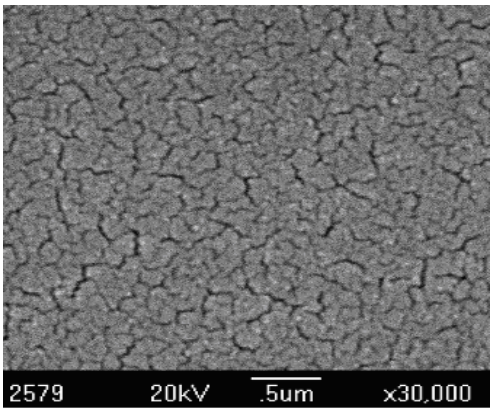

Figure 4.9 SEM planar images of 40/60 graded PZT film.

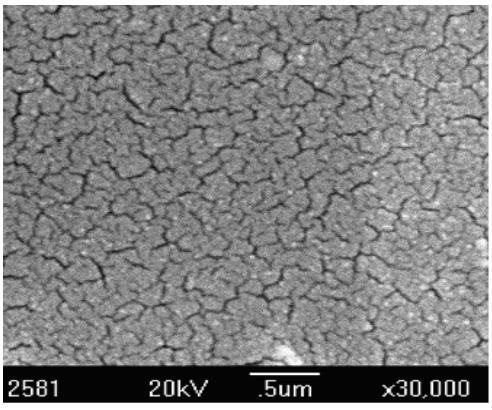

Figure 4.10 SEM planar images of 60/40 graded PZT film.

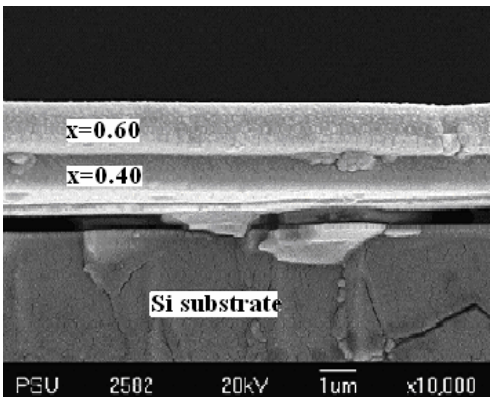

Figure 4.11 SEM cross sectional images of 40/60 graded PZT film.

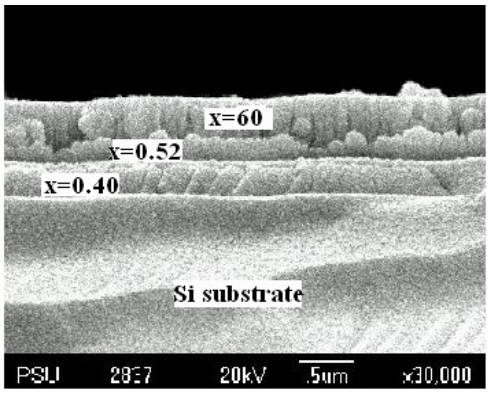

Figure 4.12 SEM cross sectional images of 40/52/60 graded PZT film.

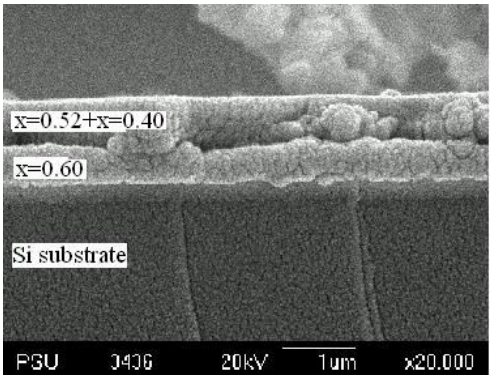

Figure 4.13 SEM cross sectional images of 60/52/40 graded PZT film.

4.4.3 Electrical characterization of the compositionally graded PZT film

Figs.4.14-4.15 show the variations of dielectric constant and dielectric loss as a function of frequency at room temperature.

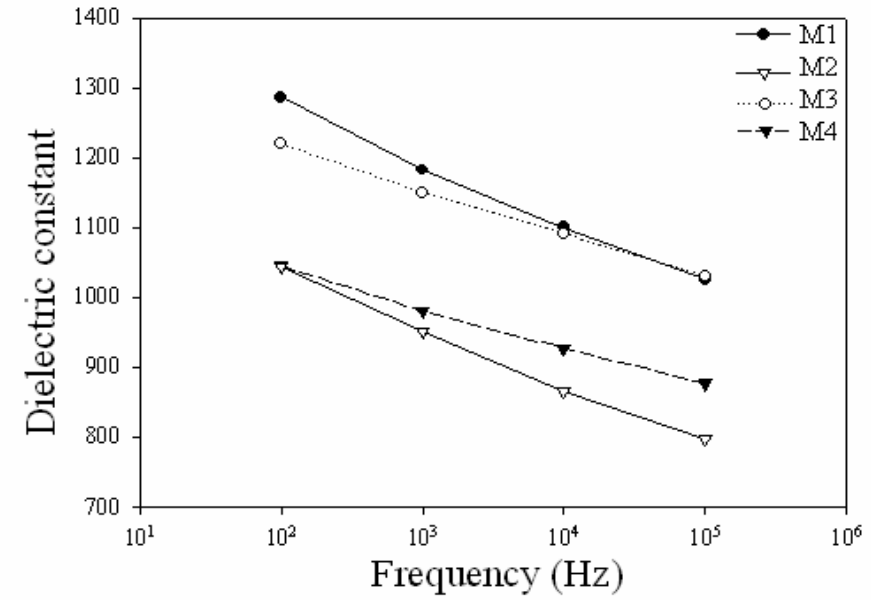

Figure 4.14 Plots of dielectric constant *vs* frequency for graded PZT films.

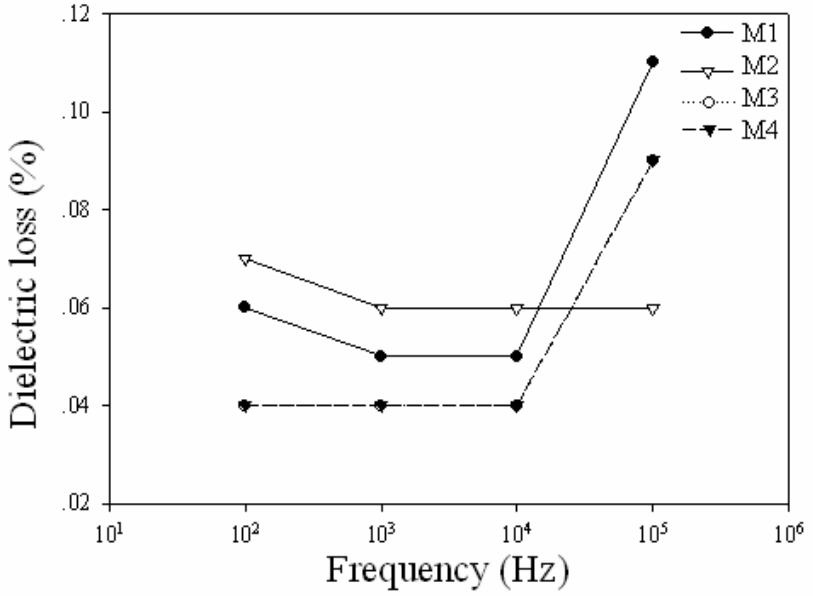

Figure 4.15 Plots of dielectric losses *vs* frequency for graded PZT films.

The dielectric constants measured at 1 kHz for M1, M2, M3 and M4 are 1182, 951, 1150 and 980, respectively. In comparison with single compositionally sol-gel PZT film, graded PZT films possessed the relatively high value of dielectric constant and it was a higher value in up-graded PZT. This was related to a uniform stress distribution in the graded ferroelectric film (Liu, Jiang and Zhu, 2000). In other ferroelectric multilayer, such as $BaTiO_3/SrTiO_3$, the dielectric enhancement previously reported that it was due to the interface space charge effect (Bao, Zhang and Yao, 2000; Bao, Yao and Zhang, 2000; O'Neill, Bowman, and Gregg, 2000; Bao *et al*., 2001a; Bao *et al*., 2001b; Bao *et al*., 2002; Xu *et al*., 2002; Zheng, Chen, and Shen, 2006). At 1 kHz, low dielectric loss of 0.12 – 0.26 was found in the films. The high dielectric loss was clearly obvious at frequencies higher than 10^5 Hz. This was probably because the fact that the graded films contained layers of different lattice parameters in accordance with tetragonal and rhombohedral compositions. Under an applied field with high operating frequency, various lattice-misfit strains between layers became additionally enhanced, resulting in the high dielectric loss in graded films (Yokohama *et al*., 2003).

Figs.4.16 and 4.17 show the well-defined *P-E* hysteresis loops of the graded PZT films. The P_r values and their corresponding coercive field values were summarised in Table 4.3. It is noted that there was no shift of the polarization along the axis. The absence of polarization offset in this work agreed with several work previously reported (Brazier, McElfresh and Mansour, 1999; Poullain *et al*., 2002; Bouregba, Rhun and Poullain, 2005).

Table 4.3 Average values of remanent polarization and coercive field (P_r, E_c) for the graded films; M1, M2, M3 and M4.

Materials/Structure $Pb(Zr_xTi_{1-x})O_3$	P_r+ ($\mu C.cm^{-2}$)	P_r- ($\mu C.cm^{-2}$)	E_c+ ($kV.cm^{-1}$)	E_c- ($kV.cm^{-1}$)
M1	23	-15	23	-51
M2	30	-16	31	-65
M3	27	-15	21	-43
M4	21	-17	31	-47

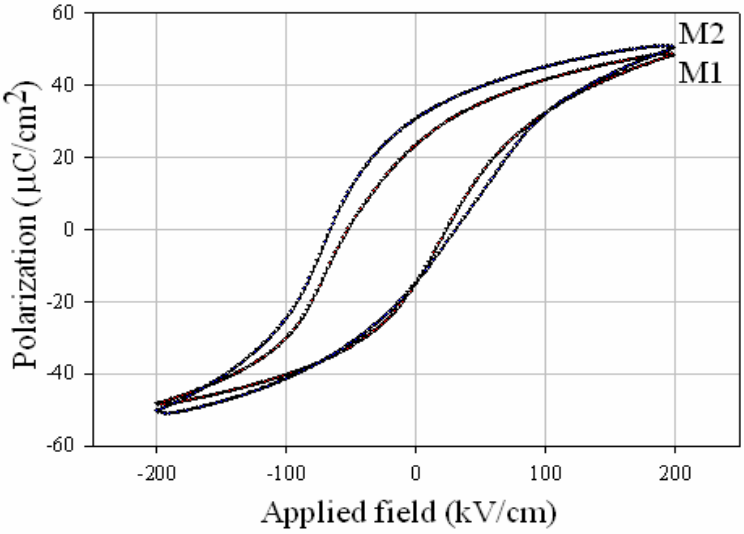

Figure 4.16 *P-E* hysteresis loops of the graded PZT films: M1 and M2.

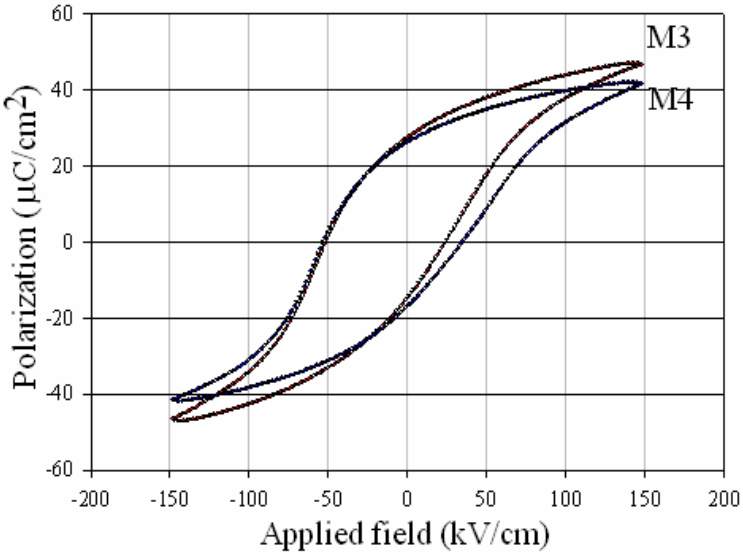

Figure 4.17 *P-E* hysteresis loops of the graded PZT films: M3 and M4.

From the *C-V* measurement at room temperature (Fig.4.18), the curves of both films revealed the expected butterfly shapes (Lee and Lee, 1999) and symmetric loops about the zero applied electric field, indicating that the films are in the ferroelectric phase and there was no obvious internal bias field at the interfaces in

the graded films. Fig. 4.18 also shows the thickness effect on the capacitance property of the PZT 40/52/60 films with different thicknesses. Compared to the 1-µm thick film, the 0.3-µm thick film had higher capacitance. This is due to the fact that the capacitance is reciprocally proportional to the film thickness and the capacitance peaks are directly related to the switching of the ferroelectric polarization.

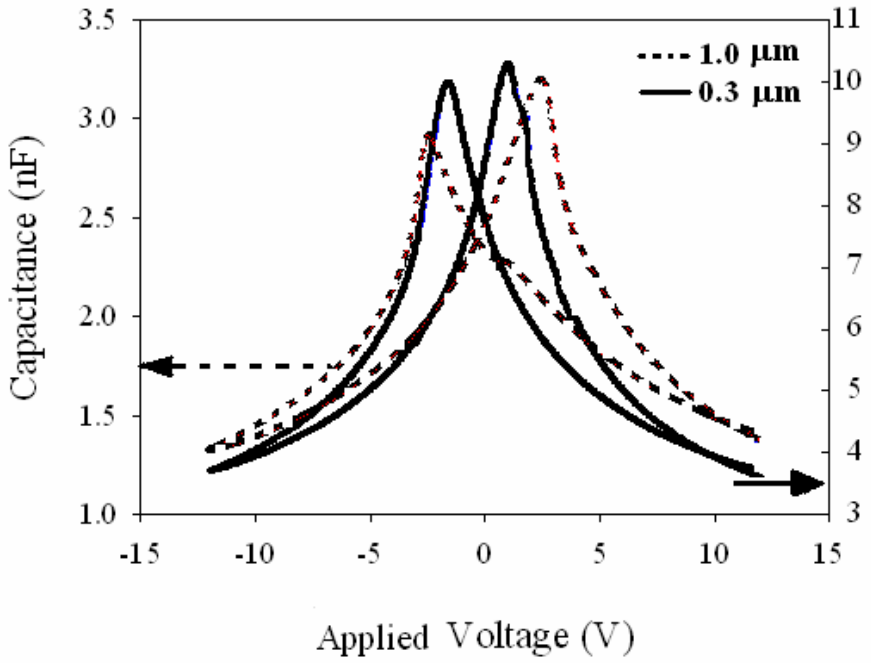

Figure 4.18 *C-V* curves for graded PZT film (M3) with different thicknesses.

The P_r, E_c and ε_r properties of these films are attractive for memory applications such as Ferroelectric Dynamic Random Access Memory (FDRAM), FRAM and Metal-Ferroelectric-Semiconductor Field Effect Transistor (MFSFET) (Uchino, 2000).

There are volatile and non-volatile memory devices in erasable semiconductor memories. DRAM is widely used because of its high integration capability, is a volatile memory. Data stored in the memory are lost when the electric power is shut off. On the contrary, non-volatile memories include a circuit-latch multiple FETs and a Si-surface-potential control Metal-Oxide-Semiconductor (MOS) FET channel. However, both types have problems in integration density and writing

time. Figure 4.19(a) shows the structure of the MOSFET. When writing, one DRAM element is chosen by *x-y* addressing; that is, voltage is applied on both the gate and the drain electrodes simultaneously, thus accumulating charge on the SiO_2 film capacitor (memorizing). Since the accumulated charge leaks, the capacitor must be recharged repeatedly (refreshing). The electron-hole pair generation around the FET by the IC package or natural radiating change the amount of charge on the capacitor, and sometimes destroys the memory (soft error). In order to retain memory, the capacitance of the memory capacitor must be higher than 30 fF (Uchino, 2000).

Since the conventional SiO_2 film plane structure cannot maintain a sufficient capacitance with decreasing element area, a multilayer type and trench type (normal hole structure on Si substrate) have been proposed. Ferroelectric materials are attractive for DRAM devices because of their high permittivities (graded film).

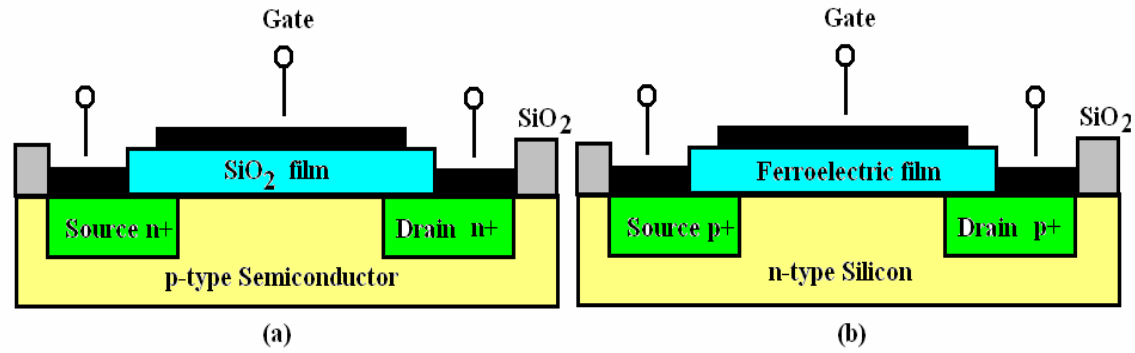

Figure 4.19 (a) MOSFET with a p-type semiconductor (b) MFSFET structure.

Because the dielectric constant of ferroelectric is typically more than 1000 (M3=1300, M1=1200 *etc.*), much larger than the dielectric constant of 3.9 for SiO_2, when a ferroelectric thin film with the same thickness as the SiO_2 film was used (Fig. 4.19b), the capacitor size to obtain 30 fF is significantly decreased, by 1/250 in term of area. Hence, much higher memory integration is possible for a ferroelectric DRAM device. However, general requirements for DRAM capacitor thin film are: (i) high dielectric constant in a thin film configuration and (ii) low leakage current. For a PZT graded structure, a leakage current less than 10^{-9} $A.cm^{-2}$ has been obtained (Brazier, McElfresh and Mansour, 1999).

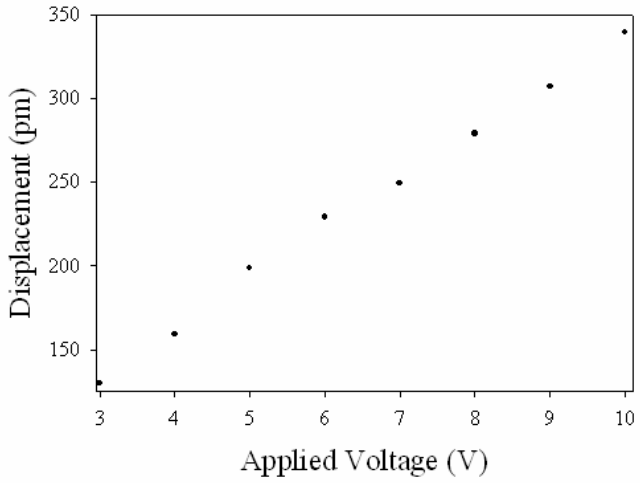

Figure 4.20 Variation of surface displacement with applied voltage measured at 5 kHz for graded PZT film (M3).

Fig. 4.20 shows the surface displacement in the graded PZT film, M3. The M1 had similar responses to that of M3. It was observed that these films required a minimum electric field to produce a linear displacement-applied voltage response. This field was 3 $MV.m^{-1}$ for M3 and 15-20 $Mv.m^{-1}$ for other films. The d_{33} coefficient was determined from a slope of the linear piezoelectric response to be 36.0 $pm.V^{-1}$ for M3 while it was 45.7 $pm.V^{-1}$ for M1. For the graded films, they have their crystalline phase corresponding to the deposition sequence of the layers. This lead to the internal stresses that differs from layer to layer in the sample (Wenbin *et al*., 2004). The complex stress possibly leads to interfacial strains in the graded films and is probably responsible for their low d_{33} values.

The other effects are also considered. At high fields, the switching domains of the top layer may exert additional stress in the under laid layers. Lattice expansion under an applied electric field between the layers of different x values resulted in localized polarization gradients and associated depolarizing field (Uchino and Giniewicz, 2003). Additionally, the polarization along certain directions depends on the crystallographic as mentioned in chapter 2. The direction (in-plane and out-of-plane polarization direction) of the spontaneous polarization in tetragonal and rhombohedral phases is different, as a result the piezoelectric activity is reduced along the polar axis. In multilayered materials as graded film, the piezoelectric response

was thus the average over all of the layers and was not due to a specific one. This trend is similar to a discussion by Kholkin *et al.* (1998), the piezoelectric coefficient was strongly depended on the orientation of the grains which is in turn affected by the grading of the composition, leading to the smaller d_{33} value in graded films when compared to those uniform films.

4.5 Conclusions

In summary, compositionally graded $Pb(Zr_xTi_{1-x})O_3$ films have been deposited by sol-gel method on $Pt/Ti/SiO_2/Si$ substrate. Both up and down graded PZT structures were prepared. The XRD results show that the layer with a Ti-rich composition was easily crystallized into the perovskite structure, triggering a good crystallization for the entire structure. A dense, smooth and pinhole-free surface morphology was obtained. Similar magnitude of the remnant polarization and a low-coercive field were observed in all graded films.

The interferometer technique was applied for the measurement of piezoelectric coefficient of the graded PZT films. The smallest value of 36 $pm.V^{-1}$ was obtained from the graded PZT (40/52/60) film. From the result in chapter 3, the magnitude of the piezoelectric coefficient of the film with MPB composition is more than twice those of the graded films, including the uniform PZT films at lower and higher Zr/Ti ratios. The effect of the substrate clamping and internal stresses between the layers of different x values in the graded PZT structures were probably responsible for the low d_{33} coefficients of the graded films.

CHAPTER 5

NANOSCALE CHARACTERIZATION AND PIEZORESPONSE OF SOL-GEL PZT FILMS

5.1 Introduction

Among the main trends in our daily society is a drive for smaller, faster, cheaper, smarter computers with ever-increasing memories. To sustain this drive the computer industry is turning to nanotechnology as a source of new processes and functional materials, which can be used in high-performance high-density electronic systems. Researchers and engineers have been focusing on ferroelectric materials for a long time due to their unique combination of physical properties. The ability of ferroelectrics to transform thermal and mechanical energy into electrical charge has been used in a number of electronic applications, most recently in non-volatile computer memories and MEMs (Alexe and Gruverman, 2004).

As mentioned in previous chapters, MEMS which combine semiconductor integrated circuits micro-assembled with mechanical, optical or other functional components (Bryzek, Petersen and McCulley, 1994), have received considerable attention because of their wide potential range of applications. These include such devices as accelerometers and gyroscopes for automotive air-bag sensors, automatic suspension and navigation systems, ‘‘smart’’ pills and catheters incorporating pressure, temperature, chemical and acoustic sensors for diagnostic use and a host of others. In many of these, the ability to integrate the active ferroelectric material in close association with a silicon signal processing array is central to the successful operation of the system. At the same time, understanding of the electromechanical coupling in nanocrystalline ferroelectrics, thin films, piezoelectric biological materials, and phase separated relaxor ferroelectrics, requires local measurements of piezoelectric coupling on the submicron and nanometer scales.

However, to meet the challenge of the "nano-era", a solid knowledge of the ferroelectric properties at the nanoscale need to be acquired. While the science of ferroelectric from micro- to larger scale is well established, the science of nanoscale ferroelectrics is still terra incognita. The properties of materials at the nanoscale show strong size dependence, which makes it imperative to perform reliable characterization at this size range. The constantly decreasing size of such devices down to a nanoscale gives rise to many fundamental questions regarding the stability of different physical properties in these low-dimensional structures. Conventional analytical techniques do not allow the determination of ferroelectric properties at this scale. The development of the atomic force microscopy (AFM) and the piezoelectric atomic force microscopy (P-AFM or PFM) has allowed the routine evaluation of surface topography of these materials, and in the last few years a number of additional techniques have been developed. (Snitka *et al*., 2006; Dunn and Whatmore, 2002).

5.2 Review of Previous Work

The PFM is based on the detection of bias-induced piezoelectric surface deformation. The tip is brought into contact with the surface and the piezoelectric response of the surface is detected as the first harmonic component of bias-induced tip deflection (Eq 5.1).

$$u = u_0 + A\cos(\omega t + \varphi) \tag{5.1}$$

The phase of the electromechanical response of the surface, φ, yields information on the polarization direction below the tip. For *c*- domains (polarization vector pointing downward), the application of a positive tip bias results in the expansion of the sample and surface oscillations are in phase with the tip voltage, $\varphi = 0$. For *c*+ domains, $\varphi = 180°$. The piezoresponse amplitude, $PR = \frac{A}{V_{ac}}$, defines the local electromechanical activity of the surface.

One of the key questions in understanding ferroelectric materials is the mechanisms for polarization switching and the role of defects, vacancies, domain walls, and other microstructural elements on switching processes. A closely related issue is the nature of the defect sites that allow domain nucleation at low electric fields (Landauer paradox) (Landauer, 1957). The application of *dc* bias to the PFM tip can result in local polarization switching below the tip, thus enabling the creation of domains, which can subsequently be imaged in real space. Studies of domain evolution with time or bias provide insight into the switching behavior and the effect of defects and disorder on switching. Recent studies by Gruverman *et al.* (2005) have shown that domain nucleation in ferroelectric capacitors during repetitive switching cycles is always initiated at the same defect regions; similarly, the grain boundaries were shown to play an important role in domain wall pinning (Kholkin *et al.*, 2004). Tybell *et al.* (2002) have used local studies of domain growth kinetics and domain wall morphology to establish the origins of disorder in ferroelectric materials (Paruch, Giamarchi and Triscone, 2005). Dawber, Gruverman and Scott (2006) interpreted the non-uniform wall morphologies as evidence for skyrmion emission during domain wall motion. Most recently, Agronin, Rosenwaks and Rosenman (2006) have observed domain pinning on structural defects.

The primary limitation of these studies of domain growth is the large time required to perform multiple switching and imaging steps. Moreover, the information is obtained on the domain growth initiated at a single point for different bias conditions, thus precluding systematic studies of microstructure influence on domain growth process. An alternative approach to study domain dynamics in the PFM experiment is based on the simultaneously measurements of the domain switching and electromechanical detection, leading to a local electromechanical hysteresis loop. In-field hysteresis loop measurements were first reported by Birk *et al*. (1991) using a scanning tunneling microscopy tip and Hidaka *et al*. (1996) using an AFM tip. In this method, the response is measured simultaneously with the application of the *dc* electric field, resulting in an electrostatic contribution to the signal. To avoid this problem, a technique to measure remanent loops was reported by Guo *et al*. (2002). In this case, the response is determined after the *dc* bias is removed,

minimizing the electrostatic contribution to the signal. However, after the bias is turned off, domain relaxation is possible.

In a parallel development, Roelofs *et al*. (2000) demonstrated the acquisition of both vertical and lateral hysteresis loops. This approach was later used by several groups to probe crystallographic orientation and microstructure effects on switching behavior (Eng *et al.*, 1998; Eng *et al.*, 1999; Rodriguez *et al.*, 2004; Kalinin, Gruverman and Bonnell, 2004; Kim *et al.*, 2005; Desfeux *et al.*, 2006; Jesse, Baddorf and Kalinin, 2006).

Recently, the PFM has been extended to an imaging mode using an algorithm for fast (30-100 ms) hysteresis loop measurements developed by Jesse, Baddorf, and Kalinin (2006). In switching spectroscopy PFM, hysteresis loops are acquired at each point of the image and analyzed to yield 2D maps of imprint, coercive bias, and work of switching, providing a comprehensive description of the switching behavior of the material at each point.

A progress in experimental methods has stimulated a parallel development of theoretical models to relate PFM hysteresis loop parameters and materials properties. A number of such models are based on the interpretation of phenomenological characteristics of piezoresponse force spectroscopy (PFS) hysteresis loops similar to macroscopic *P-E* loops, such as slope, imprint bias, vertical shift. In particular, the slope of the saturated part of the loop was originally interpreted as electrostriction; later studies have demonstrated the linear electrostatic contribution to the signal plays the dominant role.

Several groups analyzed the effect of non-uniform materials properties, including the presence of regions with non-switchable polarization on parameters such as imprint and vertical shift. In thin films, the vertical shift of the PFM hysteresis loops was interpreted in terms of a non-switchable layer by Saya *et al.* (2000). Alexe *et al.* (2001) analyzed the hysteresis loop shape in ferroelectric nanocapacitors with top electrodes, obtaining an estimate for the switchable volume of a nanocapacitor. Similar analysis was applied to ferroelectric nanoparticles developed by the self-patterning method by Ma and Hesse (2004). In all cases, the results were interpreted in terms of ~10 nm of non-switchable layers, presumably at ferroelectric-electrode interface.

There has been an attempt to relate local PFM hysteresis loops and macroscopic *P-E* measurements, often demonstrating good agreement between the two (Hanagea *et al.*, 2000). This suggests that despite the fundamentally different mechanism in local and macroscopic switching, there may be deep similarities between tip-induced and macroscopic switching processes. A framework for PFM analysis and macroscopic loops based on Landau theory was developed by Ricinshi *et al.*, (2002, 2003 and 2004) demonstrating an approach to extract local switching characteristics from hysteresis loop shape.

In parallel with tip-induced switching studies, a number of groups combined local detection by PFM with a uniform switching field imposed through the thin top electrode to study polarization switching in ferroelectric capacitor structures. Spatial variability in switching behavior was discovered by Gruverman *et al.* (2003a and 2003b) and attributed to strain and flexoelectric effects. In subsequent work, domain nucleation during repetitive switching cycles was shown to be initiated at the same defect regions, indicative of the frozen disorder in ferroelectric structures (Dehoff *et al.*, 2005; Gruverman *et al.*, 2005).

The rapidly growing number of experimental observations and recent developments in PFS instrumentation, data acquisition, and analysis methods requires understanding not only phenomenological, but also quantitative parameters of hysteresis loops, such as numerical value of the coercive bias, the nucleation threshold, *etc*. Kalinin, Gruverman and Bonnell (2004) have extended the 1D model by Ganpule *et al.* (2000) to describe PFM loop shape in the thermodynamic limit. Kholkin *et al.*, (2006a) have postulated the existence of nucleation bias from PFM loop observations, in agreement with theoretical studies by Abplanalp *et al.* (2001), Abplanalp (2001), Kalinin *et al.*(2005), Emelyanov (2005), Morozovska and Eliseev (2006). Finally, Jesse, Baddorf and Kalinin (2006) have analyzed hysteresis loop shape in kinetic and thermodynamic limits for domain formation. However, in all cases, the model was essentially 1D, ignoring the fundamental physics of domain switching.

In the case of PZT thin film, the PFM technique was selected for topography and domain switching characterization. Kholkin *et al*. (2006) presented the switching process and ferroelectric degradation of PZT thin films prepared by a sol-gel method. The piezoelectric coefficient values (d_{33}) were measured using the

PFM analyses. The results are corresponded to a report by Yang *et al*., (2003). The remanent d_{33} values are maximized near the MPB composition. This chapter presents the results of domain topographies of PZT samples and switching of a single PZT domain observed by the PFM. The piezoresponse measured by PFM, which represents the piezoelectric strain induced in the film under external field are also investigated.

Information limit in PFM

The key parameter of any microscopic technique is the minimal size of the object that can be reliably identified. In the context of PFM, this information limit corresponds to the minimal domain size that can be observed experimentally. In the assumption of the thermal noise is not presented on the topographically uniform surface, even infinitely small domain will be visible. Practically, this condition is limited by the thermal noise of the cantilever, voltage noise of the bias source, laser noise, *etc.* Also, the cantilever vibrations induced due to the lateral motion on non-uniform surface will contribute to the effective noise level. The magnitude for some of the noise components can be estimated, *e.g.* thermal noise, $\langle z^2 \rangle$, in the off resonant conditions is

$$\langle z^2 \rangle = \sqrt{\frac{4k_B TB}{Qk\omega_0}} \tag{5.2}$$

where k_B is Boltzmann constant, T is temperature, B = 1 kHz is the measurement bandwidth, Q is quality factor, k is spring constant, and ω_0 is resonant frequency. Here, we estimate Q = 20 typical for cantilever in contact with the surface, and typical value for ω_0 = 200 kHz. Note that the use of k = 1000 N/m for typical tip-surface contact leads to unphysical small estimates for noise, since the flexural oscillations of the cantilever under distributed thermal loading providing dominant contribution to thermomechanical noise are ignored. Hence, we use $k = 8k_{free}$, where k_{free} is a spring constant of freely vibrating cantilever. The full theory of the cantilever dynamic in PFM is given elsewhere (Morozovska *et al.*, 2007).

5.3 Principle of Piezoresponse Force Microscopy

The PFM has been used as a powerful tool for imaging and characterization of nanoscale domain structures in ferroelectrics (Kholkin *et al.*, 2006). The PFM detects the converse piezoelectric response of the materials under investigation and allows the mapping of the ferroelectric domains, the generation of highly localized hysteresis loops. The use of an AFM tip as a small and movable conductive probe has reduced the scale of the study of piezoelectricity to just a few tens of nanometers.

Even though the PFM technique was introduced more than ten years ago, the quantitative analysis of PFM measurements is still under debate (Seungbum *et al*., 2001; Kalinin, 2002; Kalinin and Bonnell, 2002; Alex and Gruverman, 2004). The three major issues involved in PFM contrast formation mechanism are:

(i) voltage-dependent contact mechanics of piezoelectric material that determines the PFM signal,

(ii) dynamic properties of the cantilever and transduction mechanism between the electromechanical response of the surface and electrostatic forces and resulting vertical and lateral PFM signal, and

(iii) electroelastic field distribution in the material that determines resolution, domain switching behavior, and hysteresis loop acquisition mechanism.

5.3.1 Capacitive forces

The system comprising conducting tip in a contact with the dielectric surface represents a capacitor. Therefore, an external voltage applied between the tip and the counter electrode results in an additional (capacitive or Maxwell) force that can be, in general, determined by the following equation:

$$F_{cap} = \frac{dW_{cap}}{dz} = \frac{1}{2} V^2 \frac{dC}{dz} \tag{5.3}$$

where $W_{cap} = \frac{1}{2} V^2 C$ is the energy stored in the capacitor C and z is the vertical distance. It follows that, if a combination of the *dc* and *ac* voltages ($V = V_{dc} + V_{\omega} \cos \omega t$) is applied between the tip and the counter electrode, the capacitive forces will consist of a static force F_0, a force oscillating at a driving

frequency ω ($F_\omega = V_{dc} V_\omega \frac{dC}{dz}$) and a force $F_{2\omega}$ appearing at a frequency 2ω. These forces can be essential even in contact mode (Kalinin, 2002) and must be compared with other forces including electromechanical one due to electric field-induced deformation of the sample.

The total capacitance *C* of the sample-cantilever system can be written as the sum of the capacitance of the cantilever (C_{cant}) and the capacitance of the tip (C_{tip}). The former gives rise to so-called non-local contribution to the capacitive force because of the macroscopic dimensions of the cantilever. The capacitance of the cantilever can be estimated by using the analytical expression derived by Prume *et al.* (2002):

$$\frac{dC_{cant}}{dz} = \frac{\varepsilon_0 d_c}{\tan\alpha}\left(\frac{1}{h_c} - \frac{1}{L_c \tan\alpha + h_c}\right) \tag{5.4}$$

where d_c is the width and L_c is the length of the cantilever. h_c and α are the gap and the angle between the cantilever and the sample surface, respectively. Eq.5.3 describes the non-local electrostatic force contribution F_{nl} of the cantilever to the PFM signal and can result in a signal offset appearing at 1st harmonics (PFM signal is monitored at a driving frequency ω). The typical value of the *dc* force for non-local capacitive contribution (standard Si cantilevers, L_c=450 μm, d_c=50 μm) estimated using Eq.5.4 is quite small (0.1 nN) and can be neglected for many practical cases.

In addition to capacitive forces, Coulomb attractive forces between the tip and the charged ferroelectric surface can be observed in PFM experiments (Alexe and Gruverman, 2004). This force can be estimated by using an equation:

$$F_{coul} = \frac{\sigma C V}{2\varepsilon_0} \tag{5.5}$$

where σ is the surface bound charge density and *V* is the voltage applied to the sample. Surface polarization charges giving rise to electrostatic interaction are screened by the absorbed charges of the opposite sign and thus are normally smaller than the electromechanical forces for many practical applications. For the typical polarization charge of 1 μC.cm^{-2}, tip radius ≈40 nm and bias voltage of $V \approx 1$ V the corresponding force can be estimated in the range of few nN.

5.3.2 Electromechanical forces

Applying an electric field between a cantilever and a dielectric material leads to capacitive forces as discussed above. A piezoelectric material will provide an additional response to an applied *ac* electric field due to the converse piezoelectric and electrostrictive effects. For a homogeneously polarized (in z direction), stress-free ferroelectric material its vertical (z) displacement can be expressed as follows:

$$\Delta z = d_{33}V + \frac{M_{333}}{t}V^2 \tag{5.6}$$

where V is the applied voltage, t is the sample thickness, d_{33} and M_{333} are the piezoelectric and electrostrictive constants, respectively. The second term in Eq.5.6 is typically much smaller than the first one in a polarized state (Jaffe, Cook and Jaffe, 1971). Under the external voltage $V = V_{dc} + V_{\omega}\cos\omega t$ the surface displacement will consist of a *dc* component (that cannot be measured via a lock-in detection), the signals at first and second harmonics:

$$\Delta z_{\omega} = d_{33}V_{\omega} + 2\frac{M_{333}}{t}V_{dc}V_{\omega} \tag{5.7}$$

$$\Delta z_{2\omega} = \frac{1}{2}V_{\omega}^2\frac{M_{333}}{t} \tag{5.8}$$

The sign of the converse piezoelectric signal (first term in Eq.5.7) depends on the relative orientation of the polarization and applied electric field. When a positive voltage is applied to the PFM tip and the polarization is pointing at negative z-direction (electric field is parallel to the spontaneous polarization), the sample will expand thus pushing up the cantilever and allowing measurements of d_{33}, (Fig.5.1(a)).

In this case, a positive sign is attributed to the displacement Δz. As we apply an alternating voltage, this means that the electric field and the piezoelectric signal are in phase. These measurements are referred to as *out-of-plane* (or vertical PFM, VPFM) measurements. If the polarization points at the positive z-direction, the applied electric field will be anti-parallel to the spontaneous polarization causing the ferroelectric to contract with them consequent lowering of the cantilever. The electric field and the piezoresponse signal are shifted in phase by 180°. Additionally, ferroelectric grain may contract in the film plane, which is caused by the transverse piezoelectric coefficient d_{31}. This causes additional lateral contraction of the

ferroelectrics. The anti-parallel alignment of the electric field and the spontaneous polarization lead to a vertical contraction and a horizontal expansion of the ferroelectrics, respectively. Figure 5.1(b) shows that the electric field applied orthogonally to the polarization direction results in a shear movement due to the d_{15} coefficient. This movement causes a torsional deformation of the cantilever forcing the laser spot to move horizontally (in-plane signal). Figure 5.1 (b) also presents the grain polarized in the *x*-*z* plane will contribute to the in-plane as well as to the out-of-plane signal (Kholkin *et al.*, 2006b). Figure 5.1(c) shows a grain with the polarization aligned in the *x*-*z* plane. In this case, the applied field will cause both vertical as well as torsional movement of the cantilever. A strong in-plane and a weak out-of-plane signal will indicate that the polarization has only a small component of the polarization pointing into the *z*-direction (P_z) and is mainly aligned in the film plane. Due to the cantilever asymmetry, polarization in the *y*-direction (P_y) can only be recorded by physically rotating the sample by 90° along the *z*-axis and repeating the in-plane measurement.

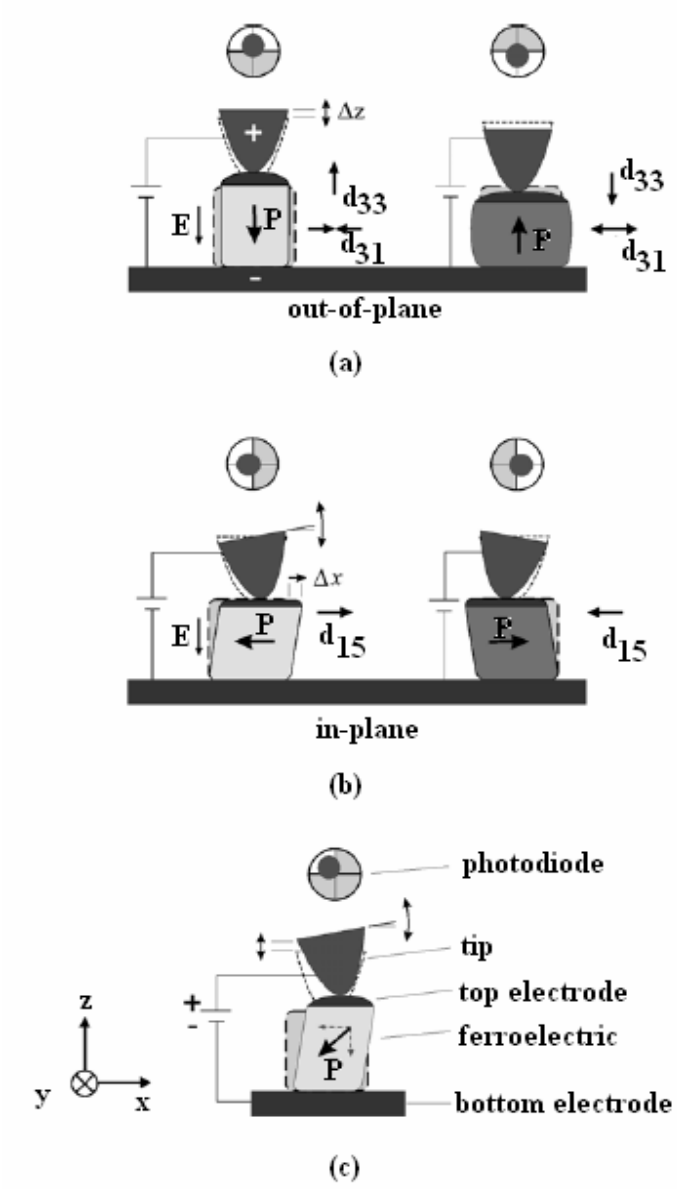

Figure 5.1 Piezoelectric effect in ferroelectrics investigated by PFM: electric field (a) aligned parallel and antiparallel to the spontaneous polarization, (b) applied orthogonal to the polarization results in a shear movement due to the d_{15} coefficient and (c) a grain polarized in the *x*-*z* plane: (Kholkin *et al.*, 2006b).

By acquiring all three components of the piezoresponse signal it is possible to perform at least semiquantitative reconstruction of polarization orientation. However, precise orientation of polarization can be calculated only if all the components of the piezoelectric tensor are known. The first attempt to relate the amplitude of the piezoresponse signal to the orientation of the ferroelectric

polarization has been undertaken by Harnagea *et al.* (2001) and detailed formalism has been later developed by Kalinin *et al.* (2005a and 2005b).

In research for multi-Gbit ferroelectric memories, the thickness of a ferroelectric film is also of great concern. Auciello, Scott and Ramesh (1998) mentioned that the thickness of less than 200 nm is necessary for future nonvolatile ferroelectric random-access memory, while Scott *et al*. (1998) discussed the possibility of thicknesses as low as 30 nm for some particular device applications. This chapter presents the thickness-dependence of the piezoresponse, the mapping of ferroelectric domain and the local piezoelectric hysteresis loops of PZT thin film with different compositions.

5.4 Materials and Methods

$Pb(Zr_xTi_{1-x})O_3$ films with x=0.3, 0.4, 0.52, 0.6, and 0.7 on the conventional $Pt(111)/Ti/SiO_2/Si(100)$ substrates were prepared by a simple sol–gel process (Budd, Dey and Payne, 1985; Perez, Vilarinho and Kholkin, 2004). The precursor with 10% excess Pb composition was prepared to compensate for the lead loss in the deposition processing. The PZT solutions were prepared in the manner as shown in Fig.3.1. Thin film fabrications were the same as those illustrated in Fig.3.2. For the thickness effect investigation, a monolayer (which is referred to one cycle of spin coating) and ten layers (ten cycles of spin coating) of PZT thin films were prepared.

To investigate nanoscale domain mapping and switching, the PFM was applied to monitor ferroelectric and topological properties of individual grains along all the three dimensions *x*, *y*, and *z* (MultiMode^{TM} SPM, Digital Instruments). This study was done in a configuration where the PFM tip served as the top electrode (Chrisman *et al.*, 2000). A weak *ac* voltage was applied between the conducting tip and bottom electrode to induce a local piezoelectric vibration, which is detected by the same tip. The experimental arrangement is schematically shown in Figs. 5.2-5.3.

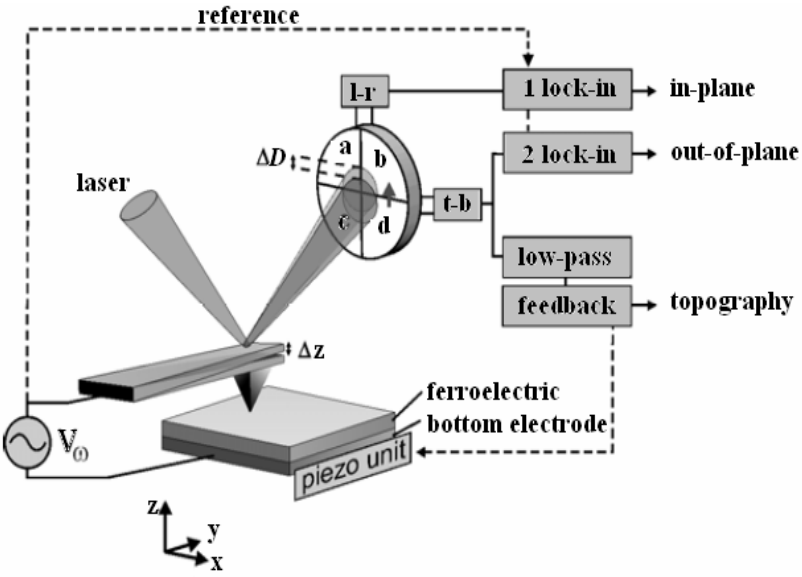

Figure 5.2 The PFM arrangement includes sample, electrode, tip, signal source, laser and lock-in amplifiers (After Kholkin *et al.*, 2006).

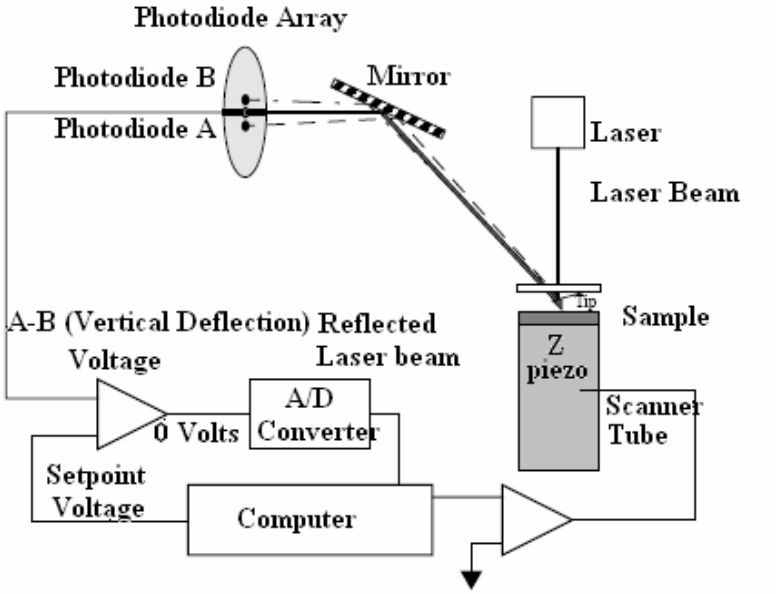

Figure 5.3 Schematic diagram of the PFM arrangement illustrates tip-cantilever system and detector.

The amplitude of the vibration signal provides information on the magnitude of the piezoelectric coefficient, while the phase signal determines the polarization direction. Due to the absence of the top electrode and consequent high resolution, one can observe the ferroelectric domains and the surface topography at

the same time and easily correlate the microstructure and the domain behavior inside individual grains.

From Fig. 5.2, a commercial AFM was connected to the lock-in amplifiers (SR830, Standard Research Systems) to detect an amplitude and phase signals from AFM detector. During the experiment, *ac* voltage of 10 V_{pp} (peak to peak with additional amplifier) at 50 kHz was applied to the AFM tip while *dc* bias voltages or bipolar single pulses with sinusoidal shape were applied to the bottom electrode. For all the experiments, the AFM tip was maintained at a fixed *x-y* position so that all the data were acquired from one position on the sample. PFM measurements were performed in a commercial setup Multimode, NanoScope IIIA, DI equipped with a lock-in amplifier Stanford Research, SR-830 and a function generator Yokagawa, FG-120. From Fig. 5.3, a commercial tip-cantilever system NCHR Nanosensors with spring constant of k=40 N.m^{-1} and tip apex radius less than 10 nm was used. Domain visualization was performed under an applied *ac* voltage of amplitude V_{ac}=5 V and frequency f = 50 kHz, scan speed 1-5 μm.s^{-1}. A sinusoidal voltage was passed between the AFM tip and the back electrode of the PZT sample, usually held at ground.

During the experiment the scan size was set to 0 nm in order to remove any topographic variation from the *z*-axis displacement with a scan rate to 0.1 Hz. The displacement of the sample surface due to the applied field was directly interpreted from the *z*-axis scale of the microscope. The microscope used was a Digital Instruments 3000 systems with series III controller. The variation in the *z*-axis displacement was plotted against the applied voltage and can be interpreted as a typical strain/field plot for the sample.

5.5 Results and Discussion

5.5.1 Domain and Piezoresponse mapping

Figs. 5.4(a)-5.8(a) show the topography and local piezoelectric behavior in the films. A variation of grain size with composition ratio was observed. The PZT film with x=0.7 show much larger grains and a very broad grain distribution as compared to x=0.3. This is because the grain sizes of PZT film strongly depend on

the composition ratio via different nucleation/growth energy. The films with higher Ti content have smaller nucleation energy as reflected in smaller size of the grains. This trend is similar to previous reports in the literature (Kuffer *et al*., 2000; Zeng *et al*., 2003a; Zeng *et al*., 2003b; Shvartsman *et al*., 2005a; Shvartsman *et al*., 2005b; Zeng *et al*., 2005). As seen from Fig. 5.8(a), the polarization distribution in the ensemble of the grains is random, indicating random crystallographic orientation, as verified by x-ray measurements (as discussed in chapter 3). Corresponding piezoresonse images are shown in Figs. 5.4(b)-5.8(b), where the areas appearing as bright and dark contrast were undoubtedly 180º domain with antiparallel polarization direction (described in Fig. 5.1). As seen from Fig. 5.8(b), grains 1 and 2 were visualized as 90º domain configurations with 100 nm in width which was clearly shown in grain 3.

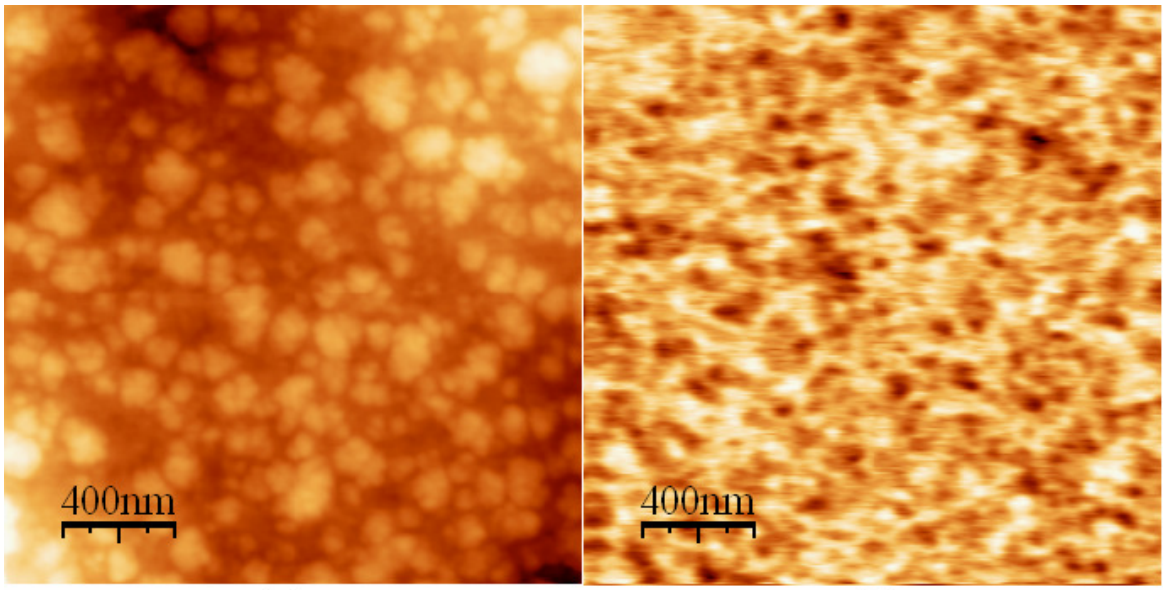

Figure 5.4 PFM image (a) topography and (b) piezoresponse of PZT film (x=0.3).

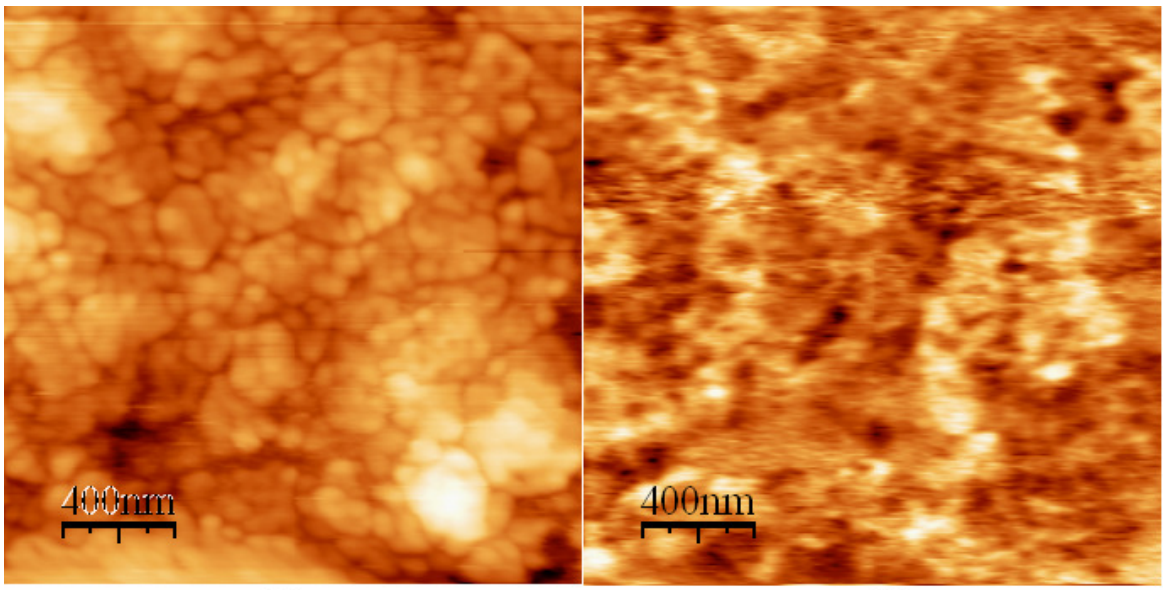

Figure 5.5 PFM image (a) topography and (b) piezoresponse of PZT film (x=0.40).

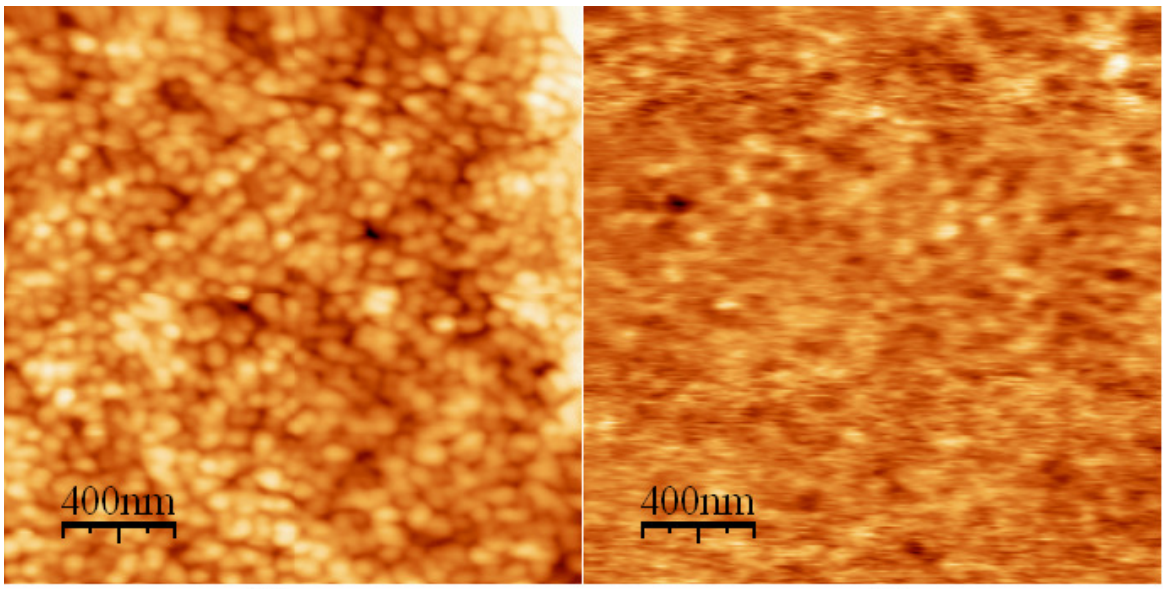

Figure 5.6 PFM image (a) topography and (b) piezoresponse of PZT film (x=0.52).

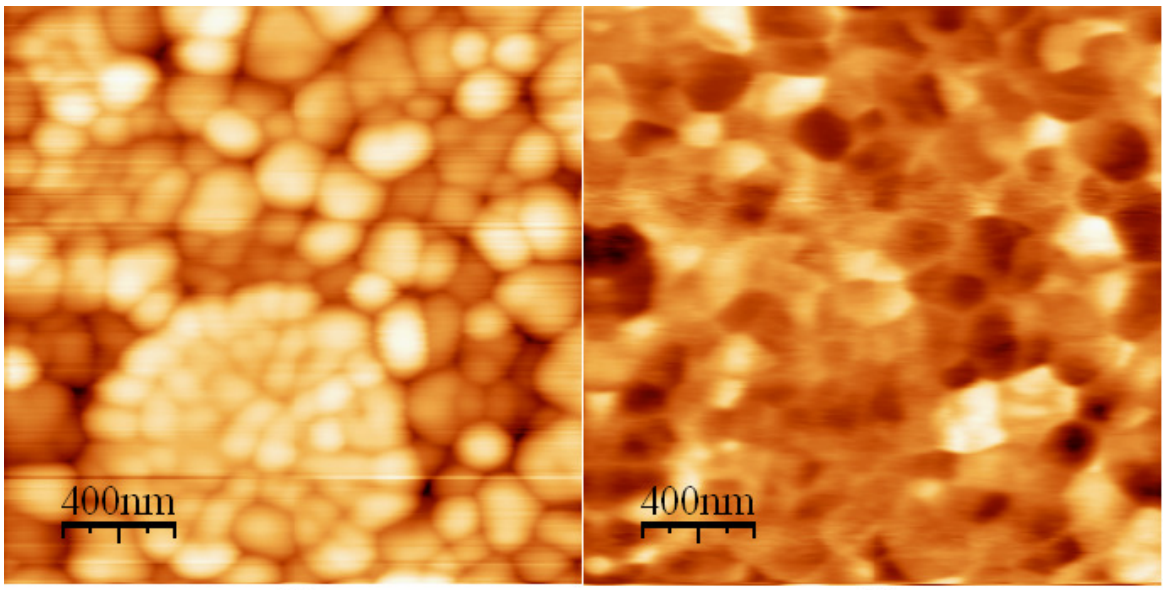

Figure 5.7 PFM image (a) topography and (b) piezoresponse of PZT film (x=0.60).

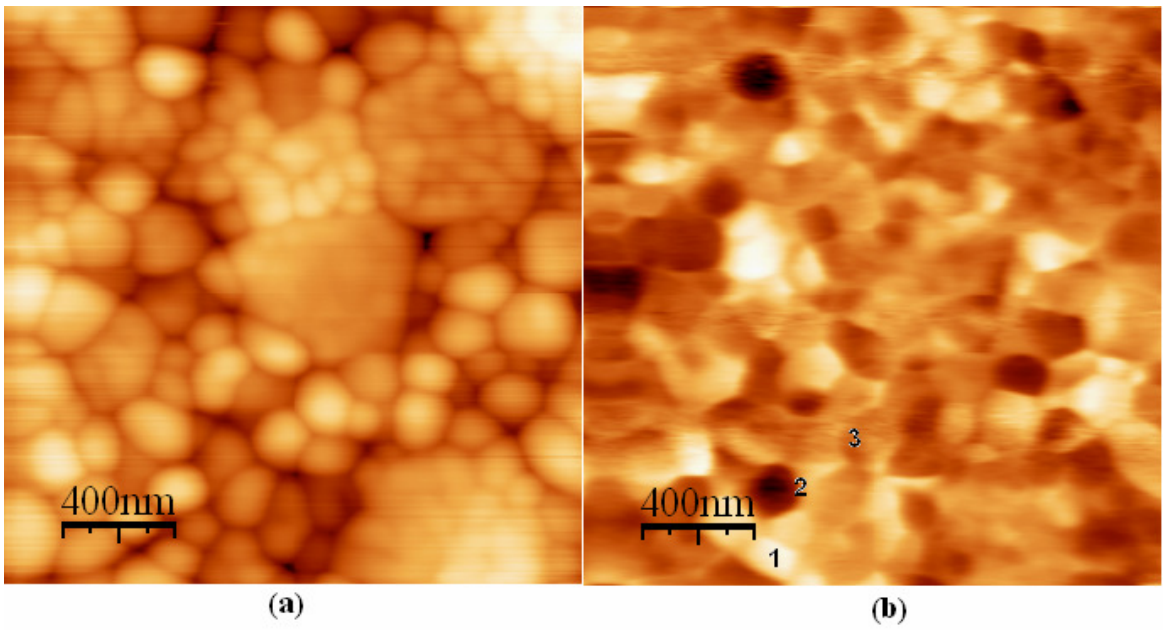

Figure 5.8 PFM image (a) topography and (b) piezoresponse of PZT film (x=0.7).

5.5.2 Piezoresponse hysteresis loops

The PFM hysteresis loops in the piezoresponse of the PZT samples are shown in Figure 5.9. A strong Zr/Ti ratios dependence of the piezoresponse is clearly seen. As discussed by Yang *et al.* (2003), the local hysteresis loops of the piezoresponse in the PFM are corresponding to the piezoelectric coefficient

measurement in the macroscopic aspect. These loops can be interpreted to the effective d_{33} of the film. From Fig. 5.9, the value of the piezoelectric response is maximum at x=0.52.

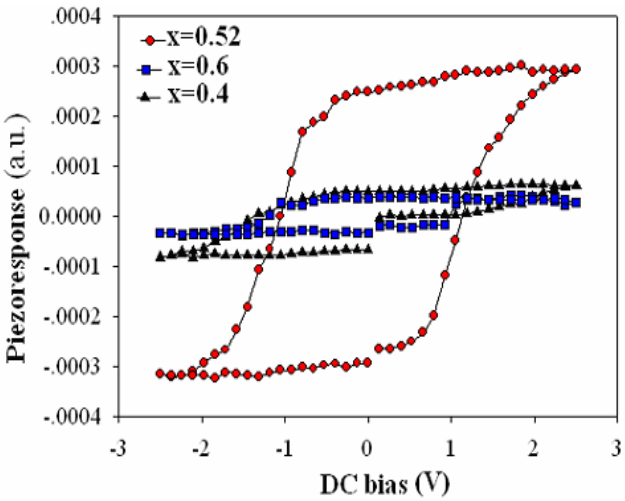

Figure 5.9 Local hysteresis loops of the PZT films with different Zr contents.

In addition, Fig. 5.9 shows a large difference between initial and final polarization states (for x=0.4). This is possibly explain by the fine size of domains and their merging upon switching by PFM tip. As a matter of fact, the coercive field of all films show a switching behavior at 250 kV.cm^{-1}. These results are consistent in the *P-E* hysteresis loop data. In the initial state, the domains in neighboring grains compensate each other while in the polarized state all domains are oriented along applied electric field and the measured value should be increased as observed in the hysteresis loop (Dunn, 2003).

As can be seen, the PFM images in Fig. 5.10(a) and (b) show the similar sun shapes of ferroelectric domain structure. Fig. 5.10(a) shows the single sun of about 10 μm in diameter produced by the first deposition.

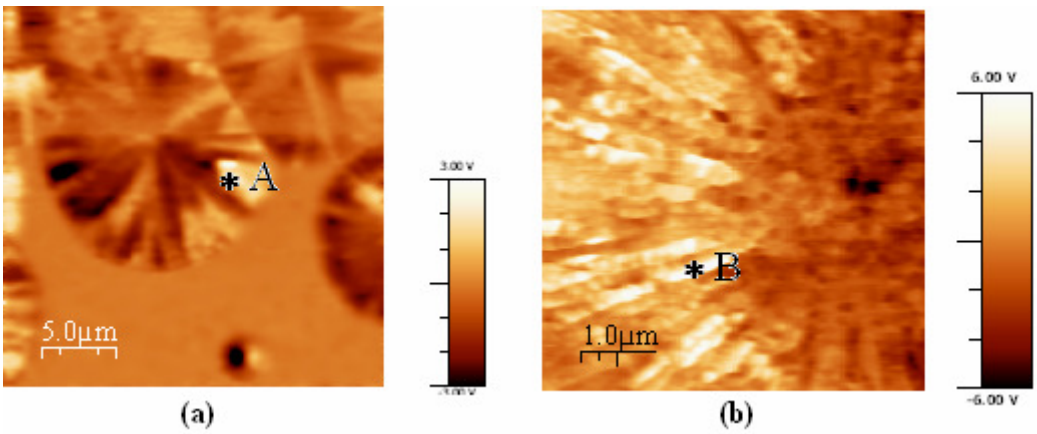

Figure 5.10 Piezoresponse of the PZT films (x=0.52) with different thickness: (a) single, and (b) ten depositions.

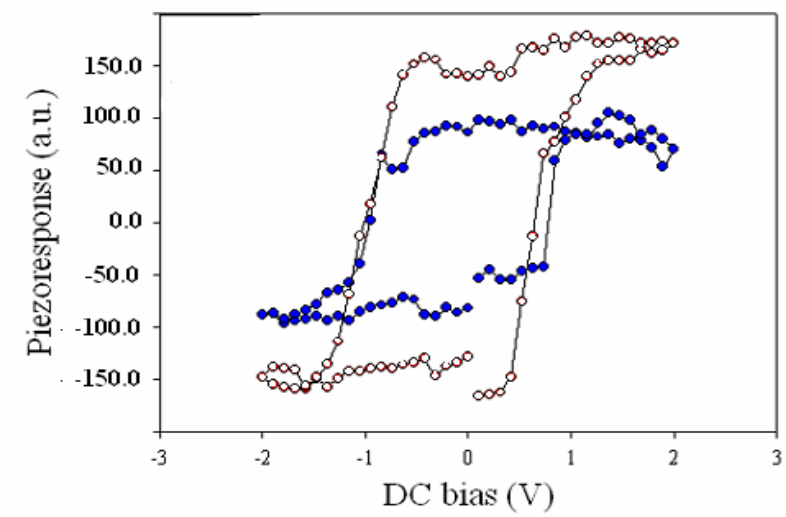

Figure 5.11 Local hysteresis loops of the PZT films (x=0.52) with different thicknesses (blue dot=single deposition and open dot=ten depositions).

Local hysteresis loops of the PZT films with different thicknesses shown in Figure 5.11 have different maximum magnitudes of piezoresponse signals after full switching. For ten-deposited film, the piezoresponse signal is higher than that of single-deposited film.

The thickness effect on the ferroelectric properties was observed in this part. The thicker film show the higher piezoresponse. Both films, however, show switching behavior and the coercive field around 30-250 kV.cm^{-1}. The piezoresponses of ferroelectric PZT thin film detected at difference domains were shown in Fig 5.12.

In Fig. 5.12(c) domain **B** and **C** are the out-of-plane polarization domain which 180º different in polarization direction, where domain (area) **A** is the in-plane polarization domain. The hysteresis of the piezoresponse of different domains was shown in Fig. 5.13.

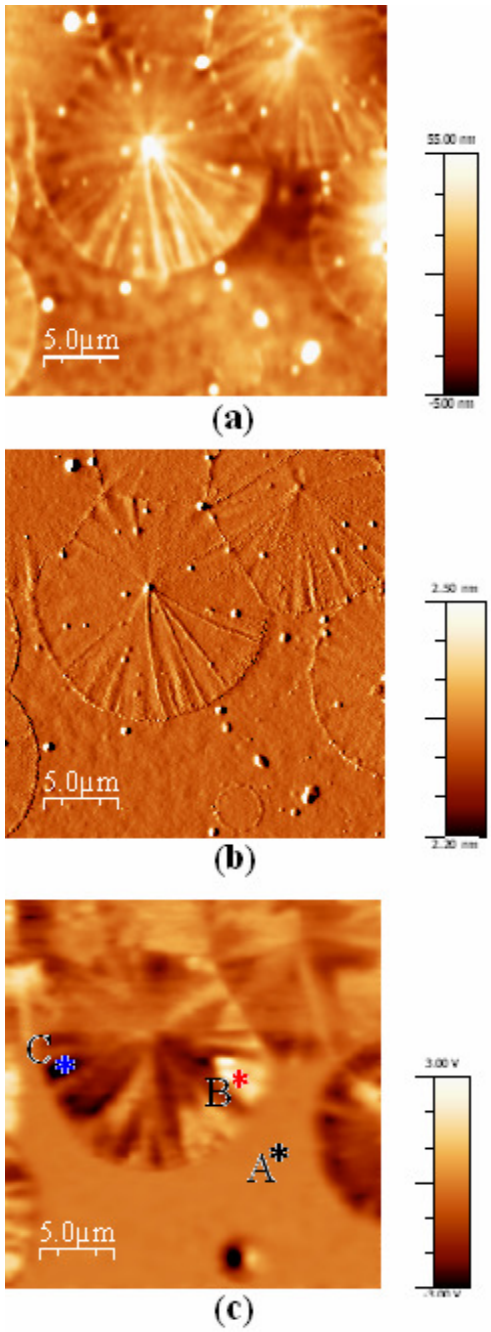

Figure 5.12 Images of out-of-plane and in-plane domains of the PZT film (x=0.52) with single deposition: (a) topography (b) deflection (*dz/dx*) and (c) piezoresponse.

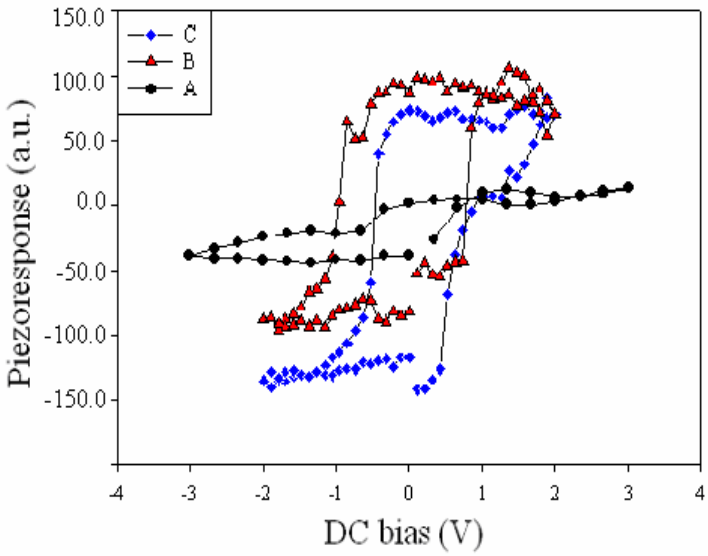

Figure 5.13 Local hysteresis loops of the PZT films (x=0.52) with different domains.

Figure 5.13 shows the local hysteresis loops from different points on the film. For **A** points, each point is placed on the substrate in a PZT-free area, therefore, there was no piezoresponse signal. For the domain along a *z*-direction which was referred as **B** points, the hysteresis loop characteristic is symmetry. This is an out-of-plane polarization (OPP) signal from the PFM measurement. For the domains along a small-angle shifted *z*-direction or **C** points, the hysteresis loop was shifted downward. This shift was due to incomplete switching during the process for obtaining loops and presented the non-switching part in piezoresponse signals. This means that the films have additional self polarization effect and additional internal position positive electric field (Roelofs *et al*., 2000).

Multidomains and their formation mechanism in low-dimensional structures are, however, not well understood. Atomic-scale details of multidomains are also scare in ferroelectric thin films. One may also wonder uncompensated depolarizing fields can yield ferroelectric phase that do not exist in the corresponding bulk material.

5.6 Conclusions

$Pb(Zr_xTi_{1-x})O_3$ thin films with different thicknesses and compositions are investigated by local piezoelectric atomic force microscopy. Islands like and sun rays type of grain and ferroelectric domain structures were found. Domains of different orientations have different shapes of hysteresis loops. A square-like *P-E* hyteresis loop indicated that all domains are well oriented along the direction of the applied electric field. The thicker film shows the higher piezoresponse signal. It is the out-of-plane polarization domains that display important role, in probing ferroelectric domains and PFM signal. Asymmetric position of local hysteresis loops point out self-polarization effect in the PZT films. The largest local piezoelectric response was observed in the films with MPB composition.

CHAPTER 6

CONCLUSIONS AND FUTURE WORK

6.1 Main Conclusions

(1) Sol-gel $Pb(Zr_xTi_{1-x})O_3$ (PZT) films with single composition (x=0.30, 0.40, 0.52, 0.60 and 0.70) were deposited on $Pt/Ti/SiO_2/Si$ substrates using a spin coating method. The PZT films with Zr/Ti ratios of 30/70 and 40/60 crystallized in the peroveskite tetragonal phase while it is the rhombohedral for the films with Zr/Ti ratios of 52/48, 60/40 and 70/30. From the microtexture of the PZT films, a uniform grain sizes in a range of 80–100 nm was obtained for all film. The film having rhombohedral crystallographic phase has ε_r' values in the frequency range of 10^2 to 10^5 Hz higher than that of the film with tetragonal phase. The film with a Zr/Ti ratio of 52/48 which is the MPB composition has a maximum ε_r' value of 1194 and low dielectric loss ($\tan\delta$) of 0.02. The PZT film with MPB composition exhibits the remanent polarization of 23.7μC.cm^{-2} and the low coercive field, E_c of 72 kV.cm^{-1}. The largest d_{33} coefficient of 117.5 ± 0.5 pm.V^{-1} was also obtained from the MPB composition PZT film. High dielectric constant and piezoelectricity of the films suggest that these films are promising for use as multilayer actuated microdevices.

(2) Sol-gel compositionally graded $Pb(Zr_x,Ti_{1-x})O_3$ films were deposited on $Pt/Ti/SiO_2/Si$ substrate by a spin-coated method. The films present crystallographic without preferred orientation**.** Well-defined depositing layers with homogeneous changing of the Zr gradient across the film thickness were observed. All graded PZT films have higher dielectric properties when compared to the single-composition PZT films. However, all graded PZT films also have higher dielectric loss. The apparent piezoelectric coefficient, d_{33} of the graded PZT film was found to be as low as 36.0 pm.V^{-1}. The compositionally graded PZT films show interior piezoelectric response possibly due to the effect of lattice mismatches, in-plane polarization and internal stress caused by the pinning of the substrate. Large

remanent polarization and smaller coercive field indicated that the graded PZT films are attractive for non-volatile memory device applications.

(3) $Pb(Zr_xTi_{1-x})O_3$ thin films with different thicknesses and compositions are investigated by local piezoelectric atomic force microscopy. Islands like and sun rays type of grains and ferroelectric domain structures were found. Domains of different orientations have the hysteresis loops with different shapes. A square-like *P-E* hyteresis loop in 52/48 film indicated that all domains are well oriented along the direction of the applied electric field. The thicker film shows the higher piezoresponse signal. It is the out-of-plane polarization domains that display important role, in probing ferroelectric domains and PFM signal. Asymmetric position of local hysteresis loops point out self-polarization effect in the PZT films. The largest local piezoelectric response was observed in the films with MPB composition.

6.2 Future Work

Some difficulties arisen during the course of this work are:

(a) the leakage current during the electrical measurements,

(b) understanding of the formation of unrelaxed stress and the prevention of the dielectric loss,

(c) initial displacements at zero applied electric fields caused by the domain switching are remained undetected.

The following topics are of considerable interest to study:

(a) measurements of the electromechanical coupling factor, *k*, an indicator of the effectiveness with which a piezoelectric material converts electrical energy into mechanical energy, or converts mechanical energy into electrical energy,

(b) measurements of the electrostrictive coefficient related to a quadratic coupling of strain and field, which is present in all materials,

(c) the integration of the sol-gel films with nowadays semiconductors or electronics technology,

(d) the fabrication of the films from the lead-free solid solution systems.

REFERENCES

Abplanalp M., (2001). *Piezoresponse scanning force microscopy of ferroelectric domains*, Dr. Nat. Sci. Thesis, Swiss Federal Institute of Technology, Zurich, Switzerland.

Abplanalp M., Fousek J., and Gunter P., (2001). Higher Order Ferroic Switching Induced by Scanning Force Microscopy, Physics Review Letters, Vol. 86, p.5799.

Agronin A., Rosenwaks Y., and Rosenman G., (2006). Direct observation of pinning centers in ferroelectrics, Applied Physics Letters, Vol. 88, p.072911.

Alexe M., Harnagea C., Hesse D., and Gosele U., (2001). Polarization imprint and size effects in mesoscopic ferroelectric structures, Applied Physics Letters, Vol. 79, p.242.

Alexe M., and Gruverman A., (2004). *Nanoscale Characterisation of Ferroelectric Materials: Scanning probe microscopy approach*, Springer-Verlag Berlin Heidelberg Pub.

Alpay S. P., Ban Z.-G., and Mantese J. V., (2003). Thermodynamic analysis of temperature-graded ferroelectrics, Applied Physics Letters, Vol. 82, p.1269.

Araujo E. B., and Eiras J. A., (2000). PZT thin films produced by oxide precursors and crystallized by conventional and RTA process, Journal of the European Ceramics Society, Vol.21, p.1513-1516.

Araujo P. de C., Scott J. F., and Taylor G. W., (1996). *Ferroelectric thin films: synthesis and basic properties*, Gordon and Breach, Amsterdam.

Arlt G., (1990). Review: Twinning in ferroelectric and ferroelastic ceramics; stress relief, Journal of Materials Science, Vol.25, p.2655-2666.

Auciello O., Scott J. F., and Ramesh R., (1998). The physics of ferroelectric memories, Physics Today, Vol.51 (Issue 7), p.22-27.

Ban Z.-G., Alpay S. P., and Mantese J. V., (2003a). Fundamentals of graded ferroic materials and devices, Physical Review B, Vol.67, p.184104.

Ban Z.-G., Alpay S. P., and Mantese J. V., (2003b). Hysteresis offset and dielectric response of compositionally graded ferroelectric Materials, Integrated Ferroelectrics, Vol.58, p. 1281-1291.

Bao D., Mizutani N., Yao X., and Zhang L., (2000). Dielectric and ferroelectric properties of compositionally graded (Pb,La)TiO_3 thin films on Pt/Ti/SiO_2/Si substrates, Applied Physics Letters, Vol. 77, p.1203.

Bao D., Zhang L., and Yao X., (2000). Compositionally step-varied (Pb,Ca)TiO_3 thin films with enhanced dielectric and ferroelectric properties, Applied Physics Letters, Vol. 76, p.1063.

Bao D., Yao X., and Zhang L., (2000). Dielectric enhancement and ferroelectric anomaly of compositionally graded (Pb,Ca)TiO_3 thin films derived by a modified sol–gel technique, Applied Physics Letters, Vol. 76, p.2779.

Bao D., Mizutani N., Zhang L., and Yao X., (2001a). Composition gradient optimization and electrical characterization of (Pb,Ca)TiO_3 thin films, Journal of Applied Physics, Vol. 89, p.801.

Bao D., Wakiya N., Shinozaki K., Mizutani N., and Yao X., (2001b). Abnormal ferroelectric properties of compositionally graded Pb(Zr,Ti)O_3 thin films with $LaNiO_3$ bottom electrodes, Journal of Applied Physics, Vol. 90, p.506.

Bao D., Yao X., Wakiya N., Shinozaki K., and Mizutani N., (2002). Structural, dielectric, and ferroelectric properties of $PbTiO_3$ thin films by a simple sol–gel technique, Materials Science and Engineering B, Vol. 94(2-3), p. 269-274.

Baythoun M. S. G., and Sale F. R., (1982). Production of strontium-substituted lanthanum manganite perovskite powder by the amorphous citrate process, Journal of Materials Science, Vol.17, p.2757.

Bell A. J., and Moulson A. J., (1985). The effect of grain size on the dielectric properties of barium titanate ceramics, British Ceramics Proceeding, p.57-66.

Birk H., Glatz-Reichenbach J., Li-Jie, Schreck E., and Dransfeld K., (1991). Journal of Vacuum Science and Technology, Vol. B (9), p.1162.

Birnie D. P., (2001). Rational solvent selection strategies to combat striation formation during spin coating of thin films, Journal of Materials Research, Vol. 16, p.1145.

Bornside D. E., Macosko C. W., and Scriven L. E., (1987). On the modeling of spin coating, Journal of Imaging Technology, Vol. 13, p.122-130.

Boyle T. J. and Schwartz R. W., (1994). An Investigation of Group (IV) Alkoxides as Property Controlling Reagents in the Synthesis of Ceramic Materials, Comments on Inorganic Chemistry, Vol.16, p.243.

Boyle T. J., Dimos D. B., Schwartz R. W., Alam T. M., Sinclair M. B., and Buchheit C. D., (1997). Aging characteristics of a hybrid sol-gel $Pb(Zr,Ti)O_3$ precursor solution, Journal of Materials Research, Vol.12, No.4.

Bouregba R., Poullain G., Vilquin B., and Le Rhun G., (2003). Polarisation Offsets of Non Graded and Graded Ferroelectric Films, Journal of Applied Physics, Vol.93, p.5583.

Bouregba R., Rhun G. L., and Poullain G., (2005). Polarization Offsets of Non Graded and Graded Ferroelectric Films, Integrated Ferroelectrics, Vol.70, p.67–78.

Brazier M., McElfresh M., and Mansour S., (1998). Unconventional hysteresis behavior in compositionally graded $Pb(Zr,Ti)O_3$ thin films, Applied Physics Letters, Vol. 72, p.1121-1123.

Brazier M., McElfresh M., and Mansour S., (1999). Origin of anomalous polarization offsets in compositionally graded $Pb(Zr,Ti)O_3$ thin films, Applied Physics Letters, Vol. 74, p. 299-301.

Brinker C. J., and Scherer G. W., (1990). *Sol–Gel Science*, Academic Press, Boston.

Bryzek J., Petersen K., and McCulley W., (1994). Micromachines on the March, IEEE Spectrum, p. 20-31.

Budd K. D., Dey S. K., and Payne D. A., (1985). Sol-gel processing of $PbTiO_3$, $PbZrO_3$, PZT and PLZT thin films, British Ceramics Proceeding, Vol.36, 107.

Budd K. D., Dey S. K., and Payne D. A., (1986). The Effect of Hydrolysis Conditions on the Characteristics of $PbTiO_3$ Gels and Thin Films, in

Better Ceramics Through Chemistry II, Eds. C. J. Brinker *et al.*, Materials Research Society Symposium Proceedings, Vol. 73, p.711-716.

Callister W. D., (1997). *Materials Science and Engineering, an Introduction*, 4th edition, John Willey&Sons Inc.

Chae H. K., Payne D. A., Xu Z., and Ma L., (1994). Molecular Structure of a New Lead Titanium Bimetallic Alkoxide Complex $[PbTi_2(\mu 3\text{-}O)(OOCCH_3)(OCH_2CH_3)_7]_2$: Evolution of Structure on Heat Treatment and the Formation of Thin-Layer Dielectrics, Chemistry of Materials, Vol.6, p.1589-1592.

Chaim N. B., Brunstein M., Grunberg J., and Seidman A., (1974). Electric field dependence of the dielectric constant of PZT ferroelectric ceramics, Journal of Applied Physics, Vol.45, p.2398.

Chen Y. H., Ma J., and Li T., (2004). A functional gradient ceramic monomorph actuator fabricated using electrophoretic deposition, Ceramics International, Vol. 30, p.683–687.

Chrisman J. A., Kim S. H., Maiwa H., and Maria J. P., (2000). Spatial variation of ferroelectric properties in $Pb(Zr_{0.3},Ti_{0.7})O_3$ thin films studied by atomic force microscopy, Journal of Applied Physics, Vol.87, No.11, p.8031-8034.

Coffman P. K., and Dey S. K., (1994). Structure evolution in the PbO-ZrO_2-TiO_2 sol-gel system: Part I-Characterization of prehydrolyzed precursors, Journal of Sol-Gel Science and Technology, Vol.1, p.251.

Cross L. E., (1996). Ferroelectric materials for electromechanical transducer applications, Materials Chemistry and Physics, Vol.43, p.108.

Danglish M., and Kemmitt T., (2000). Ferroelectric thin films-research, development and commercialization, *IPENZ Transac*., Vol.27, No.1/Gen., p.21-24.

Dawber M., Gruverman A., and Scott J. F., (2006). Skyrmion model of nano-domain nucleation in ferroelectrics and ferromagnets, Journal of Physics: Condense Matter, Vol.18, L71.

Dehoff C., Rodriguez B. J., Kingon A. I., Nemanich R. J., Gruverman A., and Cross J. S., (2005). Atomic force microscopy-based experimental setup for studying domain switching dynamics in ferroelectric capacitors, Review of Science and Instruments, Vol. 76, p.023708.

Dennis M., (1972). *Transmission electron microscopy of ferroelectric domains in $BaTiO_3$*, Ph.D. Thesis, Pennsylvania State University, USA.

Desfeux R., Legrand C., Da Costa A., Chateigner D., Bouregba R., and Poullain G., (2006). Correlation between local hysteresis and crystallite orientation in PZT thin films deposited on Si and MgO substrates, Surface Science, Vol. 600, p.219.

Dunn S., (2003). Strain behavior of thin film $PbZr_{0.3}Ti_{0.7}O_3$ (30/70) examined through piezoforce microscopy, Journal of Applied Physics, Vol.94, No.9, p.5964-5968.

Dunn S., and Whatmore R. W., (2002). Substrate effects on domain structures of PZT 30/70 sol-gel films via PiezoAFM, Journal of the European Ceramic Society, Vol. 22(6), p.825-833.

Eichorst D. J., and Payne D. A., (1988). Sol-Gel Processing of Lithium Niobate Thin-Layers of Silicon, Better Ceramics Through Chemistry III, Eds. C. J. Brinker *et al.*, Materials Research Society Symposium Proceedings, Vol. 121, p.773-778.

Emelyanov Y. A., (2005). Coherent ferroelectric switching by atomic force microscopy, Physics Review, Vol. B 71, p.132102.

Eng L. M., Güntherodt H.-J., Rosenman G., Skliar A., Oron M., Katz M., and Eger D., (1998). Nondestructive imaging and characterization of ferroelectric domains in periodically poled crystals, Journal of Applied Physics, Vol. 83, p.5973.

Eng L. M., Güntherodt H.-J., Schneider G. A., Köpke U., and Muñoz J. Saldaña, (1999). Nanoscale reconstruction of surface crystallography from three-dimensional polarization distribution in ferroelectric barium–titanate ceramics, Applied Physics Letters, Vol.74, p.233.

Falter L. M., Payne D. A., Friedmann T. A., Wright W. H., and Ginsberg D. M., (1989). Preparation of Ceramic Superconductors by the Pechini Method, British Ceramics Proceeding, Electroceramics, Vol.41, p. 261-269.

Felberg W., Mantese J. V., Schubring N. W., and Micheli A. L., (2001). Origin of the "up", "down" hysteresis offsets observed from polarization-graded ferroelectric materials, Applied Physics Letters, Vol. 78, p.524.

Fink D., Beaty H. W., and Caroll J. M., (1999). *Standard handbook for electrical engineers*, 14th edition, McGraw-Hill.

Francis L. F., Payne D. A., and Wilson S. R., (1990). Crystal Structure of a New Lead Zinc Acetate Alkoxide, $Pb_2Zn_2(C_2H_3O_2)4(C_3H_7O_2)_4$, Chemistry of Materials, Vol.2, p.645-647.

Ganpule C. S., Nagarajan V., Li H., Ogale A.S ., Steinhauer D. E., Aggarwal S., Williams E., Ramesh R., and de Wolf P., (2000). Role of 90° domains in lead zirconate titanate thin films, Applied Physics Letters, Vol. 77, p.292.

Gong W., Jing-Feng L., Xiangcheng C., and Longtu L., (2004). Effect of pyrolysis temperature on preferential orientation and electrical properties of sol-gel derived lead zirconate titanate films, Journal of the European Ceramic Society, Vol.24, p. 2977-2982.

Gruverman A., Auciello O. and Tokumoto H., (1996). Nanoscale investigation of fatigue effects in $Pb(Zr,Ti)O_3$, Applied Physics Letters, 69, 3191-3193.

Gruverman A., Rodriguez B. J., Kingon A. I., Nemanich R. J., Cross J. S., and Tsukada M., (2003a). Spatial inhomogeneity of imprint and switching behavior in ferroelectric capacitors, Applied Physics Letters, Vol.82, p.3071.

Gruverman A., Rodriguez B. J., Kingon A. I., Nemanich R. J., Tagantsev A. K., Cross J. S., and Tsukada M., (2003b). Mechanical stress effect on imprint behavior of integrated ferroelectric capacitors, Applied Physics Letters, Vol. 83, p.728.

Gruverman A., Rodriguez B. J., Dehoff C., Waldrep J. D., Kingon A. I., Nemanich R. J., and Cross J. S., (2005). Direct studies of domain switching dynamics in thin film ferroelectric capacitors, Applied Physics Letters, Vol. 87, p.082902.

Guo R., Cross L. E., Park S.-E., Noheda B., Cox D. E., and Shirane G., (2000). Origin of the high piezoelectric response in $PbZr_{1-x}Ti_xO_3$, Physics Review Letters Vol. 84, 5423-5426.

Guo H. Y., Xu J. B., Wilson I. H., Xie Z., Luo E. Z., Hong S. B., and Yan H., (2002). Study of domain stability on $(Pb_{0.76}Ca_{0.24})TiO_3$ thin films using piezoresponse microscopy, Applied Physics Letters, Vol. 81, p.715 .

Gurkovotch S. R., and Blum J. B., (1985). Crystallization of amorphous lead titanate prepared by a sol-gel process, Ferroelectrics, Vol.62, p.189-194.

Guy I. L., Muensit S., and Goldys E. M., (1999). Extensional piezoelectric coefficients of gallium nitride and aluminum nitride, Applied Physics Letters, Vol.75, p.4133.

Haas D. E., Birnie D. P., Zecchino M. J., and Figueroa J. T., (2001). The effect of radial position and spin speed on striation spacing in spin on glass coatings, Journal of Materials Science Letters, Vol. 20, p.1763.

Haertling G. H., (1991). PLZT thin films prepared from acetate precursors, Ferroelectrics, Vol. 119, p.21.

Haertling G. H., (1999). Ferroelectric Ceramics: History and Technology, Journal of American Ceramics Society, Vol.82, p.797.

Han J.-P., Gu J., and Ma T. P., (1997). $SrBi_2Ta_2O_9$(SBT) thin films prepared by electrostatic spray, Integrated Ferroelectrics, Vol.14, p.229-235.

Harnagea C., (2001). *Local piezoelectric response and domain structures in ferroelectric thin films investigated by voltage-modulated force*

microscopy, Ph.D. Thesis, Mathematisch-Naturwissenschaftlich-Technischen Fakultät, Martin-Luther-Universität Halle Wittenberg.

Harnagea C., Pignolet A., Alexe M., Hesse D., and Gosele U., (2000). Quantitative ferroelectric characterization of single submicron grains in Bi-layered perovskite thin films, Applied Physics, Vol. A 70, p.261.

Hayashi T., Ohji N., Hirohara K., Fukunaga T., and Maiwa H, (1993). Preparation and Properties of Ferroelectric $BaTiO_3$ Thin Films by Sol-Gel Process, Japanese Journal of Applied Physics, Vol. 32, p.4092.

He X. Q., Ng T., Sivashanker Y., and Liew K. M., (2001). Active control of FGM plates with integrated piezoelectric sensors and actuators, International Journal of Solids and Structures, Vol.38, p. 1641-1655.

Hidaka T., Maruyama T., Saitoh M., Mikoshiba N., Shimizu M., Shiosaki T., Wills L. A., Hiskes R., Dicarolis S. A., and Amano J., (1996). Formation and observation of 50 nm polarized domains in $PbZr_{1-x}Ti_xO_3$ thin film using scanning probe microscope, Applied Physics Letters, Vol. 68, p.2358.

Hirano S. I., and Kato K. J., (1988). Formation of $LiNbO_3$ films by hydrolysis of metal alkoxides, Journal of Non-Crystalline Solids, Vol.100, p.538.

Hsueh C. C., and Mecartney M. L., (1990). TEM Analyses of Sol-Gel Derived and Sputtered PZT Thin Films, Ferroelectric Thin Films, Materials Research Society Symposium Proceedings, 200 (219).

Hu H., Shi L., Kumar V., and Krupanidhi S. B., (1992). Rapid thermal annealing processed ferroelectric $Pb(Zr,Ti)O_3$ films, Ceramic Transactions, Vol.25 No.113.

Hunderford G., Rui Pereira M., Ferreira J. A., Viseu T. M. R., Coelho A. F., Isabel M., Ferreira C., and Suhling K., (2002). Probing Si and Ti sol-gel matrices by fluorescence techniques, Journal of Fluorescence, Vol. 12, p.397-417.

Huffmann S., Klee M., and Waser R., (1995). Structural and electrical properties of wet-chemically deposited $Sr(Ti_{1-y}Zr_y)O_3$ (y=0…1) thin films, Integrated Ferroelectrics, Vol. 10, p.155-164.

IEEE Standard Definitions of Primary Ferroelectric Terms, (1986). ANSI/IEEE Std., Published by The Institute of Electrical and Electronics Engineers, Inc., New York, NY 10017, USA

Ito Y., Ushikubo M., Yokoyama S., Matsunaga H., Atsuki T., Yonezawa T., and Ogi K., (1997). New low temperature processing of sol-gel $SrBi_2Ta_2O_9$ thin films, Integrated Ferroelectrics, Vol.14, p.123.

Jaffe B., Cook W. R., and Jaffe H., (1971). *Piezoelectric Ceramics*, Academic Press, London, p.142.

Jaffe B., and Roth R. S., (1954). Piezoelectric Properties of Lead Zirconate-Lead Titanate Solid Solution Ceramics, Journal of Applied Physics, Vol.25, p.809.

Jesse S., Baddorf A. P., and Kalinin S. V., (2006). Switching spectroscopy piezoresponse force microscopy of ferroelectric materials, Applied Physics Letters, Vol. 88, p.062908.

Jin F., Auner G. W., Nike R., Schubring N. W., Mantese J. V., and Catalan A. B., (1998). Giant effective pyroelectric coefficients from graded ferroelectric devices, Applied Physics Letters, Vol. 73, p.288.

Kalinin S. V., (2002). *Nanoscale Electric Phenomena at Oxide Surfaces and Interfaces by Scanning Probe Microscopy*, Ph.D. Thesis, University of Pennsylvania, USA.

Kalinin S. V., and Bonnell D. A., (2002), Imaging mechanism of piezoresponse force microscopy of ferroelectric surfaces, Physical Review B, Vol. 65, p.125408.

Kalinin S. V., Gruverman A., and Bonnell D. A., (2004). Quantitative analysis of nanoscale switching in $SrBi_2Ta_2O_9$ thin films by piezoresponse force microscopy, Applied Physics Letters, Vol. 85, p.795.

Kalinin S. V., Gruverman A., Rodriguez B. J., Shin J., Baddorf A. P., Karapetian E., and Kachanov M., (2005a). Nanoelectromechanics of polarization switching in piezoresponse force microscopy, Journal of Applied Physics, Vol. 97, p.074305.

Kalinin S. V., Jesse S., Borisevich A. Y., Lee H. N., Rodriguez B. J., Hanson J., Gruverman A., Karapetian E. and Kachanov M., (2005b). Recent Developments in Electromechanical Probing on the Nanoscale: Vector and

Spectroscopic Imaging, Resolution, and Molecular Orientation Mapping, Unpublished.

Khamanker R., Kim J., Jiang B., Maniar P., Moazzami R. Jone R. E., and Lee J. C., (1994). Proceeding in International Electron Device Meeting, (IEEE Press, New Jersey), p. 337.

Khaenamkeaw P., Muensit S., and Aiyarak P., (2003). Piezoelectric effects of single-crystal GaAs and multi-layered $Al_xGa_{1-x}As$/GaAs material measured by Michelson interferometer, Songklanakarin Journal of Science and Technology, Vol. 25 No. 5, p. 623-628.

Kholkin A. L., Taylor D. V., and Setter N., (1998). Piezoelectric Characterization of $Pb(Zr,Ti)O_3$ Thin Films by Interferometer Technique, Proceeding ISAF 98, p. 69-72.

Kholkin A. L., Bdikin I. K., Shvartsman V. V., Orlova A., Kiselev D., Bogomolov A. A., and Kim S.-H., (2004). Local Electromechanical Properties of Ferroelectric Materials for Piezoelectric Applications, Materials Research Society Symposium Proceedings, 839E, O7.6.

Kholkin A. L., Martins R., Aguas H., Ferreira I., Silva V., Smirnova O. A., Costa M. E. V., Vilarinho P. M., Fortunato E., and Baptista J. L., (2002). Metal-ferroelectric thin film devices, Journal of Non-Crystalline Solids, Vol. 299-302, p.1311-1315.

Kholkin A. L., Roelofs A., Kalinin S. V., Gruverman A., (2006a). *Review of ferroelectric domain imaging by piezoelectric force microscopy*, *In "Recent advancements in scanning probe microscopy*", ed. by S. V. Kalinin and A. Gruverman, Springer.

Kholkin A. L., Shvartman V. V., Kiselev D. A., and Bdikin I. K., (2006b). Nanoscale characterization of ferroelectric materials for piezoelectric application, Ferroelectrics, Vol. 341, p.9-13.

Kim D. J., Maria J. P., and Kingon A. I., (2003). Evaluation of intrinsic and extrinsic contributions to the piezoelectric properties of $Pb(Zr_xTi_{1-x})O_3$ thin films as a function of composition, Journal of Applied Physics, Vol.93, No. 9.

Kim I. D., Avrahami Y., Tuller H. L., Park Y. B., Dicken M. J., and Atwater H. A., (2005). Study of orientation effect on nanoscale polarization in

$BaTiO_3$ thin films using piezoresponse force microscopy, Applied Physics Letters, Vol. 86, p.192907.

Kingery W. D., Bowen H. K., and Uhlmann D. R., (1976). *Introduction to ceramics*, 2nd edition, John Wiley & Sons.

Kittel C., (1986). *Introduction to Solid State Physics*, 6th edition, New York, John Wiley.

Klee M., Veirman A., Weijer P., Mackens U., and Hal H. V., (1993). Large polarization and coercive force by 100% 180° domain switching in epitaxial $Pb(Zr_{0.5}Ti_{0.5})O_3$ capacitor, Philips Journal of Research, Vol.47 No. 263.

Kuffer O., Maggio-Aprile I., Triscone J.-M., Fischer ∅., and Renner C., (2000). Piezoelectric response of epitaxial $Pb(Zr_{0.2}Ti_{0.8})O_3$ films measured by scanning tunneling microscopy, Applied Physics Letters, Vol.77, No.11., p.1701-1703.

Kwok C. K., Desu S. B., and Kammerdiner L., (1993). Microstructure characterization of sol-gel derived PZT films, Journal of Materials Science, Vol.29 No.2.

Lakeman C. D. E., Xu Z., and Payne D. A., (1995). On the Evolution of Structure and Composition in Sol-Gel Derived PZT Thin Layers, Journal of Materials Research, Vol.10, p. 2042-2051.

Landauer R., (1957). Electrostatic considerations in $BaTiO_3$ domain formation during polarization, Journal of Applied Physics, Vol. 28, p.227.

Landau L. D., and Lifshitz E. M., (1980), *Statistical Physics*, Part 2, Vol. 9: *Theory of the Condensed State*, (Course of Theoretical Physics), Elsevier Pub.

Lee S. G., and Lee Y. H., (1999). Dielectric properties of Sol-Gel derived PZT(40/60)/PZT(60/40) heterolayeted thin films, Thin Solid Films, p.353.

Lefki K., and Dormans G. J., (1994). Measurement of piezoelectric coefficients of ferroelectric thin-films, Journal of Applied Physics, Vol. 76, p.1764–1767.

Liu J. -M., Pan B., Chan H. L. W., Zhu S. N., Zhu Y. Y. and Liu Z. G., (2002). Piezoelectric coefficient measurement of piezoelectric thin films: an overview, Materials Chemistry and Physics, Vol. 75, Issues 1-3, p.12-18.

Liu W., Jiang B., and Zhu W., (2000). Self-biased dielectric bolometer from epitaxially grown Pb(Zr,Ti)O_3 and lanthanum-doped Pb(Zr,Ti)O_3 multilayered thin films, Applied Physics Letters, Vol. 77, p.1047.

Lourdes C. M., Sirera R., Carmona F., and Jimenez B. J., (1995). Investigations of a Diol-base Sol-gel Process of the Lead Titanate Materials, American Ceramics Society, Vol. 78, p.1802.

Ma L., and Payne D. A., (1994). Studies on the nature of a lead zirconate titanate (PZT) precursor solution. Isolation and structural characterization of $[PbZr_2O(OOCCH_3)_2(OCH_2CH_3)_6]_2$, Chemistry of Materials, Vol.6, p.875.

Ma W., and Hesse D., (2004). Polarization imprint in ordered arrays of epitaxial ferroelectric nanostructures, Applied Physics Letters, Vol. 84, p.2871.

Mantese J. V., and Schubring N. W., (2001). Polarization-graded ferroelectrics: The dielectric analogues of semiconductor junctions devices, Integrated Ferroelectrics, Vol. 37, p.245.

Mantese J. V., Schubring N. W., Micheli A.L., and Catalan A. B., (1995). Ferroelectric thin films with polarization gradients normal to the growth surface, Applied Physics Letters, Vol.67, p. 721.

Mantese J. V., Schubring N. W., and Micheli A. L., (2001). Polarization-graded ferroelectrics: Transpacitor energy gain, Applied Physics Letters, Vol. 79, p.4007.

Mantese J. V., Schubring N. W., and Micheli A. L., (2002). Polarization-graded ferroelectrics: Transpacitor push-pull amplifier, Applied Physics Letters, Vol.80, p.1430.

Mantese J. V., Schubring N.W., Micheli A. L., Mohammed M.S., Naik R., and Auner G. W., (1997). Slater model applied to polarization graded ferroelectrics, Applied Physics Letters, Vol.71, p.2047.

Mantese J. V., Schubring N. W., Micheli A. L., Thompson M.P., Naik R., Auner G. W., Misirlioglu I. B., and Alpay S. P., (2002). Stress-induced polarization-graded ferroelectrics, Applied Physics Letters, Vol.81, p.1068.

McMillan L. D., de Araujo C., Paz A., Roberts T. L., Cuchiaro J., Scott M. C., and Scott J. F., (1992). Integrated Ferroelectrics, Vol. 2, p.351-359.

Mohammed M. S., Auner G. W., Naik R., Mantese J. V., Schubring N.W., Micheli A.L., and Catalan A.B., (1998). Temperature dependence of conventional and effective pyroelectric coefficients for compositionally graded $Ba_xSr_{1-x}TiO_3$ films, Journal of Applied Physics, Vol. 84, p.3322.

Morozovska A. N., and Eliseev E. A., (2006). Screening and size effects on the nanodomain tailoring in ferroelectrics semiconductors, Physical Review B, Vol. 73, p.104440.

Morozovska A. N., Bravina S. L., Eliseev E. A., and Kalinin S. V., (2007). Resolution Function Theory in Piezoresponse Force Microscopy: Domain Wall Profile, Spatial Resolution, and Tip Calibration, Physical Review B, Vol.75, p.174109.

Moulson A. J., and Herbert J. M., (1990). *Electroceramics – Materials, Properties & Applications*, Chapman & Hall.

Muensit S., and Khaenamkeaw P., (2002). Michelson interferometer for the piezoelectric measurements, Songklanakarin Journal Science and Technology, Vol. 24, No. 1, p.107-117.

Muralt P., Kohli M., Maeder T., Kholkin A., Brooks K., Setter N., and Luthier R., (1995). Fabrication and characterization of PZT thin-film vibrators for micromotors, Sensors and Actuators A, Vol. 48, p. 157-165.

Muralt P., (2000). Ferroelectric thin films for micro-sensor and actuator: a review, Journal of Micromechanical and Microengineering, Vol.10, p.136-146.

Newnham R. E., (1997). Molecular Mechanism in Smart Materials, MRS Bulletin, Vol.20.

Ng M. F., and Cima M. J., (1994). Crystallization of Epitaxial Lanthanum Aluminate and Spinel Thin Films Derived from Nitrate Precursors, *Epitaxial Oxide Thin Films and Heterostructures*, edited by R. Ramesh, D. K. Fork, J.

M. Phillips, and R. M. Wolf, Pittsburgh, PA., Materials Research Society Symposium Proceedings, Vol. 341.

Noheda B., Cereceda N., Iglesias T., Lifante G., Gonzalo J. A., Chen H. T., and Wang Y. L., (1995). Composition dependence of the ferroelectric-paraelectric transition in the mixed system $PbZr_{1-x}Ti_xO_3$, Physical Review B, Vol.51, p.16388.

Noheda B., Cox D. E., Shirane G., Gonzalo J. A., Cross L. E., and Park S. E., (1999). A monoclinic ferroelectric phase in the $PbZr_{1-x}Ti_xO_3$ solid solution, Applied Physics Letters, Vol.74, p. 2059.

Noheda B., Cox D. E., Shirane G., Gonzalo J. A., Park S. E., and Cross L. E., (2001). Stability of the monoclinic phase in the ferroelectric perovskite $Pb(Zr_{1-x}Ti_x)O_3$, Physical Review B, Vol.63, p.014103.

Nye J. F., (1985). *Physics Properties of Crystals*, Oxford University Press, New York.

Obata Y., and Noda N., (1996). Optimum material design for functionally gradient material plate, Archive of Applied Mechanics, Vol. 66, p.581-589.

Ogawa T., (2000). Domain structure of ferroelectric ceramics, Ceramics International, Vol.26, p.383-390.

O'Neill D., Bowman R. M., and Gregg J. M., (2000). Dielectric enhancement and Maxwell–Wagner effects in ferroelectric superlattice structures, Applied Physics Letters, Vol. 77, p.1520.

Pandey S. K., James A. R., Chandra P., Goel T. C., and Zimik K., (2004). Electrical properties of PZT thin films grown by sol-gel and using a seed layer, Materials Science and Engineering B, Vol. 112, p.96-100.

Paruch P., Giamarchi T., and Triscone J.-M., (2005). Domain Wall Roughness in Epitaxial Ferroelectric $PbZr_{0.2}Ti_{0.8}O_3$ Thin Films, Physics Review Letters, Vol. 94, p.197601.

Perez J., Vilarinho P. M., and Kholkin A. L., (2004). High-Quality $Pb(Zr_{0.52}Ti_{0.48})O_3$ Films Prepared by Modified Sol-Gel Route at low Temperature, Thin Solid Films, p.44920-44924.

Pintilie L., Boerasu I., and Gomes M. J. M., (2003). Simple model of polarization offset of graded ferroelectric structures, Journal of Applied Physics, Vol.93, p.9961.

Phillips N. J., and Milne S. J., (1991). Diol-based sol–gel system for the production of thin films of $PbTiO_3$, Journal of Materials and Chemistry, Vol.1, p.893-894.

Poullain G., Bouregba R., Viquin B., Le Rhun G., and Murray H., (2002). Graded ferroelectric thin films: Possible origin of the shift along the polarization axis, Applied Physics Letters, Vol. 81, p.26.

Praveen G. N., and Reddy J. N., (1998). Nonlinear transitent thermoelastic analysis of functionally graded ceramic-metal plates, International Journal of Solids and Structures, Vol. 35, p.4457-4476.

Prume K., Roelofs A., Schmitz T., Reichenberg B., Tiedke S., and Waser R., (2002). Compensation of the Parasitic Capacitance of a Scanning Force Microscope Cantilever Used for Measurements on Ferroelectric Capacitors of Submicron Size by Means of Finite Element Simulations, Japanese Journal of Applied Physics, Vol. 41, p. 7198-7201.

Ramamurthi S. D., and Payne D. A., (1990). Nanometer Sized ZrO_2 Particles Prepared by a Sol-Emulsion-Gel Method, Journal of American Ceramics Society, Vol. 73, p.2760-2763.

Ricinschi D., Mitoseriu L., Stancu A., Postolache P., and Okuyama M., (2004). Analysis of the Switching Characteristics of PZT Films by First Order Reversal Curve Diagrams, Integrated Ferroelectrics, Vol. 67, p.103.

Ricinschi D., Noda M., Okuyama M., Ishibashi Y., Iwata M., and Mitoseriu L., (2003). A Landau-Theory-Based Computational Study of In-Plane and Out-of Plane Polarization Components Role in Switching of Ferroelectric Thin Films, Journal of Korean Physics Society, Vol. 42, S1232.

Ricinschi D., and Okuyama M., (2002). Nanoscale Spatial Correlation of Piezoelectric Displacement Hysteresis Loops of PZT Films in the Fresh and Fatigued States, Integrated Ferroelectrics, Vol.50, p.159.

Rodriguez B. J., Gruverman A., Kingon A. I., Nemanich R. J., and Cross J. S., (2004). Three-dimensional high-resolution reconstruction of polarization

in ferroelectric capacitors by piezoresponse force microscopy, Journal of Applied Physics, Vol. 95, p.1958.

Roelofs A., Böttger U., Waser R., Schlaphof F., Trogisch S., and Eng L. M., (2000). Differentiating 180° and 90° switching of ferroelectric domains with three-dimensional piezoresponse force microscopy, Applied Physics Letters, Vol. 77, p.3444.

Rosen C. Z., Hiremath B. V., and Newnham R. E., (1992). Piezoelectricity: Key papers in physics, American Institute of Physics, p.5, 4, 13, 119, 157, and 285.

Saya Y., Watanabe S., Kawai M., Yamada H., and Matsushige K., (2000). Japanese Journal of Applied Physics, Vol. 39, p.3799.

Sawyer C. B., and Tower C. H., (1930), Rochelle Salt as a Dielectric, Physical Reviews, Vol.35, p. 269.

Sayer M., Judd B., El-Assal K., and Parsad E., (1981). Poling of piezoelectric ceramics, Journal of Canadian Ceramics Society, Vol.50.

Schubring N. W., Mantese J. V., Micheli A. L., Catalan A. B., and Lopez R. J., (1992). Charge pumping and pseudopyroelectric effect in active ferroelectric relaxor-type films, Physics Review Letters, Vol.68, p.1778.

Schubring N. W., Mantese J. V., Micheli A. L., Catalan A. B., Mohammed M. S., Naik R., and Auner G. W., (1999). Graded ferroelectrics: A new class of steady-state thermal/electrical/mechanical energy interchange devices, Integrated Ferroelectrics, Vol. 24, p.155.

Schwartz R. W., (1997). Chemical Solution Deposition of Perovskite Thin Films, Chemistry of Materials, Vol.9, p.2325-2340.

Schwartz R. W., Assink R. A., and Headley T., (1992). Solution Chemistry Effects in PZT Thin Film Processing: Spectroscopic and Microstructural Characterization, Materials Research Society Symposium Proceedings, Vol.243, p.245.

Schwartz R. W., Payne D. A., and Holland A. J., (1989). *Ceramic Powder Processing Science*; Hausner H., Messing G. R., Hirano S., (Eds.) Deutsche Keramische Gesellschaft, p. 165-172.

Scott J. F., and Araujo C. A., (1989). Ferroelectric Memories, Science, Vol.246, p.1400.

Scott J. F., Watanabe K., Hartmann A. J., and Lamb R. N., (1998). Device models for PZT/PT, BST/PT, SBT/PT, and SBT/BT ferroelectric memories, Annual Review of Materials Science, Vol. 28, p. 79-100.

Scriven L. E., (1988). Physics and Applications of Dip Coating and Spin Coating, Materials Research Society Symposium Proceedings, Vol.121, p. 717.

Sengupta S. S., Ma L., Adler D. L., and Payne D. A., (1995). EXAFS Determination of Local Structure in Sol-gel-derived Lead Titanate, Lead Zirconate and Lead Zirconate Titanate, Journal of Materials Research, Vol. 10(6), p. 1345-1348.

Seungbum S., Jong U. J., Eugene P. Y., Enrico L. C., Setter N., Kim E., and Kwangsoo N., (2001). Principle of ferroelectric domain imaging using atomic force microscope, Journal of Applied Physics, Vol. 89, No.2.

Shvartsman V. V., Kholkin A. L., Orlova A., Kiselev D., Bogomolov A. A., and Sternberg A., (2005a). Polar nanodomains and local ferroelectric phenomena in relaxor lead lanthanum zirconate titanate ceramics, Applied Physics Letters, Vol.86, p.202907-202909.

Shvartsman V. V., Kholkin A. L., Verdier C., Zhang Y., and Lupascu D. C., (2005b). Investigation of fatigue mechanism in ferroelectric ceramic via piezoresponse force microscopy, Journal of the European Ceramic Society, Vol. 25, p. 2559–2561.

Slowak R., Hoffmann S., Liedtke R., and Waser R., (1999). Functional graded high-K $(Ba_{1-x}Sr_x)TiO_3$ thin films for capacitor structures with low temperature coefficient, Integrated Ferroelectrics, Vol.24, p.169.

Snitka V., Ulcinas A., Nemciauskas K., and Lendraitis V., (2006). AFM based polarization nanolithography on PZT sol–gel films, Microelectronic Engineering, Vol. 83(4-9), p.1456-1459.

Song Y. J., (1998). *Ferroelectric thin films for high density non-volatile memories*, Ph.D. Thesis, Virginia Polytechnic Institute and State University, USA.

Takahashi Y., Matsuoka Y., Yamaguchi K., Matsuki M., and Kobayashi K., (1990). Dip coating of PT, PZ and PZT films using an alkoxide-diethanolamine method, Journal of Materials Science, Vol.25, p.3960.

Takagi K., Li J.-F., Yokoyama S., and Watanabe R., (2003). Fabrication and evaluation of PZT/Pt piezoelectric composites and functionally graded actuators, Journal of the European Ceramic Society, Vol.23 (10), p. 1577-1583.

Tang X. G., Chan H. L. W., and Ding A. L., (2003). Electrical properties of compositionally graded lead calcium titanate thin films, Solid State Communication, Vol.123, p.625-628.

Tang X. G., Wang J., Chan H. L. W., and Ding A. L., (2004). Growth and electrical properties of compositionally graded $Pb(Zr_xTi_{1-x})O_3$ thin films on $PbZrO_3$ buffered $Pt/Ti/SiO_2/Si$ substrates, Journal of Crystal Growth, Vol. 267, p.117-122.

Taya M., Almajid A. A., Dunn M., and Takahashi H., (2003). Design of bimorph piezo-composite actuators with functionally graded microstructure, Sensors and Actuators A., Vol. 107, p.248–260.

Toewee G., Boulton J. M., Lee S. C., and Uhlmann D. R., (1992). Materials Research Society Symposium Proceedings, No.234, p.255.

Tohge N., Takahashi S., and Minami T., (1991). Preparation of $PbZrO_3$-$PbTiO_3$ Ferroelectric Thin Films by the Sol-Gel Process, Journal of American Chemistry Society, Vol. 74, p.67-71.

Tybell T., Paruch P., Giamarchi T., and Triscone J.-M., (2002). Domain Wall Creep in Epitaxial Ferroelectric $Pb(Zr_{0.2}Ti_{0.8})O_3$ Thin Films, Physics Review Letters, Vol. 89, p.097601.

Tu Y. L., and Milne S. J., (1995). A study of the effects of process variables on the properties of PZT films produced by a single-layer sol-gel technique, Journal of Materials Science, Vol.30, No.10, p. 2507-2516.

Uchino K., and Giniewicz J. R., (2003). *Micromechatronics*, Marcel Dekker Inc., New York.

Uchino K., (2000). *Ferroelectric Devices*, Marcel Dekker Inc., New York.

Vest R. W., and Xu J., (1988). $PbTiO_3$ films from metalloorganic precursors, IEEE Trans. UFFC, Vol. 35, p.711.

Vilquin B., Poullain G., Bouregba R., and Murray H., (2003a). Compositionally graded $Pb(Zr,Ti)O_3$ thin films with different crystallographic orientations, Thin Solid Films, Vol. 436, p.157–161.

Vilquin B., Rhun G. Le, Bouregba R., and Poullain G., (2003b). Properties of oriented and graded PZT thin films, Materials Science and Engineering B., Vol.104, p.176–179.

Wenbin W., Wang Y., Pang G. K. H., Wong K. H., and Choy C. L., (2004). Effect of lattice-misfit strain on the process-induced imprint behavior in epitaxial $Pb(Zr_{0.52}Ti_{0.48})O_3$ thin films, Applied Physics Letters, Vol.85, p.1583.

West A. E., (1985). *Solid State Chemistry and its Applications*, John Willey & Sons Ltd.

Whatmore R. W., Zhang Q., Huang Z., and Dorey R. A., (2003). Ferroelectric thin and thick films for Microsystems, Materials Science and Semiconductors Proceeding, Vol. 5, p.65-76.

Wu X. H., Changqing C., Shen Y. P, and Tain X. G., (2002). A high order theory for functionally graded piezoelectric shells, International Journal of Solid and Structure, Vol. 39, p.5325.

Xu F., Trolier S., Ren W., and Xu B., (2001). Domain wall motion and its contribution to the dielectric and piezoelectric properties of lead zirconate titanate films, Journal of Applied Physics, Vol.89, p.1336.

Xu R., Shen M. R., Ge S. B., Gan Z. Q., and Cao W. W., (2002). Effect of the Interdiffusion Reaction on the Compatibility in PZT/PNN Functionally Gradient Piezoelectric Materials, IEEE Transaction on Component and Packaging Technology, Vol.22 No.1, p.11-17.

Yamanouchi M., Hirai T., and Shiota I., (1990). Proceedings of the First International Symposium on Functionally Gradient Materials, Japan.

Yang J.-S., Kim S.-H., Yeom J.-H., Koo C.-Y., Hwang C. S., Yoon E., Kim D.-J., and Ha J., (2003). Piezoelectric and Pyroelectric Properties of $Pb(Zr,Ti)O_3$ Films for Micro-Sensors and Actuators, Integrated Ferroelectrics, Vol. 54, p.515-525.

Yao K., and Tay F. E. H., (2003). Measurement of longitudinal piezoelectric coefficient of thin films by a laser-scanning vibrometer, IEEE-TUFFC 50, p.113–116.

Yi G., Wu Z., and Sayer M., (1988). Preparation of $Pb(Zr,Ti)O_3$ thin films by sol-gel processing: electrical, optical and electro-optic properties, Journal of Applied Physics, Vol.64(5), p.2717-2724.

Yi. G., and Sayer M., (1991). Sol-Gel processing of complex oxide films, Ceramics Bulletin, Vol. 70, p.1173.

Yokoyama S., Yoshiro H., Hitoshi M., Gouji A., Takahiro O., Takashi I., Hirofumi M., and Hiroshi F., (2003). Compositional Dependence of Electrical Properties of Highly(100)-/(011)-Oriented $Pb(Zr,Ti)O_3$ Thick Films Prepared on Si Substrates by Metalorgamic Chemical Vapor Deposition, Japanese Journal of Physics, Vol. 42, p. 5922-5926.

Zeng H. R., Li G. R., Yin Q. R., and Xu Z. K., (2003a). Nanoscale domain switching mechanism in $Pb(Zr,Ti)O_3$ thin film, Applied Physics A 76: Materials Science & Processing, p.401-404.

Zeng H. R., Li G. R., Yin Q. R. and Xu Z. K., (2003b). Local characterization of compositionally graded $Pb(Zr,Ti)O_3$ thin films by scanning force microscope, Materials Science and Engineering B, Vol.99, p.234-237.

Zeng H. R., Yu H. F., Tang X. G., Chu R. Q., Li G. R., and Yin Q. R., (2005). Piezoresponse force microscopy studied of nanoscale domain structures in ferroelectric thin film, Materials Science and Engineering B, Vol.120, p.104-108.

Zhang Q. and Whatmore R. W., (2001). Sol-Gel $Pb(Zr_xTi_{1-x})O_3$ and Mn-doped $Pb(Zr_xTi_{1-x})O_3$ Thin Films for Pyroelectric Applications, Journal of Physics D: Applied Physics, Vol. 34, p.2296-2301.

Zhang Q., Whatmore R., and Vickers M. E., (1999). A comparison of the nanostructure of lead zirconate, lead titanate and lead zirconate titanate sols, Journal of Sol-Gel Science and Technology, Vol.15, p. 13-22.

Zhang Q. M., Pan W. Y., and Cross L. E., (1988). Laser interferometer for the study of piezoelectric and electrostrictive strains, Journal of Applied Physics, Vol.63, p.2492.

Zheng F., Chen J., Li X., and Shen M., (2006). Morphotropic phase boundary (MPB) effect in $Pb(Zr,Ti)O_3$ rhombohedral/tetragonal multilayered films, Materials Letters, Vol.60, p.2733-2737.

Zhu X. H., and Meng Z. Y., (1996). Operational principle, fabrication and displacement characteristics of a functionally gradient piezoelectric ceramic actuator, Sensors Actuators A, Vol. 48, p.169–173.

Zhu T., and Yang W., (1997). Toughness variation of ferroelectrics by polarization switch under non-uniform electric field, Acta Materilia, Vol.45 (11), p.4695-4702.

Zhu X., Chong N., Chan H. L.W., Choy C.-L., Wong K.-H., Liu L., and Ming N., (2002). Epitaxial growth and planar dielectric properties of compositionally graded $Ba_{1-x}Sr_xTiO_3$ thin films prepared by pulsed-laser deposition, Applied Physics Letters, Vol. 80, p.3376.

http://www.ferroperm-piezo.com (October 5, 2007).

VITAE

Name Mr. Panya Khaenamkaew

Student ID 4623005

Educational Attainment

Degree	Name of Institution	Year of Graduation
B.Sc.(Physics)	Prince of Songkla University	2000
M.Sc.(Physics)	Prince of Songkla University	2003

Scholarship Awards during Enrolment

UDC grant from Kasetsart University, 2002-2006

The 7th Royal Golden Jubilee Ph.D. Program, Thailand Research Fund, 2003-2006

Work – Position and Address

Position	Address
Teacher Assistant	Physics Department, Prince of Songkla University
Research Assistant	Material Physics Research Unit, Prince of Songkla University
Part Time Lecturer	Faculty of Science and Technology, Hatyai University, Songkla
Full Time Lecturer	Faculty of Resources and Environment, Kasetsart University

List of Publications and Proceedings

Publications

1. **Khaenamkaew P.**, Muensit S., Bdikin I. K. and Kholkin A. L., **(2007)**. Effect of Zr/Ti ratio on the Microstructure and Ferroelectric Properties of Lead Zirconate Titanate Thin Films, Materials Chemistry and Physics, Vol.102, p.159-164.
2. **Khaenamkaew P.**, Bdikin I. K., Kholkin A. L., and Muensit S., **(2007)**. Microstructure and Ferroelectric Properties of Sol-gel Graded PZT (40/52/60) and (60/52/40) Thin Films, Ceramics International (*online*).
3. **Khaenamkaew P.**, Bdikin I. K., Kholkin A. L., and Muensit S., **(2008)**. Local piezoresponse and ferroelectric property of sol-gel $Pb(Zr_x,Ti_{1-x})O_3$ film, Songklanakarin Journal of Science and Technology, Vol. 30, Jan-Feb (*in press*).

Proceedings

1. Panya Khaenamkaew, Pruittikorn Smithmaitrie and **Supasarote Muensit**, **(2008)**. Electrically induced strains in sol-gel up-graded and down-graded PZT thin films, International Conference on Electroceramics (ICE 2007), 31 July-3 August 2007, Arusha,Tanzania.
2. **Panya Khaenamkaew**, Igor D. Bdikin, Andrei L. Kholkin, and Supasarote Muensit, **(2005)**. Comparative study of single-composition and graded sol-gel PZT films, Asian Meeting on Electroceramics (AMEC'05), 11-14 December 2006, Sofitel Central Plaza, Bangkok, Thailand.
3. **Panya Kheanumkeaw** and Supasarote Muensit, **(2004).** Effective Piezoelectric Coefficient of Sol-gel PZT Films, The International Conference on Smart/Intelligent Materials and Nanotechnology (SmartMat-'04), 1-3 December 2004, Imperial Mae Ping, Chiang Mai, Thailand.
4. **Panya Kheanumkeaw** and Supasarote Muensit, **(2004).** Nanofrabrication and Characterization of PZT Thin Films, RGJ Seminar Series XXX: Biosciences and Biotechnology for the Development of Southern Thailand, Thailand Research Fund, 13 August 2004, Faculty of Agro-Industry, Prince of Songkla University.